2013

Air Cooling of PV Panels

Frantzis Iakovidis
University of Windsor

Air Cooling of PV Panels

by

Frantzis Iakovidis

A Thesis
Submitted to the Faculty of Graduate Studies
Through Mechanical, Automotive, and Materials Engineering
in Partial Fulfillment of the Requirements for
the Degree of Master of Applied Science at the
University of Windsor

Windsor, Ontario, Canada

2013

Library and Archives Canada

Published Heritage Branch

395 Wellington Street
Ottawa ON K1A 0N4
Canada

Bibliothèque et Archives Canada

Direction du Patrimoine de l'édition

395, rue Wellington
Ottawa ON K1A 0N4
Canada

Your file Votre référence
ISBN: 978-0-494-85111-1

Our file Notre référence
ISBN: 978-0-494-85111-1

Air Cooling of PV Panels

by

Frantzis Iakovidis

APPROVED BY:

_____

Dr. Paul Henshaw
Department of Civil and Environmental Engineering

_____

Dr. Amir Fartaj
Department of Mechanical, Automotive and Materials Engineering

_____

Mr. Steve Ray, Industrial Advisor
Essex Energy

_____

Dr. David Ting, Advisor
Department of Mechanical, Automotive and Materials Engineering

_____

Dr. Vesselin Stoilov, Chair of Defense
Department of Mechanical, Automotive and Materials Engineering

January 23, 2013

DECLARATION OF ORIGINALITY

I hereby certify that I am the sole author of this thesis and that no part of this thesis has been published or submitted for publication.

I certify that, to the best of my knowledge, my thesis does not infringe upon anyone's copyright nor violate any proprietary rights and that any ideas, techniques, quotations, or any other material from the work of other people included in my thesis, published or otherwise, are fully acknowledged in accordance with the standard referencing practices. Furthermore, to the extent that I have included copyrighted material that surpasses the bounds of fair dealing within the meaning of the Canada Copyright Act, I certify that I have obtained a written permission from the copyright owner(s) to include such material(s) in my thesis and have included copies of such copyright clearances to my appendix.

I declare that this is a true copy of my thesis, including any final revisions, as approved by my thesis committee and the Graduate Studies office, and that this thesis has not been submitted for a higher degree to any other University or Institution.

ABSTRACT

In the current study fluid flow and heat transfer characteristics over a heated flat plate were investigated in a closed loop wind tunnel. Two free stream flow regimes were considered; Laminar (turbulence intensity, Tu < 0.5%) and Turbulent. For the laminar free stream case, velocities ranging from 4 to 10 m/s that resulted in Reynolds numbers (Re) up to 346,670 were examined. For the turbulent free stream case, Tu=4%, 8% 12%, and Λ=0.015, 0.021 0.030m were set at the leading edge of the 0.34 by 0.52m heated plate. The aluminum flat plate was heated with supplying powers of 52W and 224W.

The heated flat plate was positioned at 0° and 20° tilt and the local heat transfer coefficient in terms of Nusselt number (Nu) was determined along the centreline span of the plate in the streamwise coordinate. Effects of Reynolds number, turbulence intensity (Tu) and integral length scale (Λ/x) on Nusselt number were investigated. The convection heat transfer rate increased in the range of 15% ~ 40% while the turbulent intensity was raised from 4% to 8%. It was observed that the effect of integral length scale (Λ/x) on heat transfer rate is more significant at larger turbulence intensities.

DEDICATION

Firstly to God, and Second to my late father Anestis, my Mother Ekaterini, Brother Theodoros, my fiancée Kristine, my nieces Kristina and Katerina.

"For after all what is man in nature? A nothing in relation to infinity, all in relation to nothing, a central point between nothing and all and infinitely far from understanding either. The ends of things and their beginnings are impregnably concealed from him in an impenetrable secret. He is equally incapable of seeing the nothingness out of which he was drawn and the infinite in which he is engulfed" (Blaise Pascal, Pensees#72).

I first read this quote while taking Dr.Ting's Turbulence course, Thank You.

ACKNOWLEDGEMENTS

I would like to express my sincere gratitude to Dr. David Ting for his excellent guidance and support during this study. The invaluable comments and assistance from the committee members are gratefully acknowledged. Technical assistance from the staff of the University of Windsor is appreciated. Gratitude goes to Mr. Steve Colbert of the OCE (Ontario Centre of Excellence) and to Mr. Steve Ray (Essex Power) who made my research possible.

The financial support from the Department of Mechanical, Automotive and Materials Engineering in the form of a Graduate Assistantship is acknowledged.

TABLE OF CONTENTS

LIST OF TABLES

LIST OF FIGURES

NOMENCLATURE / ABBREVIATIONS

A	Ampere
A_s	Cross-sectional Area, (m^2)
C_p	Specific Heat Capacity, (J/kg-K)
C_0, C_1, C_2, C_3, C_4	Hot Wire Calibration Coefficients
E	Voltage, (V)
G_t	Solar Irradiance, (W/m^2)
h	Heat Transfer Coefficient, (W/m^2-K)
h_x	Local Heat Transfer Coefficient, (W/m^2-K)
K	Shape Factor
L	Flat Plate Length, (m)
M	Auto-Correlation Counting Parameter
N	Sample Size
NOCT	Nominal Operating Cell Temperature (°C)
Nu	Nusselt Number
Nu_x	Local Nusselt Number
$Nu_{x,oG}$	Nusselt Number in Absence of Turbulence Generator
P_{ext}	Pressure Outside of the Boundary Layer
Pr	Prandtl Number
PV	Photovoltaic
$\dot{Q}_{cond}$	Energy Transfer due to Conduction, (W)
$\dot{Q}_{conv}$	Energy Transfer due to Convection, (W)

$\dot{Q}_{rad}$ Energy Transfer due to Radiation, (W)

$\dot{Q}_{total}$ Total Power, (W)

Re Reynolds Number

Re_x Local Reynolds Number

Re_c Critical Reynolds Number

Re_t Turbulent Reynolds Number

T_c PV cell/panel Temperature, (^{o}C)

T_a Ambient Temperature, (^{o}C)

T_{ref} Reference Temperature, (^{o}C)

T_f Film Temperature, (^{o}C)

T_s Surface Temperature, (^{o}C)

T_{sx} Local Surface Temperature, (^{o}C)

T_{sky} Sky Temperature, (^{o}C)

T_∞ Free Stream Temperature, (^{o}C)

Tu Turbulence Intensity, (%)

U Free Stream Velocity, (m/s)

U_{ext} External Velocity, (m/s)

U_{mean} Free Stream Mean Velocity, (m/s)

u_{rms} Root Mean Square Velocity, (m/s)

u' Instantaneous Fluctuating Velocity, (m/s)

V Velocity, (m/s)

x Distance from Leading Edge of the Flat Plate

Greek Symbols

ρ	Density, (kg/m^3)
δ	Boundary Layer Thickness
ν	Kinematic Viscosity, (m^2/s)
μ	Dynamic Viscosity, (mPa-s)
ε	Emissivity
k	Thermal Conductivity, (W/m-K)
β	Temperature coefficient
η_c	Efficiency of Solar cell
η_{Tref}	Reference Efficiency of Solar cell
Λ	Integral Length Scale, (m)
τ_Λ	Integral Time Scale (s)
σ	Stefan Boltzman nConstant, ($W\ m^{-2}K^{-4}$)

CHAPTER 1

INTRODUCTION

1.1. Introduction and Motivation

It is known that temperature plays a key role in the photovoltaic (PV) conversion process. The PV panel temperature is dependent upon many factors such as solar radiation, ambient temperature, wind speed and wind turbulence. This temperature directly affects some basic parameters including the voltage and current of the PV generator, the output electrical power of the PV cell and its efficiency [1]. Therefore, in recent years the influence of the panel temperature on PV cells has been given a great amount of attention in the scientific community.

In the literature, different equations have been used to express the PV cell temperature T_c as a function of the ambient temperature (T_a), the local wind speed (V) and the solar irradiance (G_t) [2]. Many of the technologies and/or techniques in recent years focus on increasing the incoming radiation on the PV cell surface in an effort to reduce the required PV cell area [3]. It goes without saying that these techniques and technologies bring forth higher operating temperatures on the PV cell which negatively affect its efficiency [1].

With an increase in the solar panel temperature, its electrical efficiency decreases. The result is that a more significant amount of the absorbed solar radiation by the cell is not converted into electricity. Furthermore, this increasing temperature of the panel affects other components of the photovoltaic system, including thermal stress which may result in premature failures in the photovoltaic system. Consequently, a method to cool the solar

panels is desirable. The long-term objective of this project is to enhance the performance of the solar panel by attempting to enhance the convection heat transfer and hence decrease the PV cell temperature; simply, $\uparrow \eta_c$ by $\downarrow T_c$.

In the current research, a heated flat plate with a roughly uniform heat flux was placed horizontally in the wind tunnel and exposed to laminar and turbulent free stream flows. The surface of the flat plate was cooled at a rate which was dependent on the Reynolds number (Re), turbulent intensity (Tu), and integral length scale (Λ). Eighteen Type T thermocouples were located beneath the surface of the flat plate which were used to measure the surface temperature of the flat plate in order to determine the convective heat transfer coefficient. For turbulence generation, three perforated plates with hole diameters of approximately 25, 37.5 and 50 mm in different distances upstream of the leading edge of the flat plate were used to control the different characteristics of the turbulence which was produced. Experiments performed in the wind tunnel were briefly compared to field data obtained from Essex Energy, who is the industry partner for the current endeavor.

1.2. Objectives

A point form summary of the objectives of this project is as follows;

- to determine the effect that the Reynolds number has on the heat transfer coefficient,
- to determine the effect that the turbulence intensity has on the heat transfer coefficient, and
- to determine the effect that the turbulence integral length scale has on the heat transfer coefficient.

CHAPTER 2

REVIEW OF LITERATURE

2.1 Heat Transfer of a Flat Plate in Cross-Flow

Flow over a flat plate has been studied for many years, however, it remains a topic of interest for many researchers [for example 4-7]. One reason for this is that solar panels can be approximated as flat plates with reasonable accuracy [8].

Heat transfer can be defined as thermal energy in transit due to a temperature difference. According to the second law of thermodynamics heat is transferred from a higher temperature body to a lower temperature body [9]. The three major heat transfer mechanisms are conduction, convection and radiation. The convection heat transfer is generally categorized in terms of being natural or forced. In forced convection, the fluid is forced to flow over a surface by external means such as a blower, or a fan. Forced convection heat transfer is calculated using Newton's law of cooling which states that the rate of heat transfer from a solid surface of area (A_s) at a temperature of T_s to a fluid at a temperature of T_∞ is [10]

$$Q_{convection} = hA_s (T_s - T_\infty) \quad (1)$$

where h ($W/m^2 \cdot °C$) is the convection heat transfer coefficient. The convection heat transfer coefficient is the rate of heat transfer between a solid surface and a fluid per unit surface area and per unit temperature difference.

When a Newtonian fluid is forced to flow over a solid surface that is nonporous, it is observed that the fluid in motion comes to a complete stop at the surface and assumes a zero velocity relative to the surface. Accordingly, a thin layer of fluid is generated near

the surface in which the velocity changes from zero at the surface to the free stream value some distance away from the surface (see Figure 2.1). This layer is called the boundary layer [11].

As can be seen in Figures 2.1 and 2.2, if the flat plate is long enough, the flow goes through the following stages starting with the leading edge [12]:

(1) Stable laminar flow following the leading edge.

(2) Laminar flow with two dimensional Tollmien-Schlichting waves.

(3) Development of unstable, laminar, three dimensional waves and vortex formation.

(4) Bursts of turbulence in places of very high local vorticity.

(5) Formation of turbulent spots in places when the turbulent velocity fluctuations are large.

(6) Coalescence of turbulent spots into fully developed turbulent boundary layer.

The convective heat transfer coefficient depends on:

(i) Surface geometry

(ii) Surface roughness

(iii) Type of fluid flow (laminar, transitional or turbulent). By increasing the fluid velocity (V), the convection heat transfer coefficient can be increased.

The convection heat transfer coefficient also depends on the fluid properties in the following manner:

(iv) By decreasing the dynamic viscosity (μ) of the fluid, convection heat transfer coefficient can be increased. The lower viscosity causes the fluid to move more freely thus transferring more heat.

(v) By increasing the thermal conduction of the flowing fluid, convection heat transfer coefficient can be increased. Increasing the thermal conduction between the surface and the fluid naturally causes an increase in the convection as well.

(vi) By increasing the specific heat (C_p), convection heat transfer coefficient can be increased.

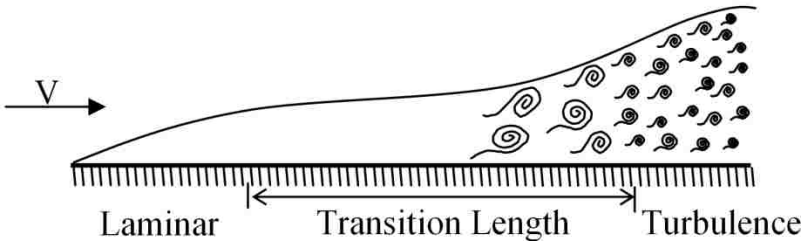

Figure 2.1: Flow over a flat plate.

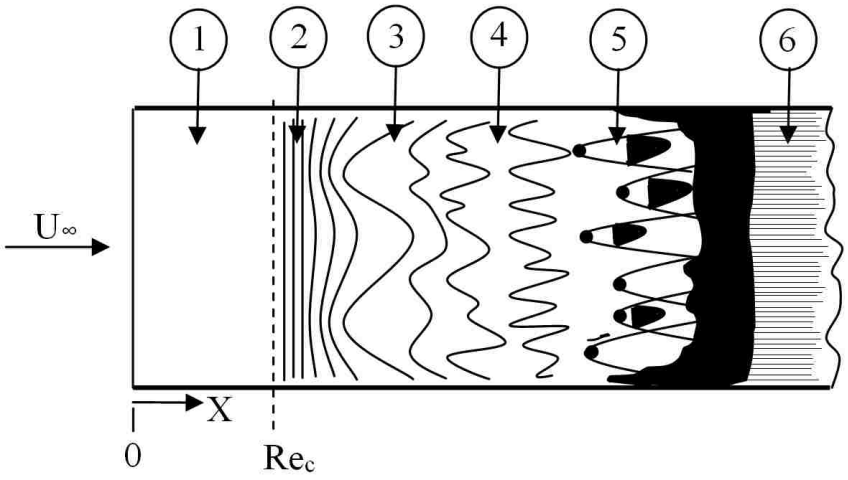

Figure 2.2: Transition from laminar to turbulent. Numbers correspond to stages described in text.

2.2 Fluid Flow Effects on Heat Transfer from a Flat Plate

The first step in the treatment of any convection problem is to determine whether the boundary layer is laminar or turbulent. Convection heat transfer rates depend strongly on which of these conditions exists [10]. The heat transfer from a flat plate occurs via convection, radiation, and conduction. For the present study, the effect of radiation and conduction on the top surface of the heated plate under study was negligible, leaving convection as the primary driver. The heat transfer problem can thus be characterized by the Nusselt number which is a function of the Reynolds number, turbulence intensity, and flow length scale, among many other parameters such as surface roughness etc. Nu = f(Re,Tu,Λ/L); where these parameters are defined as follows [11]

Nusselt number, $Nu = hL/k_{air}$

Reynolds number, $Re_L = UL/\nu$ and $Re_x = Ux/\nu$

Turbulence intensity, $Tu(\%) = (u_{rms}/U_{mean}) \times 100$

Turbulence length scale, $\Lambda = U_{mean}.\tau_{\Lambda}$

where u_{rms} is root mean square velocity, the Λ is the large integral length scale and the τ_{Λ} is the integral time scale.

2.3 Laminar Flow

In the case of photovoltaic panels, the heat transfer is neither a uniform temperature nor a uniform heat flux situation. Therefore both cases will be considered.

Incropera and DeWitt [13] expressed the Nusselt number for laminar forced convection flow over a flat plate as a function of Reynolds and Prandtl number as follows;

For Constant Surface Temperature

$$Nu_x = 0.332\ Re_x^{0.5}\ Pr^{1/3} \qquad \text{for } 0.6 < Pr \tag{2}$$

The average Nusselt number over the entire plate is expressed as

$$Nu_L = 0.664\ Re_L^{0.5}\ Pr^{1/3} \tag{3}$$

For Uniform Heat Flux

$$Nu_x = 0.453\ Re_x^{0.5}\ Pr^{1/3} \qquad \text{for } 0.6 < Pr \tag{4}$$

For this situation the average Nusselt number is expressed as

$$Nu_L = 0.680\ Re_L^{0.5}\ Pr^{1/3} \tag{5}$$

One of the earliest experimental studies of laminar forced convection was done by McAdams [14] on a 0.5 m^2 copper plate in a wind tunnel and subjected to a uniform heat flux. The resulted relation for heat transfer coefficient and Nusselt number from this study was:

$$h = 5.7 + 3.8V \qquad \text{for } V<5m/s \tag{6}$$

$$Nu = 0.085Re^{0.73} \tag{7}$$

Watmuff et al. [15] later claimed that the McAdams relation may include free convection and radiation effects too, so they modified the McAdams correlation into Equations (8) and (9):

$$h = 2.8 + 3.0V \qquad \text{for } V<5m/s \tag{8}$$

$$Nu = 0.024Re^{0.8} \tag{9}$$

Sparrow & Ramsey [16] studied laminar forced convection over small rectangular cassettes containing naphthalene in a wind tunnel. The cassettes had ratios of span-wise width to streamwise length of 0.4 and 2.5 and were placed in wind tunnel and subjected

to various air speeds and different attack angles. They proposed the following expression for heat transfer coefficient and Nusselt number in a Reynolds range of $2x10^4<Re<9x10^4$:

$$h = 4.96V^{1/2}L^{-1/2} \quad (10)$$

$$Nu = 0.75Re^{0.5} \quad (11)$$

where the characteristic length L, according to their study, is four times the plate area divided by the plate perimeter. There are many other studies on laminar convection flow over a flat plate. Some of the main experimental studies with a focus on the laminar heat transfer from a heated flat plate are summarized in Table 2.1. It is impossible to have a laminar wind flow under field conditions; therefore, all of the laminar studies are done in wind tunnel.

Table 2.1: Some studies on laminar heat transfer from a flat plate inside wind tunnel.

Author	Equation	Test condition	Main studied parameters
MacAdams [14]	$h = 5.7 + 3.8V$	0.5 m^2 copper plate Stands vertically $V<5$ m/s	Heat transfer coefficient versus flow velocity
Watmuff et al.[15]	$h = 2.8 + 3.0V$	$V<5$ m/s	Heat transfer coefficient versus flow velocity
Sparrow & Ramsey [16]	$h = 4.96V^{1/2}L^{-1/2}$ $L = \frac{4 \times \text{Plate area}}{\text{Plate perimeter}}$	Small rectangular cassettes $2x10^4<Re<9x10^4$	Geometry of plate, attack angle, Reynolds number of air
Lunde [17]	$h = 4.5 + 2.9V$	$V<5$ m/s	Heat transfer coefficient versus flow velocity
Sartori [18]	$h=3.83V^{0.5}L^{-0.5}$	Laminar solution coming from the boundary layer theory ($Re<4 \times 10^5$)	Heat transfer coefficient versus flow velocity

2.4 Turbulent Flow

The transition from laminar to turbulent flow does not occur suddenly; rather, it occurs over some region in which the flow hesitates between laminar and turbulent flows before it becomes fully turbulent (recall Figures 2.1 and 2.2). Transition from laminar to turbulent depends on many factors including:

- Surface geometry
- Surface roughness
- Free stream disturbance
- Temperature difference

In order for a flow to be turbulent it must possess the following characteristics:

- irregularity or randomness
- unsteadiness, fluctuating randomly in the spatial and time domains.
- must be dissipative, and highly vortical
- must be highly diffusive

The Reynolds number at which the flow becomes turbulent from laminar is called the "critical Reynolds number". This critical value differs for different geometries. For the current case, flow over a smooth flat plate, the generally accepted value of the critical Reynolds number is $Re_c = 5 \times 10^5$ [10]. Fluid motion in the turbulent flow is highly irregular and is characterized by velocity fluctuations. These fluctuations enhance the transfer of momentum, and energy, and hence increase convection heat transfer rates. The effect of the flow regime on convection heat transfer rate is shown in Figure 2.3 which is a drawing that shows how convection heat transfer coefficient (h_x) decreases with boundary layer thickness. Almost all flows in real engineering applications are turbulent in nature [19], thus making it imperative to study its characteristics and behavior.

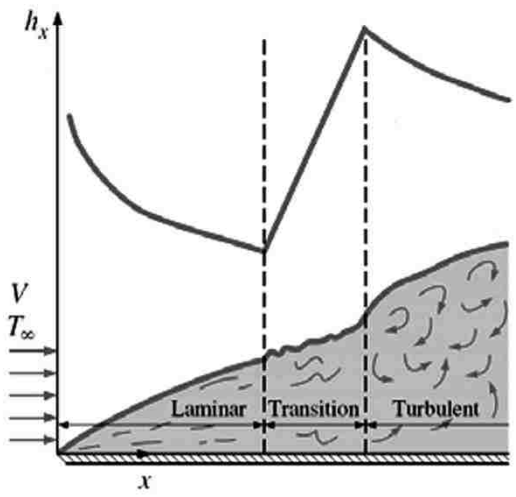

Figure 2.3: Effect of boundary layer thickness on the convection heat transfer coefficient.

For laminar flow, only the Reynolds number is required to characterize the flow. However in turbulent flow, in addition to the Reynolds number, there are many other parameters which categorize the flow as such; i.e. turbulence intensity (Tu), and length scale (Λ) are the two main ones. Incropera and DeWitt [13] proposed the following sets of equations for turbulent convection over a flat plate.

For Constant Surface Temperature

$$Nu_x = 0.0296\, Re_x^{4/5}\, Pr^{1/3} \qquad 5 \times 10^5 \leq Re_x \leq 10^7 \quad \text{and} \quad 0.6 \leq Pr \leq 60 \qquad (12)$$

where, the average Nusselt number for the whole plate is:

$$Nu_L = 0.037\, Re_L^{4/5}\, Pr^{1/3} \qquad (13)$$

For Uniform Heat Flux

$$Nu_x = 0.0308\, Re_x^{4/5}\, Pr^{1/3} \qquad 5 \times 10^5 \leq Re_x \leq 10^7 \quad \text{and} \quad 0.6 \leq Pr \leq 60 \qquad (14)$$

where, the average Nusselt number for the whole plate is:

$$Nu_L = 0.0385\, Re_L^{4/5}\, Pr^{1/3} \qquad (15)$$

2.5 Turbulence Intensity and Length Scale Effects on Heat Transfer

Hori & Junzo [20] studied the correlation of Nusselt number with turbulence intensity and integral length scale. Their experiments were conducted at Tu% range of 1 to 5 while the integral length scale was chosen to be 5 mm, 10 mm, 20 mm and 30 mm. This study indicates that at larger integral length scales the Nusselt number is more sensitive to turbulence intensity. With an increase of Tu% in 1 to 5 at an integral length scale of 5mm, the Nusselt number increases around 2%. However, the increase is more than 20% when the integral length scale is 30 mm. This is summarized in Figure 2.4. $Nu_{x,0G}$ is the local Nusselt number in the absence of the grid, i.e. no turbulence generator.

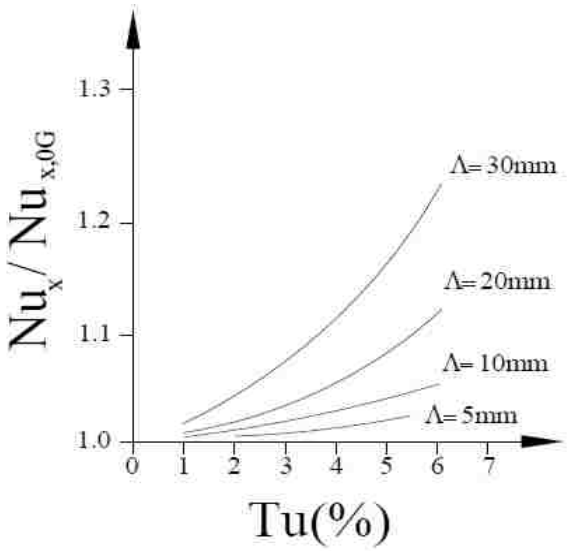

Figure 2.4: Effect of integral length on Nu-Tu relationship [20], $Re_x < 1.7 \times 10^6$.

They also studied the variation of Nusselt number ratio with turbulent Reynolds number Re_t and turbulence intensity Tu. The Re_t was defined as $Re_t = \sqrt{\overline{u'^2}}L/\upsilon$ in which u' and L are velocity fluctuations and characteristic length respectively. As is illustrated in

Figure 2.5, they depicted Nusselt number versus $Tu^{0.3}Re_t^{1.5} \times 10^{-4}$ and compared it with those of Blair [21] and Sugawara et al. [22].

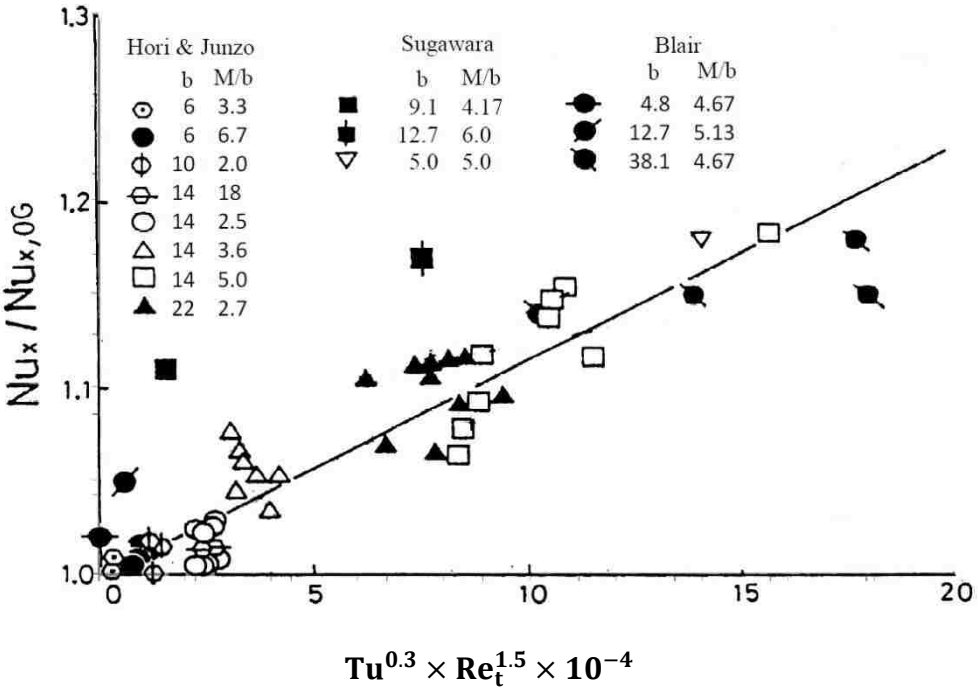

Figure 2.5: Nusselt number ratio versus turbulence intensity and turbulent Reynolds number [20].

The solid line indicates values calculated by the empirical equation $\frac{\mathrm{Nu_x}}{\mathrm{Nu_{x,0G}}} = 1.15 \times 10^{-6} \times \mathrm{Tu}^{0.3}\mathrm{Re_t}^{1.5} + 1$. This equation can be used for turbulence intensity up to Tu=5%. Applying the definition of turbulence intensity as $= \sqrt{\overline{u'^2}}/\mathrm{U}$, the $\mathrm{Re_t}$ can be replaced by $\mathrm{Tu} \times \mathrm{Re}$ where Re is the free stream Reynolds number. Therefore, the correlated equation can be rewritten as $\frac{\mathrm{Nu_x}}{\mathrm{Nu_{x,0G}}} = 1.15 \times 10^{-6} \times \mathrm{Tu}^{1.8}\mathrm{Re}^{1.5} + 1$. This three-variable function is depicted in Figure 2.6. As can be seen, at each constant turbulence intensity, the Nusselt number ratio increases with Reynolds number. Also, at each constant Reynolds number the Nusselt number ratio increases with turbulence intensity.

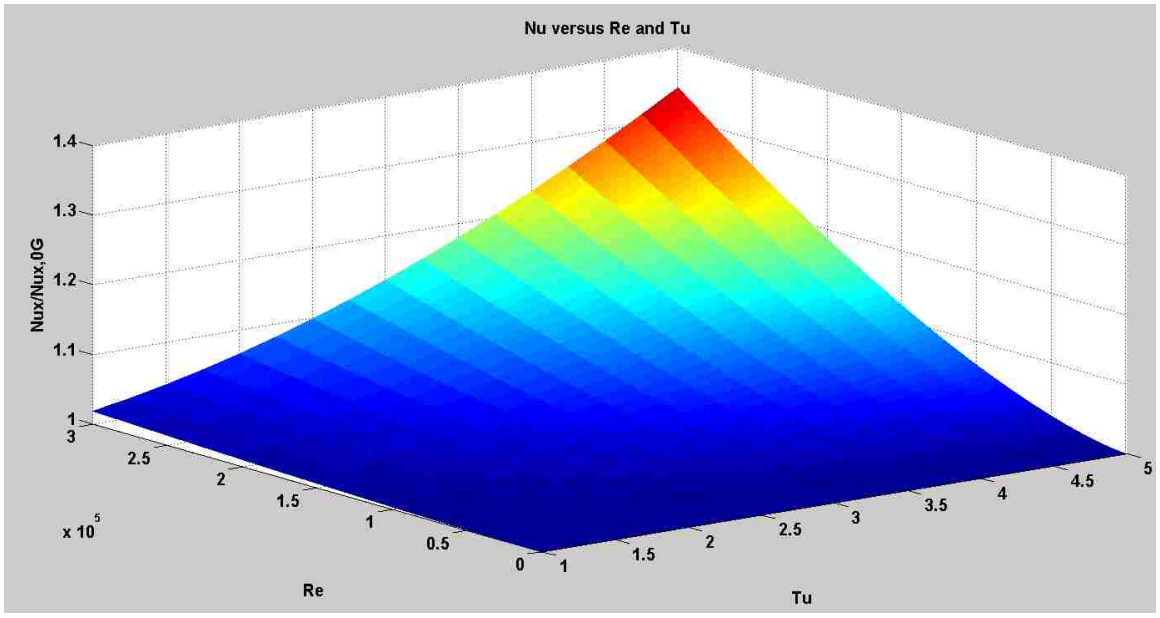

Figure 2.6: Nusselt number ratio versus turbulence intensity and free stream Reynolds number.

To clarify further, this three dimensional diagram is illustrated in Figure 2.7 in two-dimensional format at turbulence intensities of 2 and 4%.

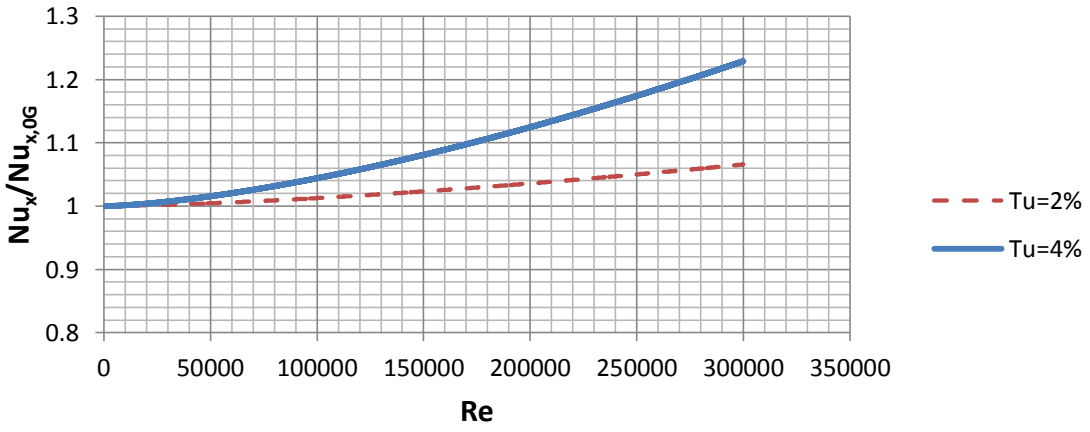

Figure 2.7: Nusselt number ratio versus free stream Reynolds number at Tu=2 and 4%.

Hubble & Pavlos [23] investigated the effects of turbulence intensity and integral length scales on heat transfer from boundary layer flow. They conducted their experiments in a

water tunnel. Kind et al. [24] worked on a heated plate in a wind tunnel at different angles, which was a 1:32 scale model of a single family residence roof mounted solar collector. The airflow was both shear and turbulent, and their results show that the sensitivity of the heat transfer coefficient to turbulence was low. Table 2.2 shows the heat transfer coefficient of a flat plate in turbulent flow from different studies. The turbulent case can be studied through field measurements as well as wind tunnel tests. Some of wind tunnel experiments and outdoor measurements which have been done on a flat plate in natural wind are included in this table.

Table 2.2: Wind tunnel and outdoor tests by various researchers focusing on the heat transfer from a flat plate via turbulent flow.

	Equation	**Test condition**	**Main studied parameter**
Wind Tunnel Tests			
Hori & Junzo [20]	$\frac{\mathrm{Nu_x}}{\mathrm{Nu_{x,0G}}} 1.15 \times 10^{-6} \mathrm{Tu}^{0.3} \mathrm{Re_t^{1.5}} + 1$	Uniform heat flux: 250 W/m^2 Average flow speed: 20m/s. $Tu^{0.3}Re_t^{1.5}$ changes in the range of 0-0.02. $R_t\sqrt{\overline{u'^2}}$ x integral length scale $/\nu$	Turbulent intensity and length scale
Sartori [18]	$h=5.74V^{0.8}L^{-0.2}$	Fully turbulent flow, solution coming from the boundary layer theory ($Re>4 \times 10^5$)	Heat transfer coefficient versus flow velocity
Outdoor Tests			
Test et al. [39]	h = 8.55 + 2.56V	1.22 m×0.81 m plate	Different wind velocity
Sturrock & Cole [40]	h = 11.4 + 5.7V	Flat plate solar collector	Different wind velocity
Sharples & Charlesworth [41]	h = 6.5+ 3.3V (for the wind parallel to the plate)	A 1.81 m×0.89 m flat plate solar collector with 35^o tilt angle	-Different wind velocity -Incident angle

Smith & Kuethe [25] performed experiments at free stream Reynolds number of 5×10^5 to determine the effect of turbulence on heat transfer from a flat plate. A grid turbulence up to 6% was imposed and as a result the heat transfer was increased approximately 30%. Colombo et al. [26] studied convection heat transfer over a ribbed flat plate to show the effects of the turbulence on the rate of heat transfer from the plate. Their results show that the heat transfer from the ribbed plate is much higher in comparison with the smooth one. This is attributed to the boundary layer regime which is more turbulent over the ribbed plate. Sanz et al. [27] studied the boundary layer transition over a flat tilted plate by means of heat transfer measurements. They define the dimensionless pressure gradient parameter as a shape factor K, ($K = -\frac{dP_{ext}}{dx} \times \frac{\delta}{\mu U_{ext}/\delta}$), where δ is the momentum boundary layer thickness, U_{ext} the external velocity, P_{ext} the pressure outside of the boundary layer and the x axis is parallel to the surface. They found that the critical Reynolds number increases exponentially with the pressure gradient parameter. Some researchers used a combination of experimental data and analytical solutions to study heat transfer over a heated flat plate. For instance, Li &Yan [28] used an inverse method to estimate the space- and time-dependent heat flux from the temperature measurements taken inside the flow. In the inverse method the conjugate gradient method is adopted for the estimation of the unknown wall heat flux. The problem was solved as an optimization problem which minimizes the summation of the square of the differences between the estimated dimensionless temperatures and the measured dimensionless temperatures. They showed that heat flux and temperature distribution over the flat plate. In addition, the variation of local Nusselt number along the plate was investigated.

In addition to these experimental efforts, some researchers used computational fluid dynamics CFD to study convection heat transfer over flat plate. For instance, Karava et al. [29] applied RANS turbulence model to examine wind flow over the roof surface of a low-rise building. They studied effects of turbulence intensity on convection heat transfer coefficient, and found a 40% increase in Nusselt number while the free stream turbulence intensity was increased from 19 to 35%. Turgut & Onur [30] conducted a three-dimensional numerical simulation to study turbulence effects on the convection heat transfer over a rectangular flat plate model collector, flush-mounted on the roof of a model residential house. They investigated heat transfer and fluid friction for hydrodynamically fully developed thermally developing three dimensional steady turbulent flow in a horizontal trapezoidal duct with constant surface. They showed that increasing the Reynolds number increases the Nusselt number and the thermal entrance region increases with an increase in the Reynolds number. They also presented new engineering correlations for the friction and heat transfer coefficients in the form of power law. Peneau et al. [31] conducted an LES simulation of flow over a flat heated plate at Re of 8×10^4. They changed the free stream turbulence intensity from 1.5 to 10% to examine the influence of free-stream turbulence on the development of boundary layer. Their simulations underscored the higher sensitivity of the thermal field to free-stream turbulence. There are many other CFD studies on flow over a heated flat plate in the literature including works by Garcia & Balenzategui [32], Juncu [33], Lioznov et al. [34], Wu [35], Kendoush [36], Campo [37], Ribando et al. [38]. All of these CFD observations confirmed significant effects of turbulence parameters on the rate of convection heat transfer from the flat plate.

Most of the equations presented in Tables 2.1 and 2.2 were developed for convection heat transfer coefficient in terms of velocity. However, the length of the plates they used in their experiments was not the same. Therefore these equations must be normalized with respect to plate length and fluid properties to make a comparison meaningful. Hence, the non-dimensional groups of Nu and Re are illustrated for these cases in Figure 2.8. The shaded areas represent the standard curve band for the laminar data points respectively.

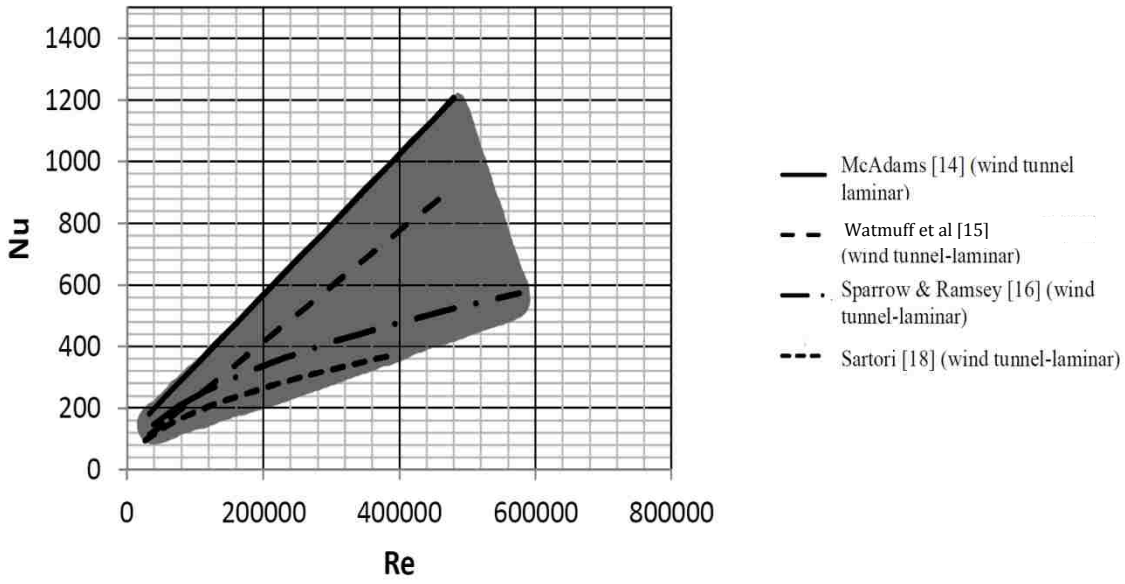

Figure 2.8: Comparison of Nusselt number in flow over a flat plate obtained by different sets of wind tunnel experiments.

CHAPTER 3

EXPERIMENTAL DETAILS

3.1 Wind Tunnel

The experiments in this study were conducted in a closed-loop wind tunnel as depicted in Figure 3.1. The cross section of this wind tunnel at the entrance is square with dimensions of 0.762 m by 0.762 m. The cross-sectional area increases gradually downstream to overcome the boundary layer phenomenon which builds up on the wind tunnel ceiling, floor, as well as the two side walls. Due to this gradual increase, the dimensions of the end portion of the working section are approximately 0.762m wide and 0.800m high. The maximum achievable mean velocity inside the wind tunnel is approximately 20 m/s and the turbulent intensity falls within 0.35% and 0.62% in the empty wind tunnel; in the absence of any turbulence generator.

Figure 3.1: Closed Looped Wind Tunnel.

3.2 Instruments

In the following sections all instruments used in the experimental part of current project including hot-wire, data acquisition system, traverse system, turbulence generators, pitot tube, variable voltage supplier, thermocouples, thermocouple toggle and heat flux sensors are respectively described.

3.2.1 Hotwire and Data Acquisition System

For flow velocity measurement, a 1D hot-wire probe (DANTEC type 55p15) was connected to a DANTEC Streamline 55C90 with a constant temperature hot-wire anemometer -CTA- Module. The output signal was sent to a desktop computer through a National Instrument ATMIO-16E-10 multifunction data acquisition board with a 12-bit resolution. The complete measuring system consists of the following:

Hot-wire probe 55P15, probe support 55H21, and 4-m BNC probe cable 9055A1863.

The Frame including two 55C90 CTA Modules contains a constant temperature anemometer, signal conditioner together with a calibration Module 90H10, controller, and power supply.

3.2.2 Traverse System

The 1 D hot-wire probe, together with the temperature probe, were mounted on a light-duty 2-D traversing system, as shown in Figure 3.2. The horizontal and vertical traverse lengths were 558 mm and 520 mm, respectively. The entire system was supported by a frame made of aluminum sheets. Two servomotors were responsible for the horizontal

and vertical motion. The traversing system works as either a fully 2-D system or only as a 1-D system with a spatial resolution of 0.0254 mm.

Figure 3.2: The light-duty 2-D traversing mechanism.

3.2.3 Turbulence Generator

Turbulence generation was obtained by using one of the three perforated plates with different hole diameters of 25.4 mm, 38.1 mm, and 50.8 mm all with the same solidity ratio of approximately 41%. The solidity ratio is defined as the ratio of the total area of the aluminum plate to the total hole area. These plates were made of aluminum, each with a thickness of 6 mm. The 50.8 mm perforated plate is shown in Figure 3.3. All holes have a chamfer of approximately 41°. The sharp edge of the plate faced the incoming flow, this is done to reduce the thickness effect of the plate on the turbulence structure. The plates were placed at various distances from the leading edge of the flat plate to achieve the desired turbulence intensity and integral length scale as detailed in Liu et al. [42].

Figure 3.3: Perforated plate used for the production of turbulence.

3.2.4 Pitot Static Tube

The free stream velocity in the wind tunnel was measured via a pitot-static tube, which was connected to a digital manometer (Dwyer series 475 mark II). The accuracy for the manometer is ±0.5% of the pressure reading and had a resolution of 0.0001 kPa. The operation range of this Pitot tube is between 249 Pa (1 inch water column) to 1034 kPa (150 psi).

The free stream speed was measured at the center of the test section close to the entrance of the wind tunnel. Approximately thirty seconds were needed to allow the manometer to stabilize, and after the pitot-static tube was removed from the wind tunnel to prevent its interference with the flow and the small opening in the wind tunnel was sealed.

3.2.5 Variable Voltage Supplier

A variable voltage supplier was used to supply the power needed to heat the flat plate (see Figure 3.4). It is capable of supplying power at different voltages ranging from 0 to 120V. In the current project the voltage was chosen to be 20 and 40V which corresponds to supplying power of 52 and 224W, respectively. The current corresponding to each case was 2.6 and 5.6 A, respectively. The resolution of this voltage supplier is about 4V.

Figure 3.4: Variable Voltage Supplier.

3.2.6 Thermocouple Readers and the Toggle Box

Figures 3.5 and 3.6 depict the equipment used to measure the temperature of the thermocouples. All 18 (Type T manufactured by Omega) thermocouples are wired into a toggle box as shown in Figure 3.6 and from the toggle there are connections for the thermocouple reader. The thermocouple readers were manufactured by Fluke (Model # 51 Series II). The reader has an accuracy of ± [0.05% + 0.3ºC] and a display resolution of 0.1ºC.

Figure 3.5: Thermocouple Reader.

Figure 3.6: Thermocouple Toggle.

3.2.7 Heat Flux Sensor

The heat flux sensor shown in Figure 3.7 was used to measure the heat coming through the top surface of the flat plate. The heat flux sensor is manufactured by Hukseflux, model PU-11, and has an accuracy of ±5% of the reading taken in millivolts.

Figure 3.7: Actual Heat Flux Sensor.

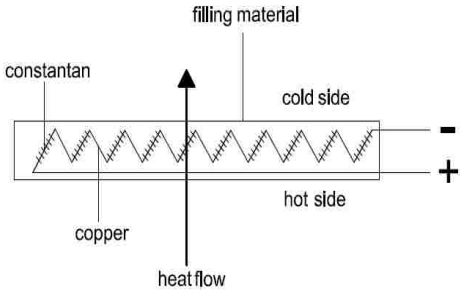

Figure 3.8: Heat Flux Sensor Schematic.

3.3 Flat Plate Setup

The installation of the flat plate on an inclining base made it possible to position the plate from 0° to 90° as shown in Figure 3.9. By tightening the bolts the plate was able to remain in its respective positions. The flat plate is heated by a 0.4572 m×0.3048 m flexible heater as shown in Figure 3.10. The total maximum power of the heater is 2160 Watts. The power input was controlled using a variable voltage transformer (see Figure 3.4). To reduce the bottom heat losses, a carbon fiber fabric was placed between the heater and the wood.

The flat plate that was used in this study was 0.52 m long by 0.34 m wide by 0.021 m thick (see Figure 3.11). The dimensions of the flat plate were restricted by the size of the wind tunnel. The surface of the flat plate was made from polished aluminum with a surface roughness of several nano-meters.

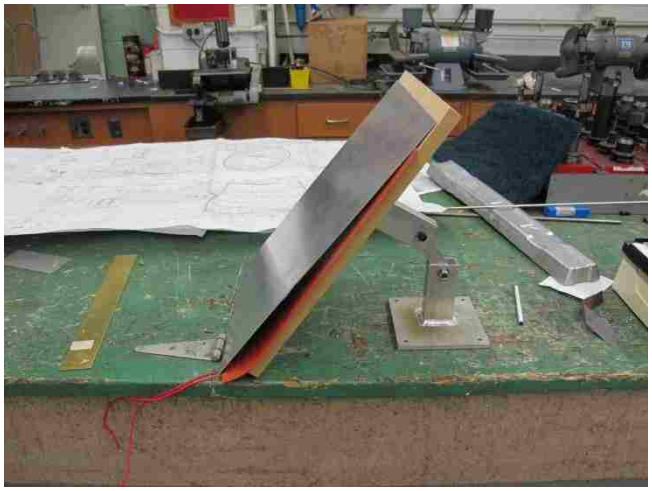

Figure 3.9: Inclining base where flat plate is installed.

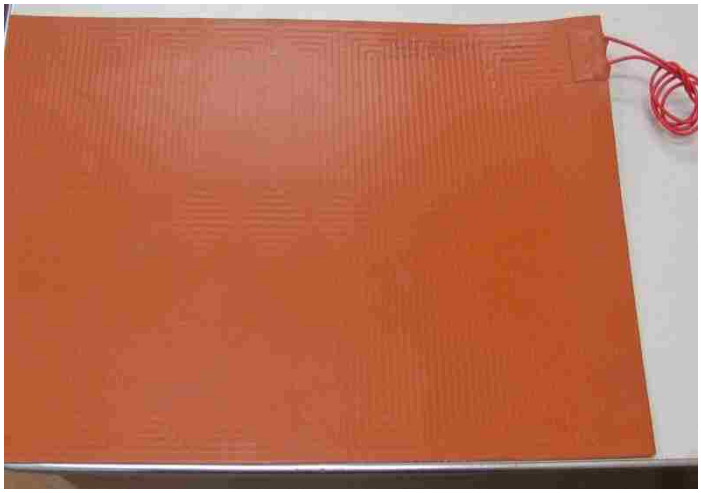

Figure 3.10: Flexible heater used to heat flat plate.

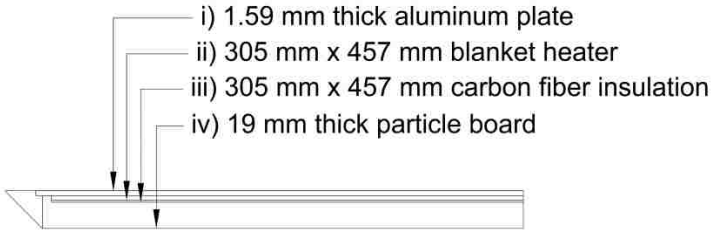

Figure 3.11: Schematic of the flat plate.

Figure 3.12 shows the thermocouple arrangement on the bottom of the aluminum surface. Each thermocouple is shown with $T_{x,z}$ in which x and z are the distance from the leading edge and the middle line in centimeter respectively. Negative values of z mean the thermocouples are located on the left hand side of the middle line. The values read from the thermocouples located on the middle line were used to determine the heat transfer coefficient h, i.e. $T_{3.5,0}, T_{7,-2}, T_{7,2}, T_{12,0}, T_{18,0}, T_{25,-2}, T_{25,2}, T_{32,0}, T_{37,0}, T_{40,-2}$ and $T_{40,2}$. The purpose of the other thermocouples was to observe the edge losses.

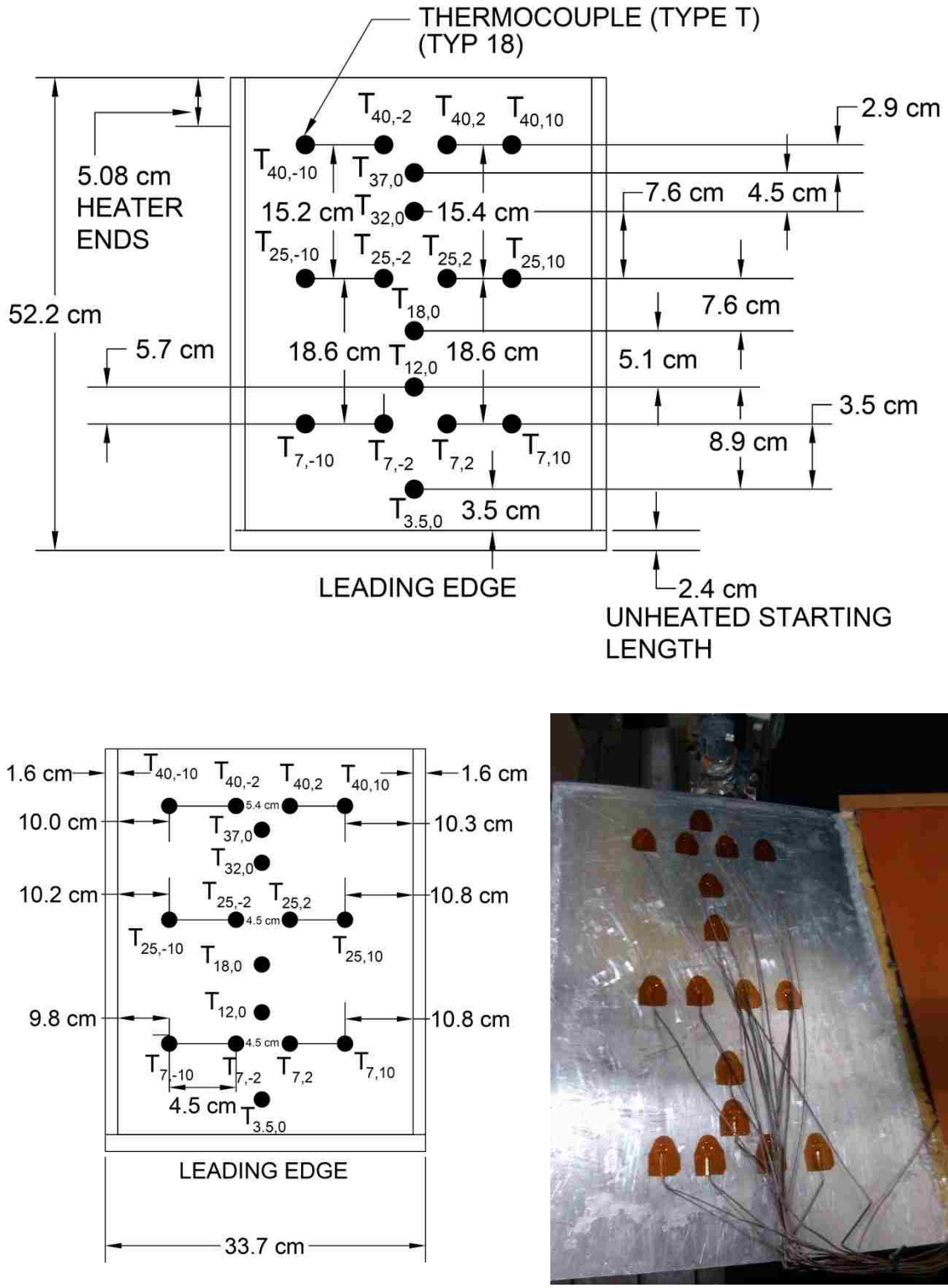

Figure 3.12: Top view of the thermocouple arrangement.

Figure 3.13 shows the data recorded at room temperature by thermocouples installed on the flat plate center line. It is observed that there is a difference of 0.3 ℃ in values recorded by different thermocouples.

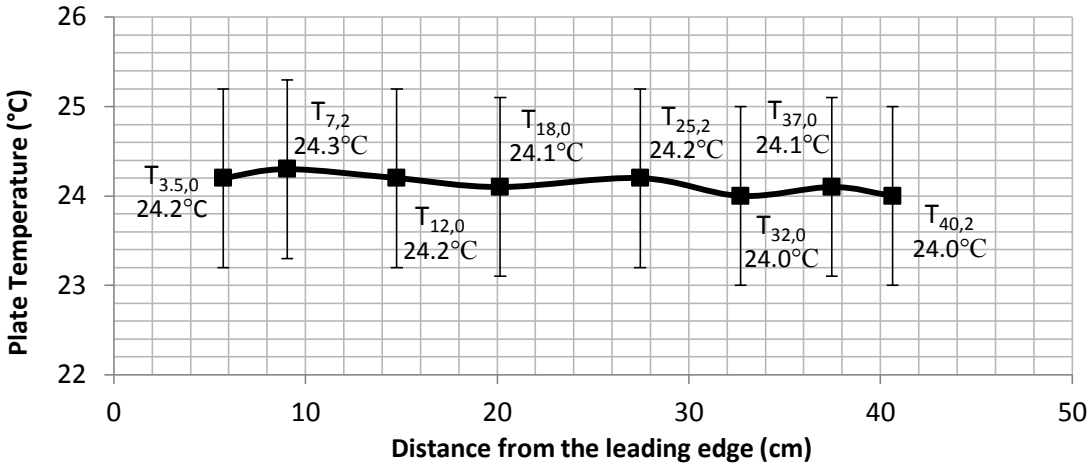

Figure 3.13: Temperature distribution at room temperature.

The flat plate was installed 32 cm from the bottom of the wind tunnel, approximately in the middle of the wind tunnel cross section (see Figure 3.14).

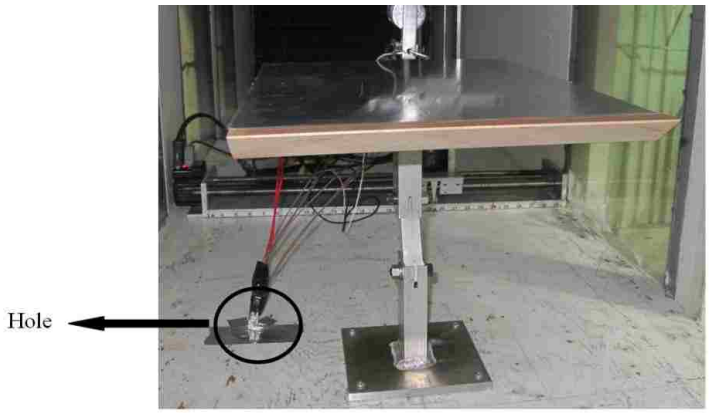

Figure 3.14: Front view of the flat plate installed in the wind tunnel (looking downstream).

Figure 3.15 shows a schematic of the orientation of the flat plate installed in the wind tunnel. Via a hole located at the bottom of the wind tunnel the power supply cord from the heater was allowed to exit the wind tunnel (as shown in Figure 3.14.) to be connected to the main power supply. Also in the same figure, the traverse system and hot wire can be seen behind and above the plate respectively.

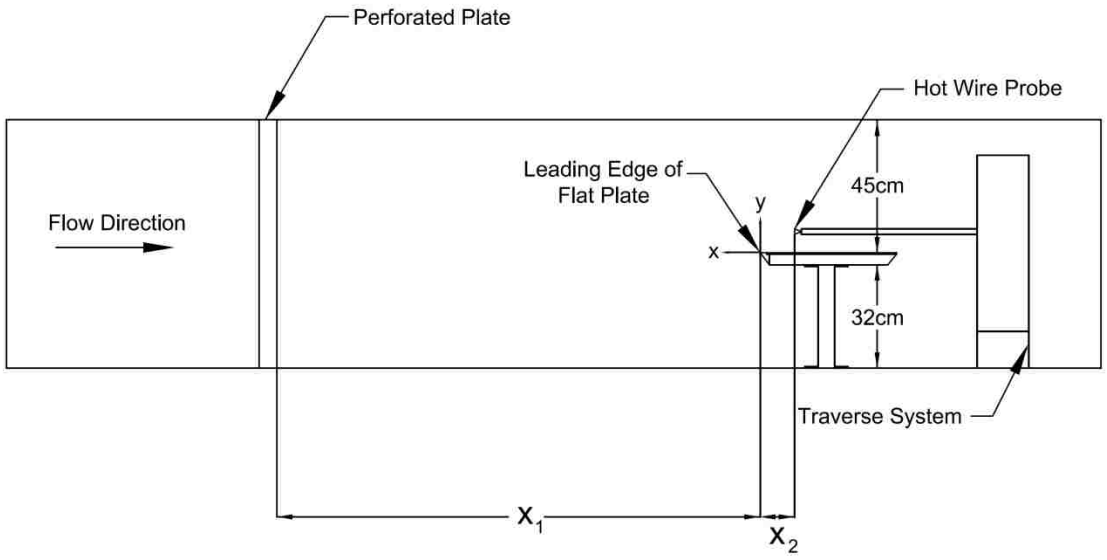

Figure 3.15: Wind tunnel configuration of the experimental setup.

3.4 Experimental Cases

Table 3.1 and Table 3.2 show the test matrix for both the laminar and turbulent case, as well as the operating conditions for both cases. During the test the air temperature varied between 24°C and 26°C. The tests for the laminar case were conducted at a background turbulence intensity of the empty wind tunnel of approximately. 0.5%. Tests were done by using voltages of 20 and 40 V which correspond to supplying powers of 52 and 224W

respectively to examine the effect of increasing the supplying power. It was concluded that using a higher voltage gives more accurate results as all measuring devices used perform within their tolerance range. However, the equipment used (more specifically the heat flux sensor) also limited the voltage that may be supplied, and 40 volts was the maximum that could be reached. The wind tunnel was capable of generating velocities from 1 m/s to approximately 20 m/s, however at velocities over 10 m/s there were rapid fluctuations in the thermocouple readers prohibiting accurate data.

Table 3.1: Operating conditions for laminar case.

Tu	**Inclination**	**Power**	**U_{air}**	**Re_x at 1st and last location on flat plate (5.71cm and 40.64cm)**	**# of Tests**
≈0.5%	0° 20°	52 W 224 W	4 m/s 6 m/s 8 m/s 10 m/s	13,290 and 92,603 20,210 and 142,069 29,264 and 208,137 34,029 and 242,027	16

Table 3.2: Operating conditions for turbulent case.

Tu	**Λ**	**Inclination**	**Power**	**U_{air}**	**Re_x at 1st and last location on flat plate (5.71cm and 40.64cm)**	**# of Tests**
4% 8% 12%	0.030 m 0.021 m 0.015 m	0° 20°	224 W	4 m/s 8 m/s	13,290 and 92,603 29,264 and 208,137	36

CHAPTER 4

DATA COLLECTION AND PROCESSING

4.1 Hot Wire Data Analysis

The DANTEC hot wire provided voltage values which are converted to flow velocities through the calibration equation. This equation is obtained from the calibration data. The fully computer-controlled calibration system consists of a calibration Module (DANTEC 90H10) and a separate flow unit where pressurized air (6 to 8 bars) enters through an external filter that filters away particles and oil. A precision regulator inside the Flow Unit ensures a stable input pressure to the Flow Control. The Flow Unit is able to set velocities from 0.5 m/s to 60 m/s through different nozzles. To calibrate the hot-wire probe, the probe is installed near the exit of a jet. The Flow Unit has a venturi nozzle which produces a low-turbulent air stream The probe is then exposed to a set of known velocities, U, and then records the voltages, E. The following polynomial curve fit represents the transfer function to be used when converting data records from voltages into velocities

$$U = C_0 + C_1E^1 + C_2E^2 + C_3E^3 + C_4E^4 \quad (1)$$

The acceptable curve errors are less than 1%. The constant coefficients of this equation (C_0, C_1, C_2, C_3, and C_4) are generated by the automated system. The voltage values E are also corrected by the system for temperature variations during the calibration and measurement.

The sample value of the time-averaged velocity (U) can be calculated by using

$$\overline{U} = \sum_{i=1}^{N} \frac{U_i}{N} \tag{2}$$

where N represents the number of times the hot wire repeats the reading, which was 10^7 with a sampling frequency of 80 kHz used in this experiment. The difference between the instantaneous velocity U and mean velocity $\overline{U}$ is the instantaneous fluctuating (u) value. The root mean square value for the velocity at any location is

$$u_{rms} = \sqrt{\sum_{i=1}^{N} \frac{(U_i - \overline{U})^2}{N-1}} \tag{3}$$

The relative turbulence intensity (Tu) is

$$Tu = 100\,x\,\frac{u_{rms}}{\overline{U}} \tag{4}$$

The integral length scale represents the scale of the energy-containing eddies. The magnitude of the integral length scale is largely dependent on the dimensions of the size of the holes and the spacing between them. It is evaluated from the area under the curve of the correlation function of the fluctuation velocity (u) value in the streamwise direction.

The integral time scale for discrete samples can be deduced from

$$\tau_\Lambda = \frac{\frac{1}{N-M}\sum_{i=1}^{N-M}(u_i u_{i+m})}{\frac{1}{N}\sum_{i=1}^{N} u_i^{\,2}} \tag{5}$$

Here M is the auto-correlation counting parameter which is an integer. It should be changed from 0 to N-1 in a numerical algorithm, which at each M a discrete time is being calculated as $M\Delta t$.

The value of τ_Λ in Figure 4.1 is a rough measure of the interval over which u(t) is correlated with itself.

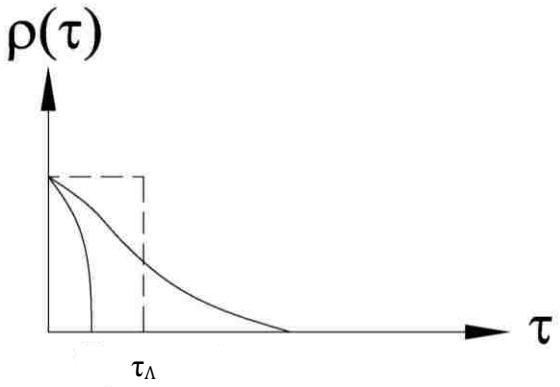

Figure 4.1: Integral and Taylor micro time scales

Then the integral length scale can be found by multiplying the integral time scale by the time averaged velocity.

$$\Lambda = \overline{U} \cdot \tau_\Lambda \tag{6}$$

4.2 Fluid Flow and Heat Transfer Data Processing

In the following section, all required equations to post process the both raw wind tunnel and field data are presented.

4.2.1 Data Processing for Wind Tunnel Experiments

In the current study, the Reynolds number defined as,

$$\mathrm{Re} = \frac{\bar{U}L}{\nu} \tag{7}$$

where the mean velocity, $\bar{U}$, was measured using a manometer and pitot static tube as described in Chapter 3, the total plate length L=0.52 m was measured using a ruler, and

the kinematic viscosity, ν = 18.27 x 10^{-6} m^2/s was determined at standard atmospheric pressure and temperature. The value for the kinematic viscosity was found from tables in reference [9].

The local Reynolds number is,

$$Re_x = \frac{\bar{U}x}{\nu} \tag{8}$$

where x is the distance from the leading edge to a point along the flat plate (Figure 3.12) and was measured using a ruler, and the kinematic viscosity, ν, was determined at standard atmospheric pressure at the film temperature, T_f. The film temperature is defined as,

$$T_f = \left[\frac{(T_{s,x} + T_\infty)}{2}\right] \tag{9}$$

where $T_{s,x}$ is the surface temperature of the flat plate, and T_∞ is the ambient temperature. The heat transfer due to convection can be expressed as,

$$Q_{conv} = h_x A_s (T_{s,x} - T_\infty) \tag{10}$$

where $T_{s,x}$ is the local surface temperature of the flat plate, T_∞ is the free stream temperature measured in the wind tunnel, A_s is the surface area, and h_x is the local heat transfer coefficient. The heat flux which is defined as,

$$\text{heat flux} = \left[\frac{Q_{conv}}{A_s}\right] \tag{11}$$

was measured using a heat flux sensor manufactured by Huskeflux (Model# PU-11).

The overall average heat transfer coefficient h_{avg} was calculated as,

$$h_{avg} = \left[\frac{\int_{x_1}^{x_8} h_x \, dA}{\int_{x_1}^{x_8} dA}\right] \quad (12)$$

After discretizing the above integration it becomes,

$$h_{avg} = \left[\frac{\sum_{i=1}^{N=8} h_i \Delta x_i}{\sum_{i=1}^{N=8} \Delta x_i}\right] \quad (13)$$

where Δx_i is the distance from thermocouple to thermocouple meant to represent length of influence of the thermocouple. The above equation is the average of the local heat transfer coefficients calculated along the plate.

In order to have a sense of the order of magnitude of the heat flux sensor and the heat transfer coefficient which was calculated using Equations 10 and 13, an energy balance equation that takes into consideration all the heat gains and heat losses was used. The energy balance can be written as,

$$Q_{total} = Q_{convection} + Q_{conduction} + Q_{radiation} \quad (14)$$

Figure 4.2 illustrates the input and output energies of the flat plate. At steady state condition, the incoming energy into the flat plate Q_{total} is equal to the energy which is transferred from the flat plate to the free stream through the convection $Q_{convection}$, conduction $Q_{conduction}$ and radiation $Q_{radiation}$.

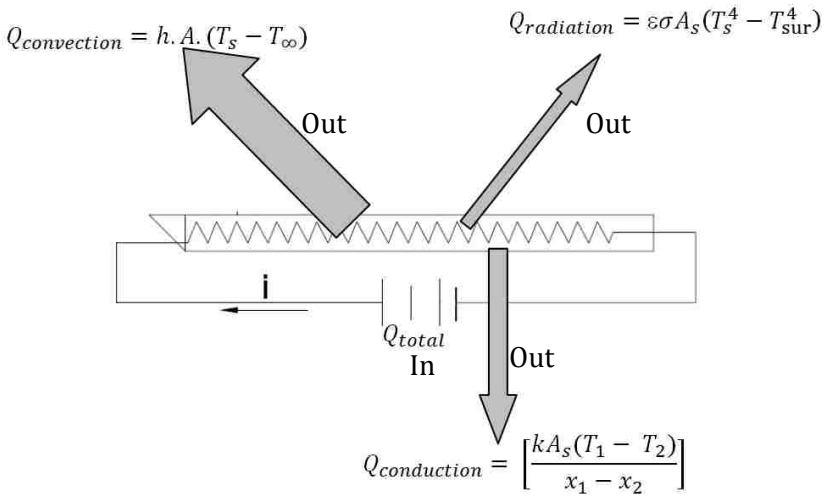

Figure 4.2: Schematic of heat balance on flat plate.

The loses by radiation to the surrounding air can be estimated as,

$$Q_{radiation} = \varepsilon\sigma A_s(T_s^4 - T_{sur}^4) \tag{15}$$

where ε is the emissivity of the polished aluminum surface, taken to be approximately 0.05 [11] and σ is the Stefan-Boltzmann constant (σ =5.67 x 10^{-8} W m^{-2} K^{-4}). It was assumed that $T_{sur} = T_\infty$. Finally, the losses by conduction can be estimated as,

$$Q_{conduction} = \left[\frac{kA_s(T_1 - T_2)}{x_1 - x_2}\right] \tag{16}$$

where k is the thermal conductivity of the particle board, T_1 and T_2 are the temperatures of the particle board at locations x_1 and x_2 respectively as shown in Figure 4.3.

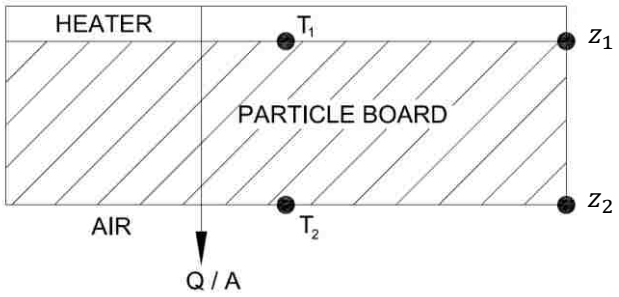

Figure 4.3: Heat transfer by conduction of the flat plate.

Subsequently, the effects of laminar and turbulent flows on the heat transfer from the flat plate were related by using the dimensionless form of the heat transfer coefficient which is the Nusselt number. The Nusselt number is defined as the ratio of heat transfer by convection over heat transfer by conduction under the same conditions and can be written as,

$$\mathrm{Nu} = \frac{\mathrm{Q_{conv}}}{\mathrm{Q_{cond}}} = \frac{\mathrm{hL}}{\mathrm{k_{air}}} \tag{17}$$

where k_{air} is the thermal conductivity of air and is determined at the film temperature with the use of tables in reference [9].

As an example, the convection heat transfer and the total incoming heat of the laminar flow at free stream velocity of 4 m/s are plotted in Figure 4.4 to show the conduction and radiation heat losses. The supplying power is of this case is 224W. Ramirez et al. [43] affirmed that the assumption uniform heat flux condition is reasonably valid in an interval of $\pm 10\%$ of the average convection heat flux. These margins are shown in Figure 4.4 using dashed lines. Therefore, according to the criterion defined by Ramirez et al. [43], for the most of the flat plate the convection heat flux can be considered uniform. As it is illustrated by the cross markers, just around the leading edge and trailing edge the

convection heat transfer cannot be considered a uniform heat flux case. The same condition was observed in all other cases.

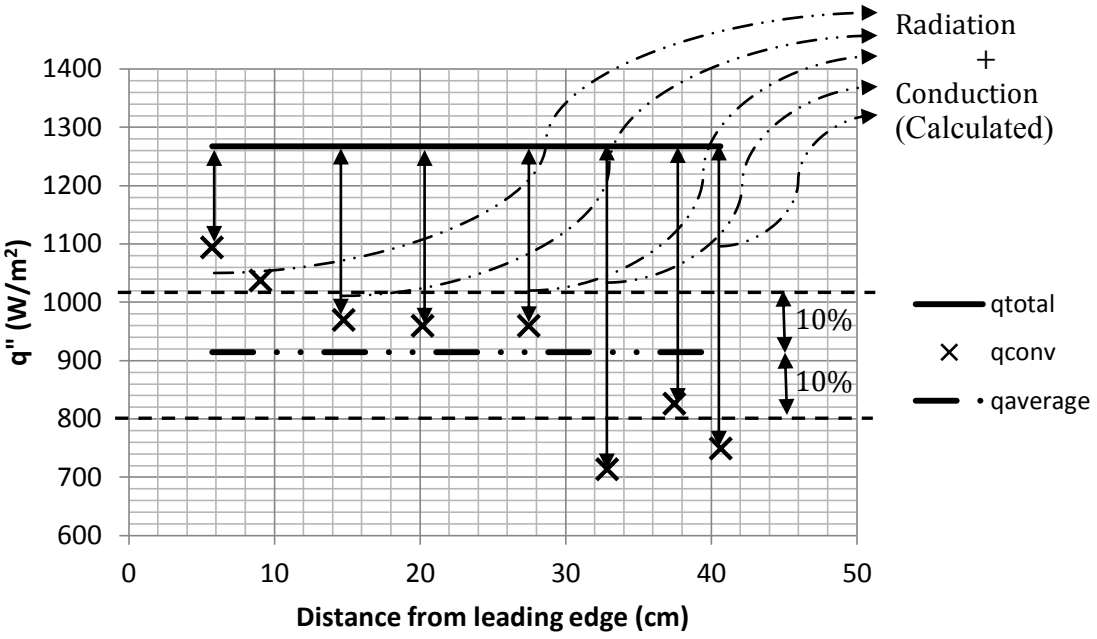

Figure 4.4: Heat flux losses due to radiation and conduction through the backside of the heated plate.

4.2.2 Data Processing for Field Solar Data

All fluid properties are chosen at the film temperature T_f. The film temperature is defined as,

$$T_f = \left[\frac{(T_c + T_a)}{2}\right] \tag{19}$$

where T_c, is the temperature of the solar panel, and T_a is the ambient temperature. The heat transfer on a solar panel can be expressed in a similar manner as the flat plate. The heat transfer due to convection is defined as,

$$Q_{conv} = hA_s(T_c - T_a) \tag{20}$$

And the loses by radiation to the surrounding bodies can be estimated as,

$$Q_{radiation} = \varepsilon\sigma A_s\left(T_{sky}^4 - T_a^4\right) \quad (21)$$

where ε is the emissivity of the glass surface, taken to be approximately 0.92 [9], σ is the Stefan-Boltzmann constant, and T_{sky} is the sky temperature. The sky temperature is estimated by using the following relation proposed by Evans & Florschuetz [44].

$$T_{sky} = 0.0552T_a^{1.5} \quad (22)$$

The sky temperature can also be estimated using the data found in Chapter 14 in the 2009 ASHRAE Fundamentals Handbook titled "Climatic Design Information" [45].

CHAPTER 5

RESULTS AND DISCUSSION

Results obtained for both laminar and turbulent cases are presented in this chapter. All tests were done at quasi-steady-state conditions. The following table shows an example of achieving the quasi-steady-state temperature distribution on the flat plate. This table corresponds to the laminar convection heat transfer at a free stream velocity of 6 m/s and supplying power of 224 Watts.

Table 5.1**:** Temperature time history recorded by the thermocouples.

Thermocouple, $T_{x,z}$	**Surface Temperature (°C)**				
	30 min	60min	90min	120min	150min
$\mathbf{T_{3.5,0}}$	52.2	53.8	54.0	54.1	54.3
$\mathbf{T_{7,-2}}$	51.8	53.3	53.6	53.5	53.7
$\mathbf{T_{7,2}}$	52.2	53.8	54.0	53.9	54.0
$\mathbf{T_{12,0}}$	53.9	55.6	55.9	55.8	55.9
$\mathbf{T_{18,0}}$	56.5	58.7	59.0	58.9	59.0
$\mathbf{T_{25,-2}}$	59.6	62.0	62.5	62.4	62.5
$\mathbf{T_{25,2}}$	59.4	62.0	62.5	62.4	62.5
$\mathbf{T_{32,0}}$	58.6	61.3	61.8	61.9	62.0
$\mathbf{T_{37,0}}$	61.3	64.6	65.1	65.4	65.4
$\mathbf{T_{40,-2}}$	55.0	57.8	58.3	58.4	58.5
$\mathbf{T_{40,2}}$	55.3	58.1	58.6	58.7	58.6
$\mathbf{T_{7,-10}}$	53.3	54.9	55.1	55.0	55.0
$\mathbf{T_{25,-10}}$	59.8	62.4	62.7	62.7	62.8
$\mathbf{T_{40,-10}}$	56.1	59.2	59.7	59.9	59.9
$\mathbf{T_{7,10}}$	53.6	55.2	55.5	55.3	55.3
$\mathbf{T_{25,10}}$	61.0	63.5	63.9	63.8	63.8
$\mathbf{T_{40,10}}$	59.3	62.0	62.5	62.5	62.3

As is seen, in first 90 minutes the temperature increased around 1.8 degrees, then in the next 30 minutes it decreases 0.1 degrees and in the last 30 minutes it increased only around 0.1 degrees which signifies that a steady state condition has been reached. Figure 5.1 displays the temperature time-history captured for thermocouple T18. Temperature increases with time and finally it reaches quasi-steady-state.

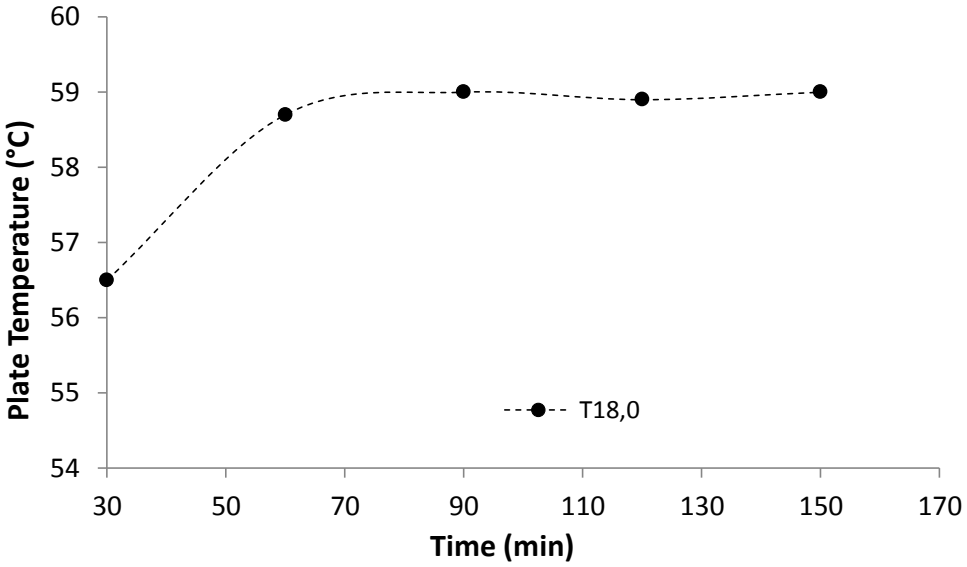

Figure 5.1: Quasi steady state recorded by thermocouple T_{18}.

5.1 Laminar Heat Transfer Over the Flat Plate

The laminar tests were done at tilt angles of 0° and 20°. These two configurations are respectively illustrated in Panels (a) and (b) of Figure 5.2. In each of these cases, the flat plate was heated by two different supplying powers of 52 and 224 W. Tests were conducted at free stream velocities of 4, 6, 8 and 10 m/s.

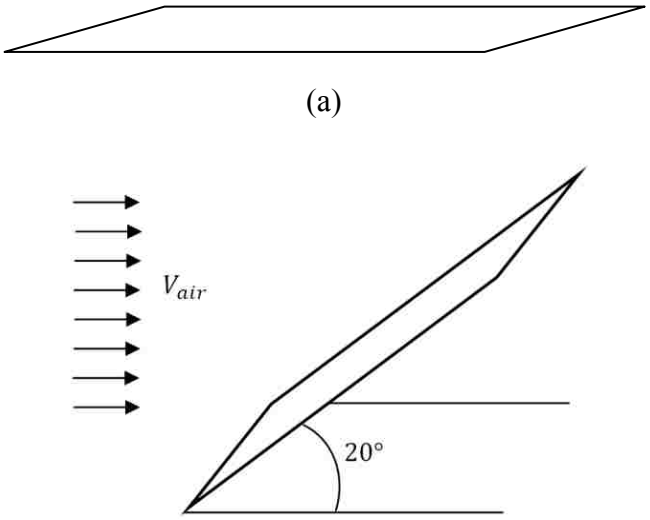

Figure 5.2: (a) Inclined angle of 0°, (b) Inclined angle of 20° with schematic stream-lines downstream of the plate .

Figures 5.3a and 5.3b illustrate the temperature distribution of the flat plate at a tilt angle of 0° for supplying powers of 52W and 224W respectively. The exact locations of the thermocouples are presented in Figure 5.3a. Figure 5.4 shows this distribution at an angle of 20°. As can be seen, in both tilt angles, the supplying power has no significant effect on the temperature distribution trend along the flat plate, i.e. the temperature along the plate increases as the distance from the leading edge increases and then starts to decrease as it approaches the end of the plate. It should be pointed out that the temperature increase from thermocouple number 6 (located around x=32.7 cm) to thermocouple

number 7 (located around x=37.15 cm) in Figures 5.3a and 5.3b may be due to the uncertainty of the sensors which are reported to be $\pm 0.5^{\circ}$ by the manufacturer. The temperature drop around the trailing edge is possibly due to the interference between flow and the power cord which is immediately after the trailing edge in the middle. It could be due to the difference between the length of the heater and the aluminum plate, i.e. the heater does not cover the total surface of the aluminum plate. As shown in Figure 5.5, there is an approximately 5.08 cm unheated distance which creates a negative gradient in the temperature of the aluminum surface close to the trailing edge due to conduction effect. To better clarify, an infrared photo was taken of the heated plate (see Figure 5.6) using a FLIR camera model T300. The unheated areas are clearly seen close to the edges of the plate.

(a)

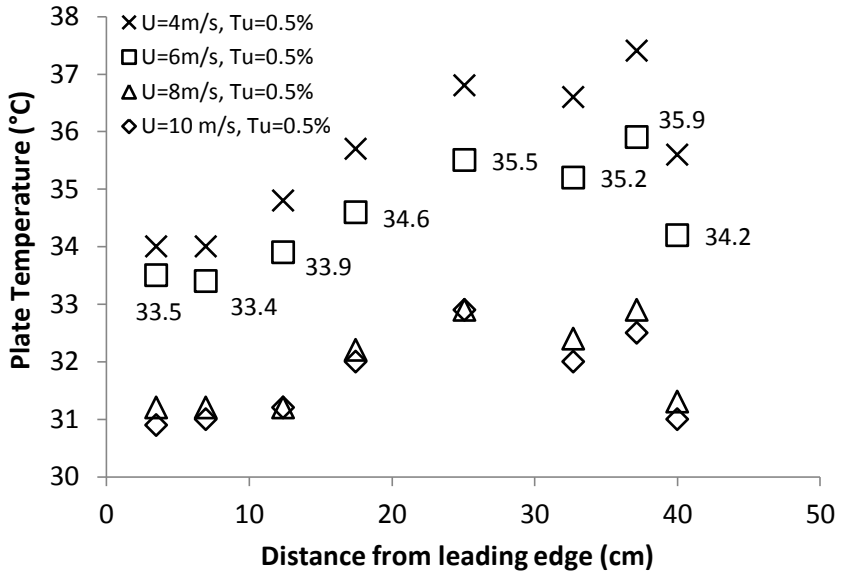

(b)

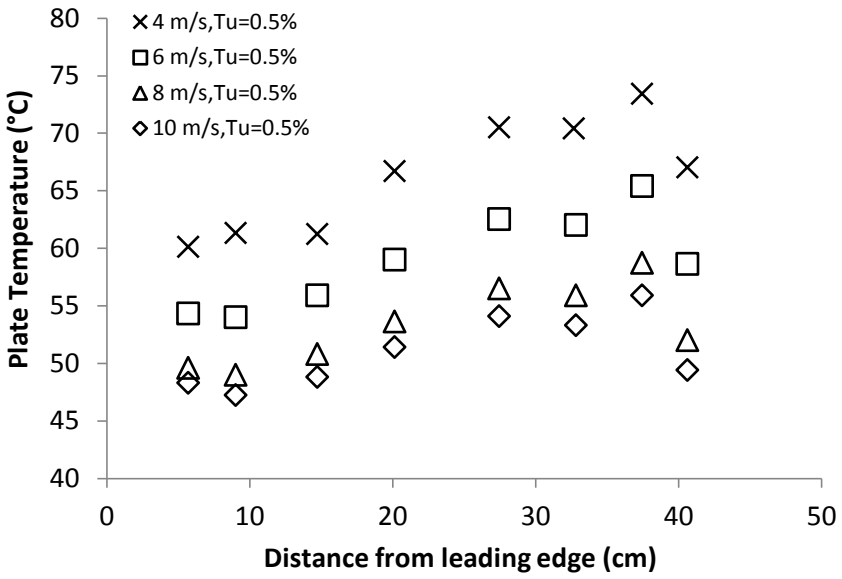

Figure 5.3: Flat plate temperature vs. distance from leading edge for tilt of 0°; (a) 52W, (b) 224W.

(a)

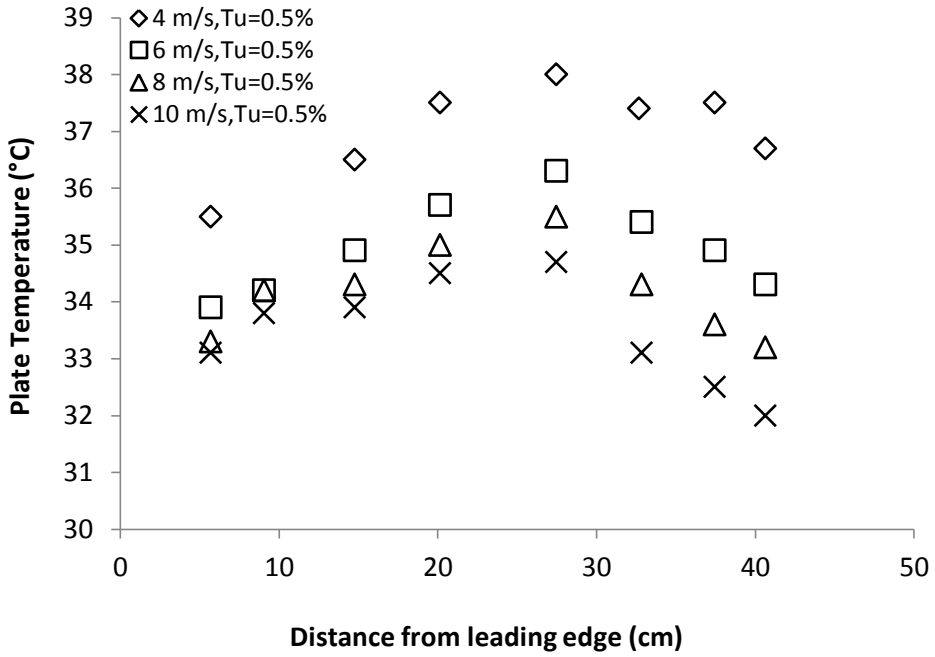

(b)

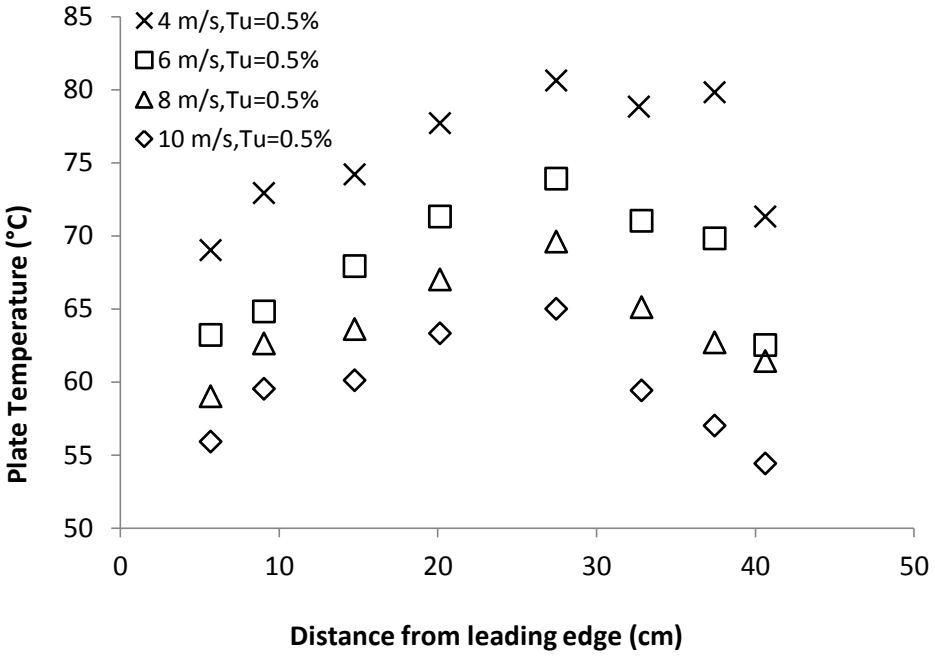

Figure 5.4: Flat plate temperature vs. distance from leading edge for tilt of 20°; (a) 52W, (b) 224W.

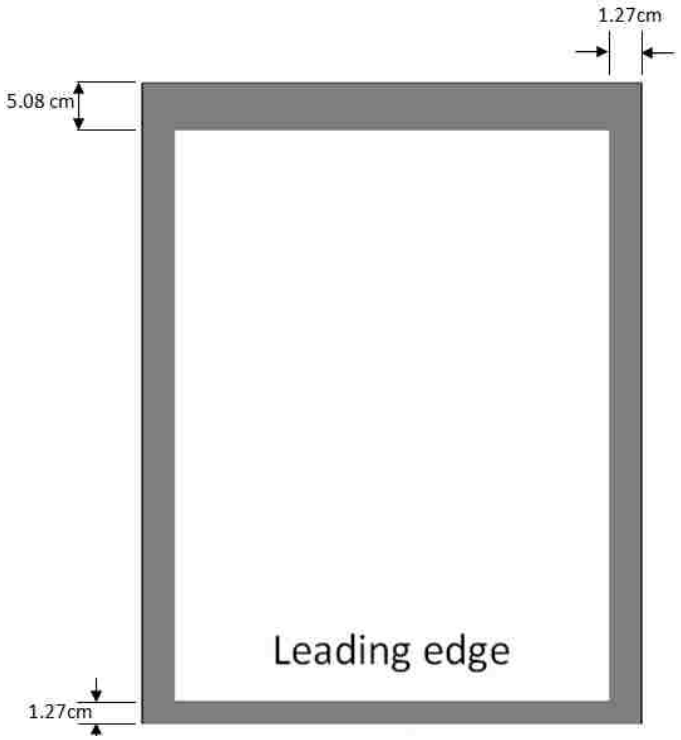

Figure 5.5: Top view of the flat plate, gray area shows the unheated surface of the flat plate. The middle white surface shows the heater.

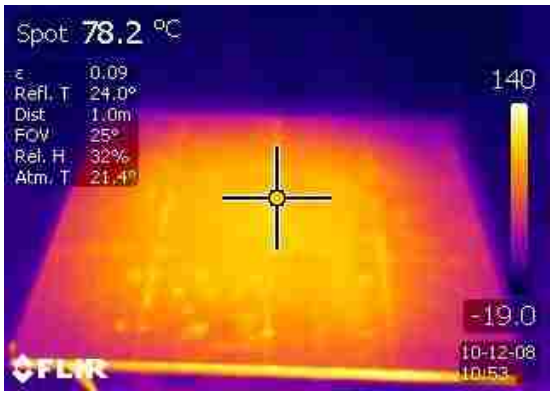

Figure 5.6: Photo of the heated plate taken by infrared camera.

Figure 5.7 depicts the local Nusselt number versus local Reynolds number at a tilt angle of 0° for supplying powers of 52 and 224 Watts. It is observed that in both wattages the

Nusselt number varies in the same range 50~430. Figure 5.8 shows the local Nusselt number versus local Reynolds number at a tilt angle of 20° for supplying powers of 52 and 224 Watts. In the ideal scenario the Nusselt number is a function of Reynolds number and the effect of free stream velocity is included in the Reynolds number. However, the present results indicate a variation of Nu with the free stream velocity. This variation is smaller for the supplying power of 224W compared to the case of 52W. For the tilt angle of 0°, the maximum variation is approximately 20 and 15% for the supplying powers of 52 and 224W, respectively. The percent of variation is calculated based on the highest value. For the tilt angle of 20°, the maximum percents of variations increased to approximate values of 49 and 43% for supplying powers of 52 and 224W, respectively. This can be attributed to the more uniform temperature distribution on the flat plate in higher supplying powers. In the current project, the supplier with variable voltage had the ability of increasing the incoming voltage up to 120V which provides a power of approximately 2000W. However, the heat flux sensor used could not stand temperatures more than 90°C, and at an input power of 224W, the maximum temperature of the flat plate surface was very close to 90°C.

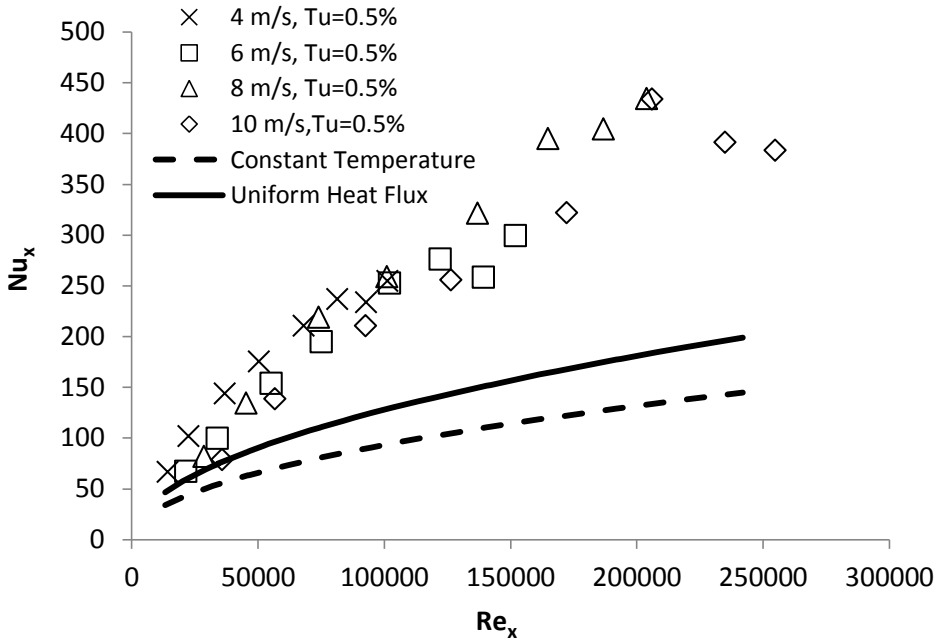

(a)

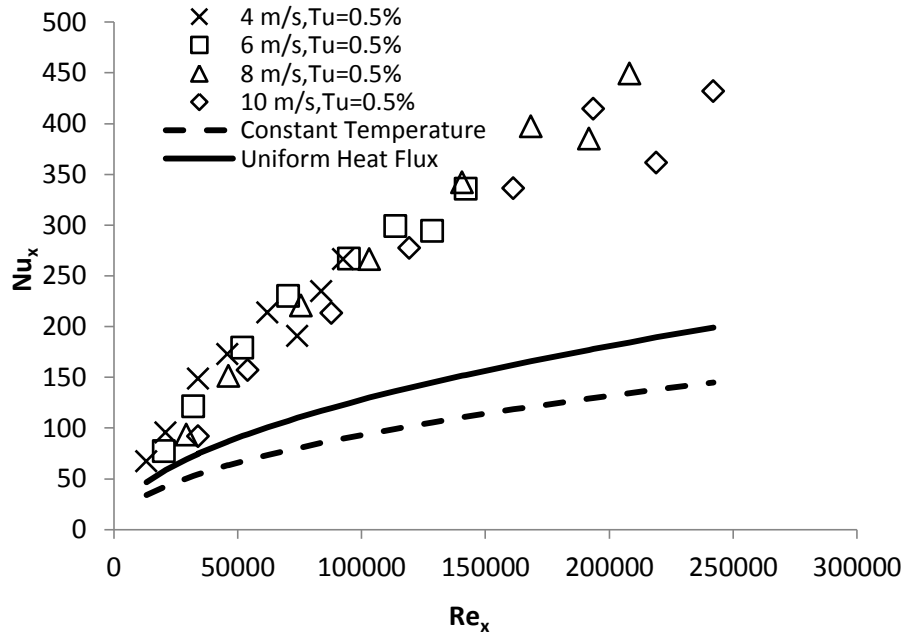

(b)

Figure 5.7: Nusselt number vs. Reynolds number for tilt of 0°; (a) 52W, (b) 224W. The presents results are compared with data reported by Cengel and Boles [10], solid line is for the case of uniform heat fux and dashed line represents the constant temperature case.

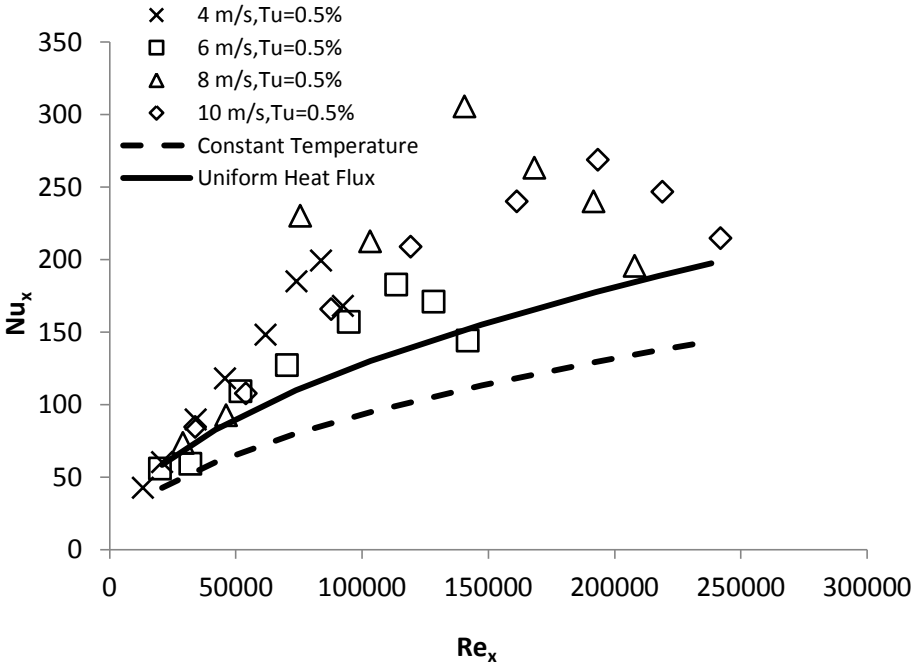

(a)

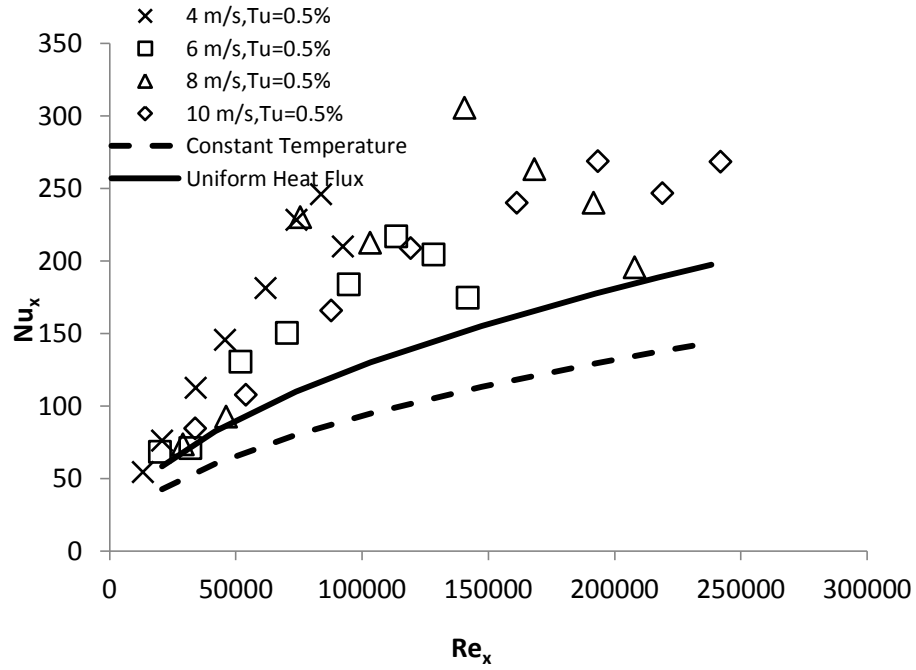

(b)

Figure 5.8: Nusselt number vs. Reynolds number for tilt of 20°; (a) 52W, (b) 224W. The presents results are compared with data reported by Cengel and Boles [10], solid line corresponds to uniform heat fux and dashed line represents the constant temperature for tilit angle of 0.

Data reported by Cengel and Boles [10] are also plotted in Figures 5.7 and 5.8. Dashed lines correspond to the constant surface temperature conditions and solid lines represent the uniform heat flux condition. It should be mentioned that in the current experimental work, none of these conditions are perfectly established. However, our conditions are closer to the uniform heat flux than constant temperature, with reference to Figure 4.4. It is observed that our Nu values are higher than those obtained based on the expressions of Cengel and Boles [10].

The convection heat transfer coefficient is depicted versus distance in Figures 5.9 and 5.10 for tilt angles of 0° and 20º respectively. It is observed that convection heat transfer coefficients decrease with distance from the leading edge. According to the definition of the convection heat transfer coefficient ($h = \frac{-k(\frac{\partial T}{\partial y})_{wall}}{T_s - T_\infty}$) and the sharp drop at the surface temperature close to the trailing edge observed in Figures 5.3 and 5.4, the convection heat transfer decreases at a higher rate around the trailing edge for the 20° tilt. The other point which is observed in both Figures 5.9 and 5.10 is the jump in the local convection heat transfer coefficient with increasing free stream velocity from 4 to 6 m/s.

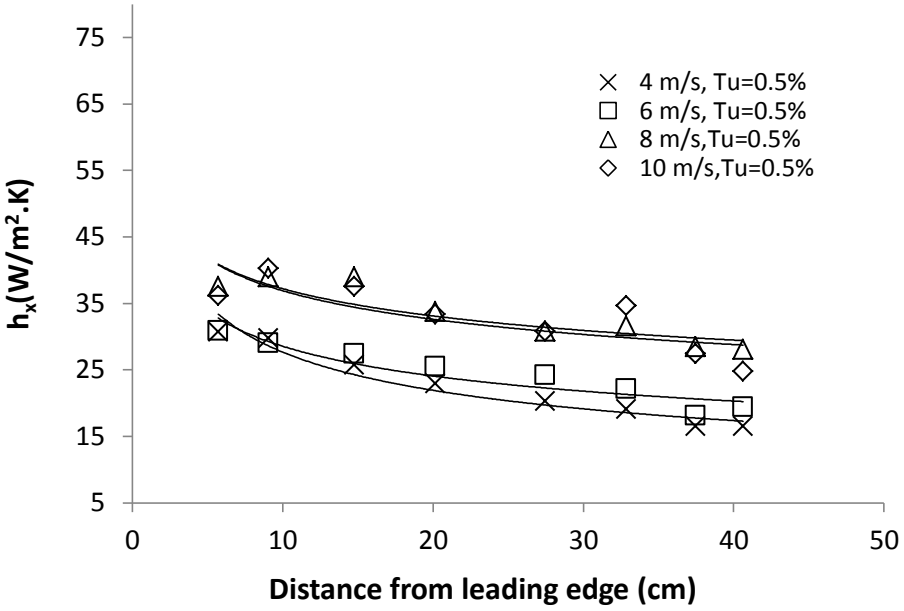

(a)

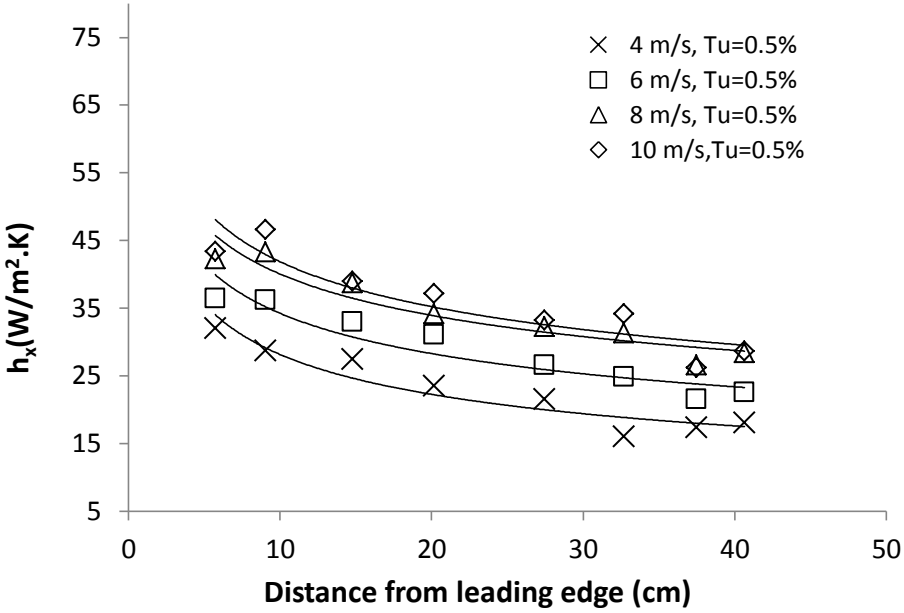

(b)

Figure 5.9: Local heat transfer coefficient vs. distance for tilt of 0°; (a) 52W, (b) 224W.

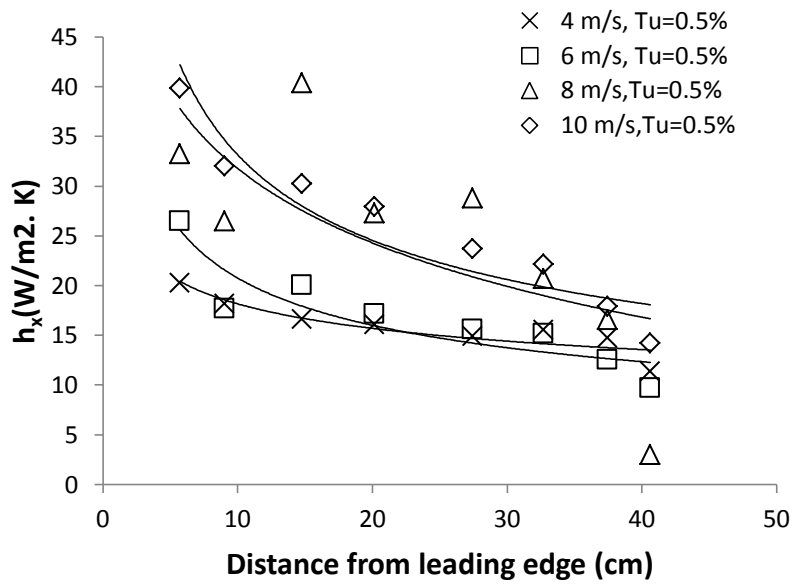

(a)

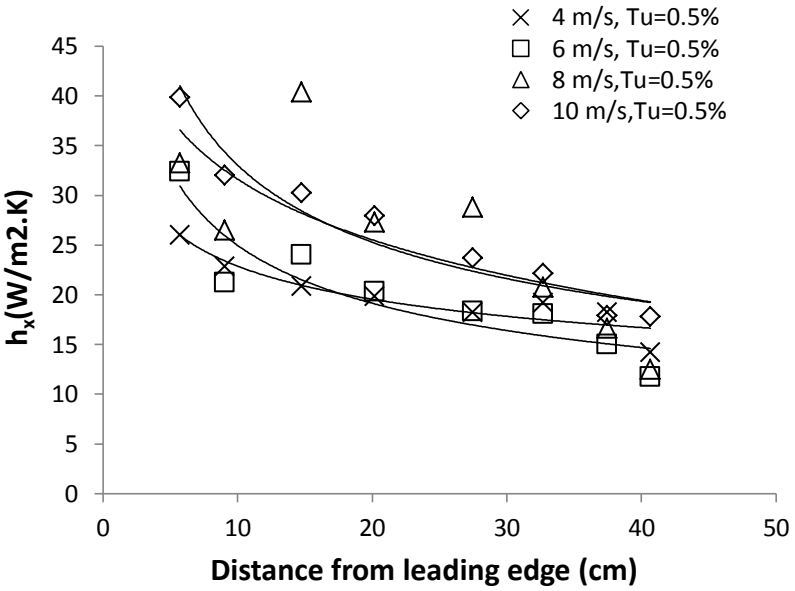

(b)

Figure 5.10: Local heat transfer coefficient vs. distance for tilt of 20°; (a) 52W, (b) 224W.

5.2 Turbulent Heat Transfer Over the Flat Plate

The effects of turbulence on the convection heat transfer were investigated through conducting separate experiments at three different turbulence intensities Tu=4.0%, 8.0% and 12.0% all at an integral length scale of 0.015 m. Then, all of these tests were repeated for two more integral length scales of 0.021 m and 0.030 m to realize how length scale affects convection heat transfer. All of the turbulent tests were done at a supplying power of 224W. Since this wattage produced a total heat flux of approximately 1267 W/m^2, which was very close to what a PV panel is exposed to in the field, it was deemed as a good choice.

5.2.1 Integral Length Scale of 0.015 m

Figure 5.11 illustrates a temperature distribution at a free stream velocity of 8 m/s. Panels (a) and (b) correspond to tilt angles of 0° and 20° respectively. It is observed that in both tilt angles, the local temperature decreases with turbulence intensity, i.e. better cooling. Figure 5.12 confirms this fact at a free stream velocity of 4 m/s. The other point which is realized from Figures 5.11 and 5.12 is that temperature continuously increases in the horizontal case, while in the case of tilt=20° there is a decrease around x=30 cm. This can be attributed to the flow separation.

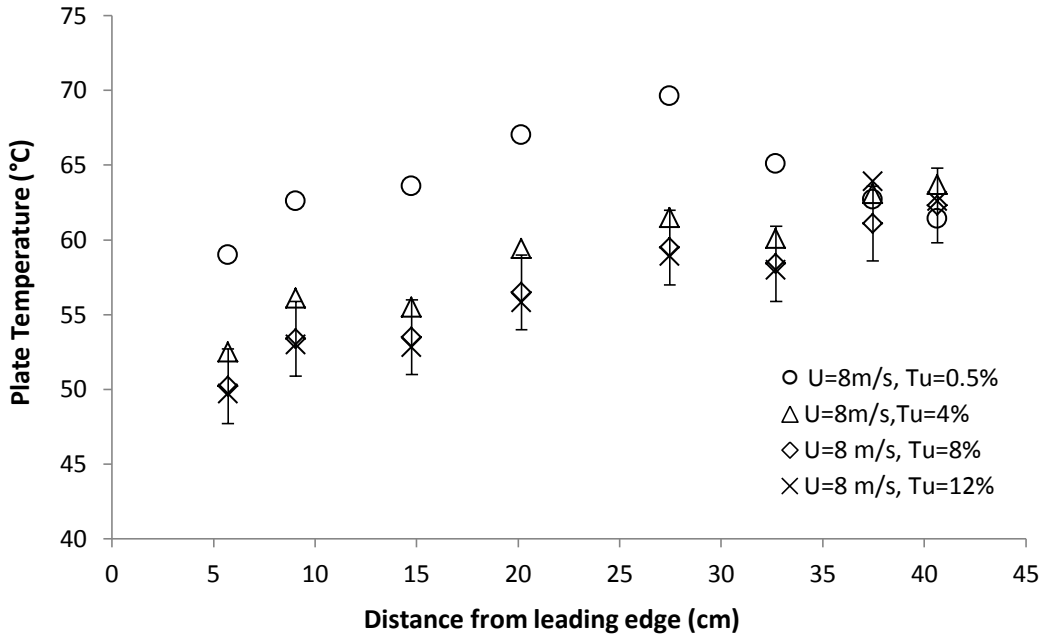

(a)

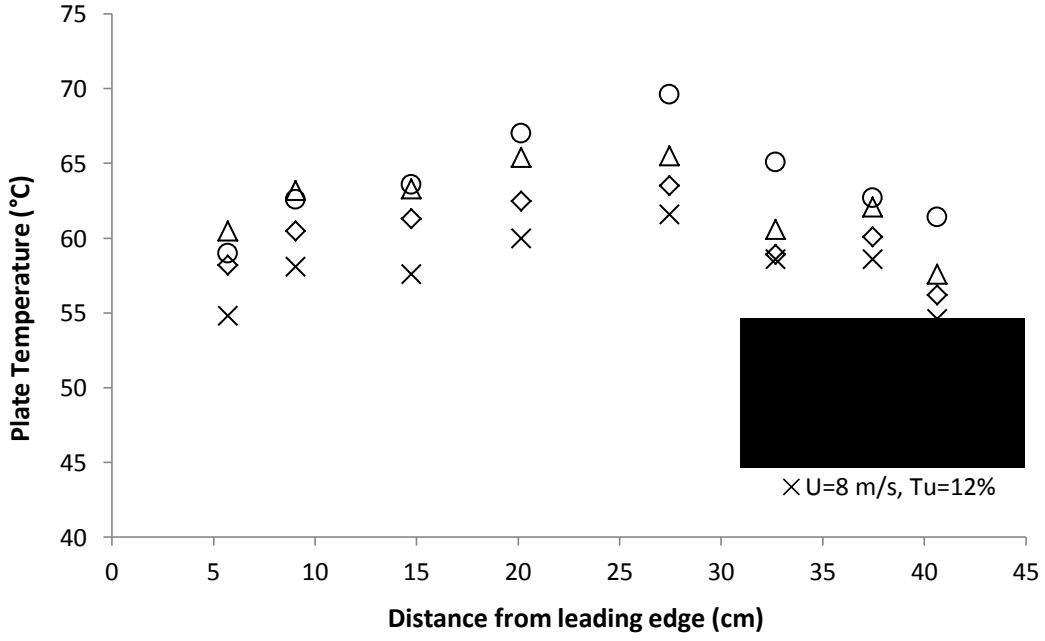

(b)

Figure 5.11: Flat plate temperature vs. distance from leading edge at free stream velocity of 8m/s and integral length scale of 0.015m; (a) tilt of 0°, (b) tilt of 20°.

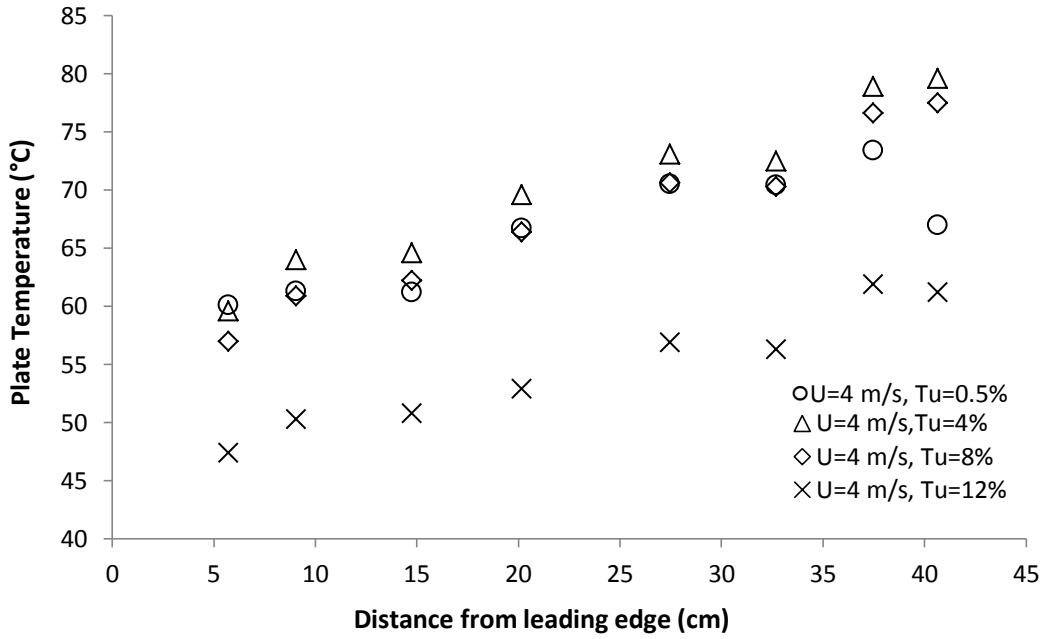

(a)

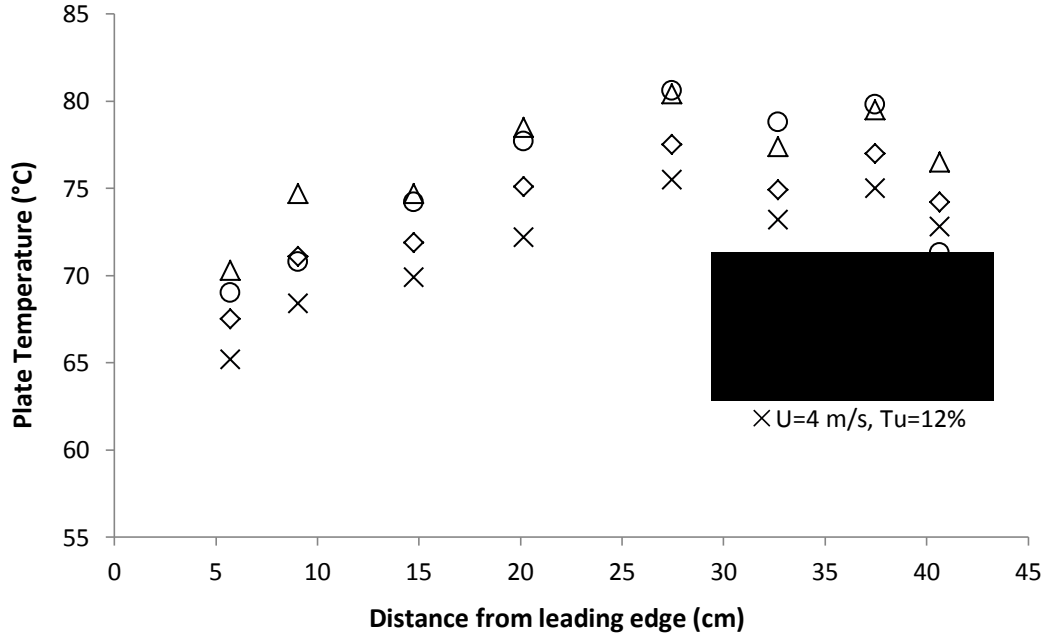

(b)

Figure 5.12: Flat plate temperature vs. distance from leading edge at free stream velocity of 4m/s and integral length scale of 0.015m; (a) tilt of 0°, (b) tilt of 20°.

Figures 5.13 and 5.14 respectively show the local heat transfer coefficient versus location for free stream velocities of 8 and 4 m/s. It is observed that the convection heat transfer coefficient continuously decreases along the plate; however, it goes down with higher rate close to the end of the plate. This is due to the approximately 5.08 cm (2 inch) unheated distance which creates a negative gradient in the temperature close to the trailing edge. The other major point that emerges from these diagrams is the increase of the convection heat transfer coefficient with the turbulence intensity for both horizontal and tilted cases. However, this increase appears to be more significant for the horizontal case. By comparing Figures. 5.13 and 5.14 it is observed that at tilt angle of 0° the turbulence intensity is more effective at lower free stream velocity. For instance, for the horizontal flat plate, while turbulence intensity goes from 4 to 12%, the local heat transfer coefficient increases approximately 80 and 10% for the free stream velocities of 4 and 8 m/s, respectively.

Figures 5.15 and 5.16 depict local Nusselt number versus local Reynolds number at free stream velocities of 8 m/s and 4 m/s respectively. As shown, the local Nusselt number increases with the local Reynolds number along the plate, however, there is a decrease close to the end of the flat plate. This decrease corresponds to the huge drop at the end of the heat transfer coefficient diagram, which is due to the unheated area close to the trailing edge.

The other significant point which is understood from Figure 5.15 and Figure 5.16 is the relatively great difference in the Nu value which corresponds to the tilt angles of 0° and 20°. It is observed that in the case of tilt=0°, Nu is higher and there is better cooling. Thus, strictly for the topic of cooling, it would be concluded that the horizontal case

would be a better choice for PV panels. However, the best tilt angle to obtain the optimum efficiency is dependent on many other parameters including snow shedding. For example, adjusting the panels to a steeper angle in the winter makes it more likely that they will shed snow; a panel covered in snow produces little or no power (See Appendix D for more information regarding effects of snow build up on the PV panels). By putting all effective parameters together, articles on solar energy often give the advice that the tilt should be equal to the latitude, plus 15 degrees in winter or minus 15 degrees in summer [46-53].

(a)

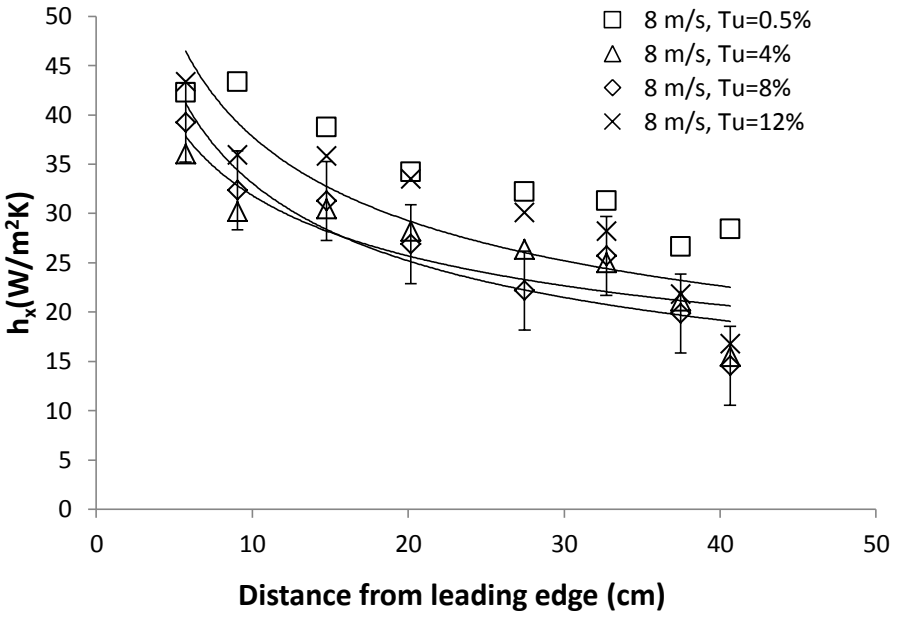

(b)

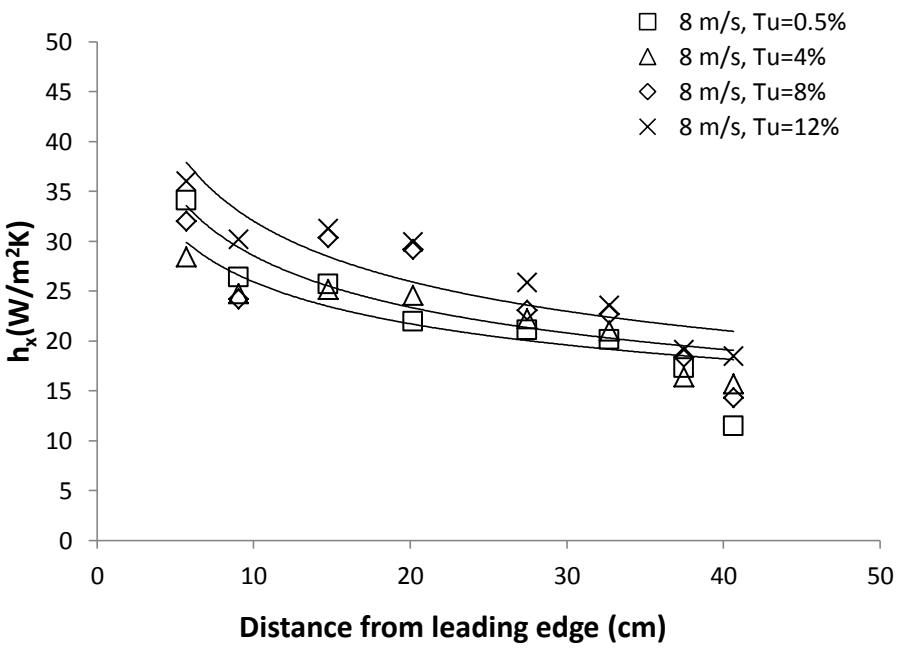

Figure 5.13: Local heat transfer coefficient vs. distance at free stream velocity of 8 m/s and integral length scale of 0.015m; (a) tilt of 0°, (b) tilt of 20°.

(a)

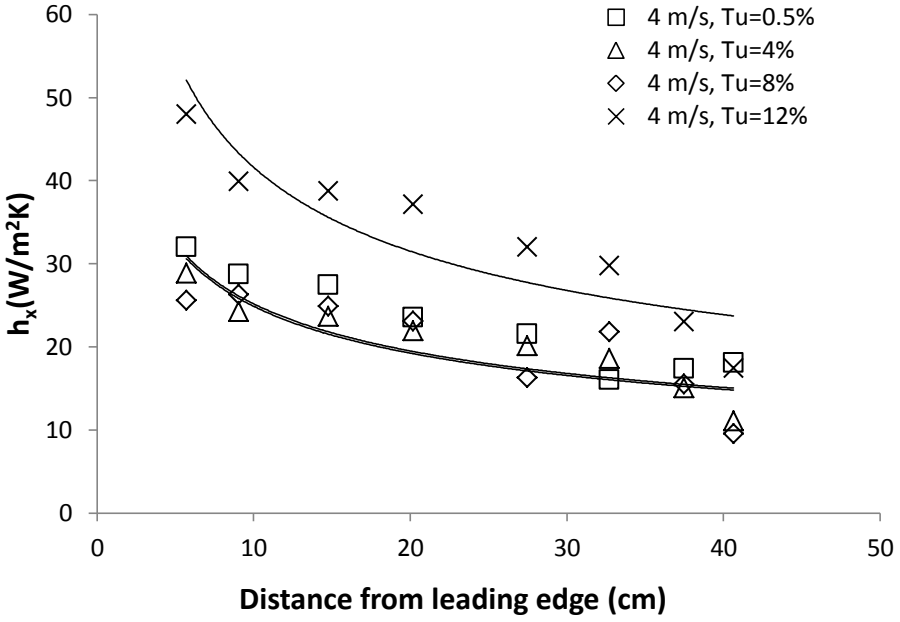

(b)

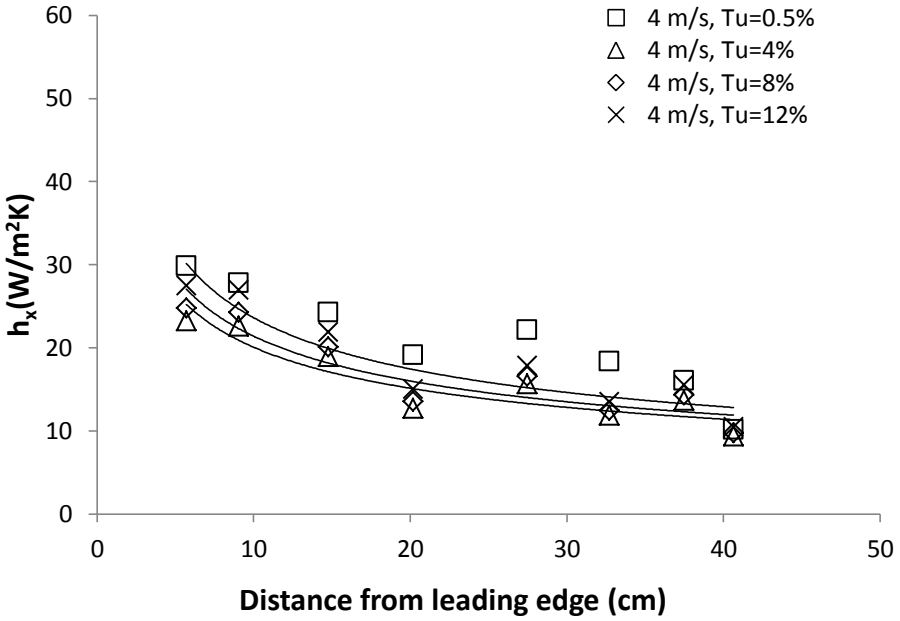

Figure 5.14: Local heat transfer coefficient vs. distance at free stream velocity of 4 m/s and integral length scale of 0.0150m; (a) tilt of 0°, (b) tilt of 20°.

(a)

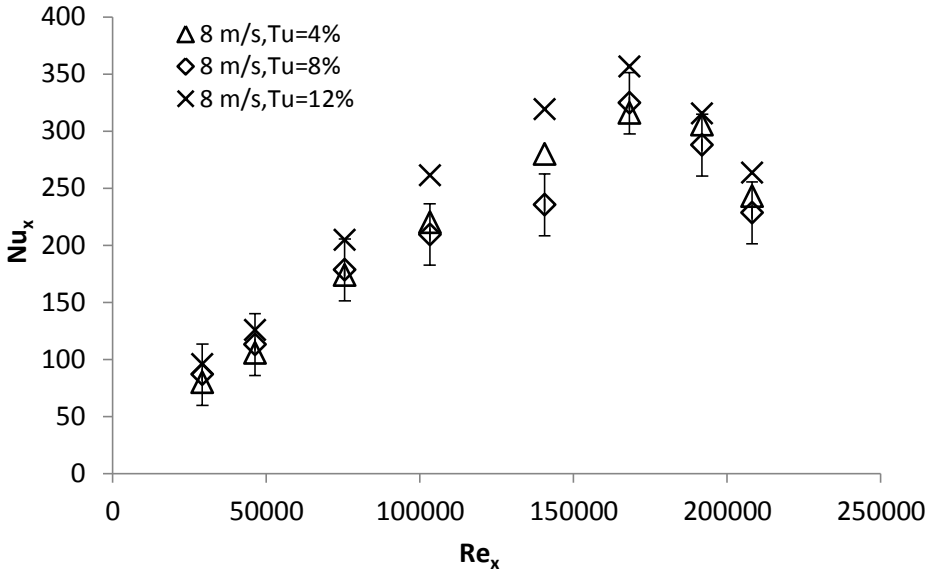

(b)

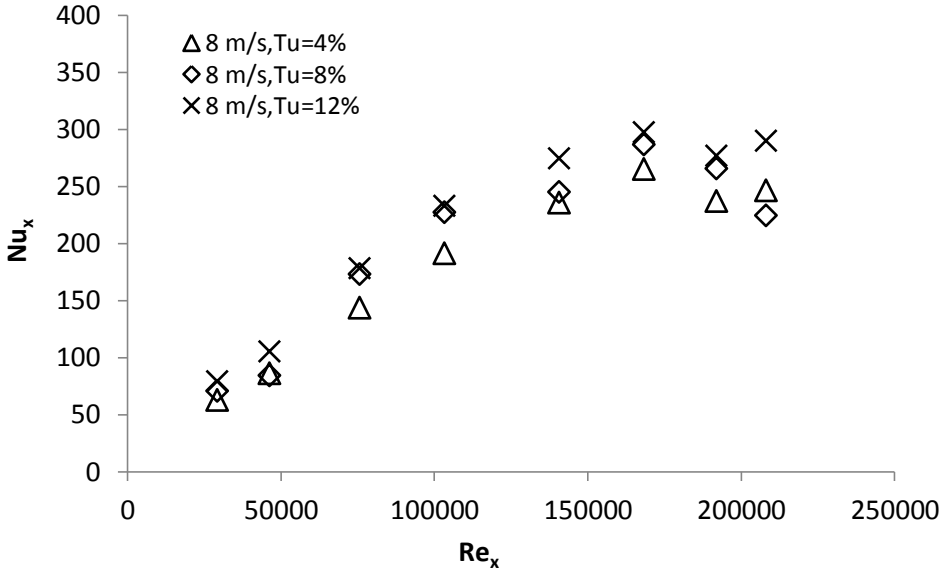

Figure 5.15: Nusselt number vs. Reynolds number at free stream velocity of 8 m/s and integral length scale of 0.0150m; (a) tilt of 0°, (b) tilt of 20°.

(a)

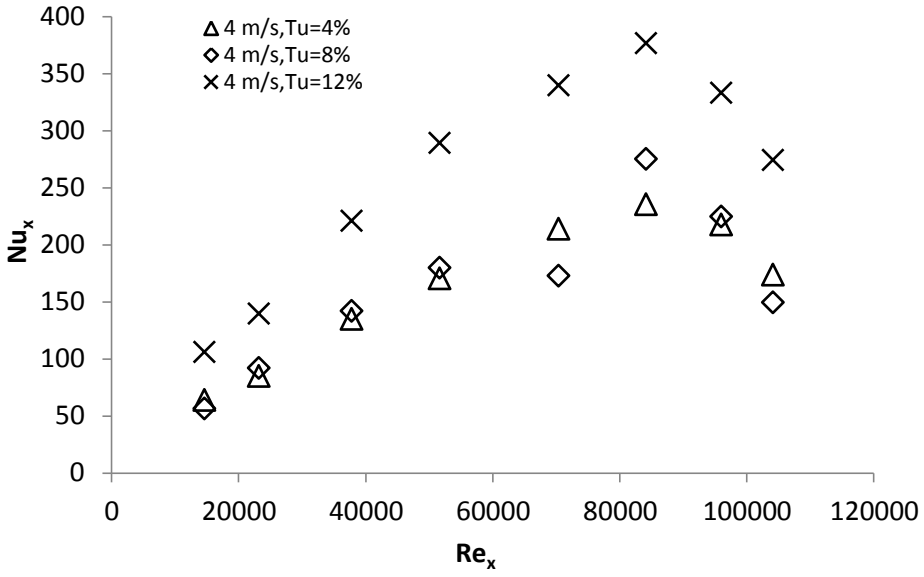

(b)

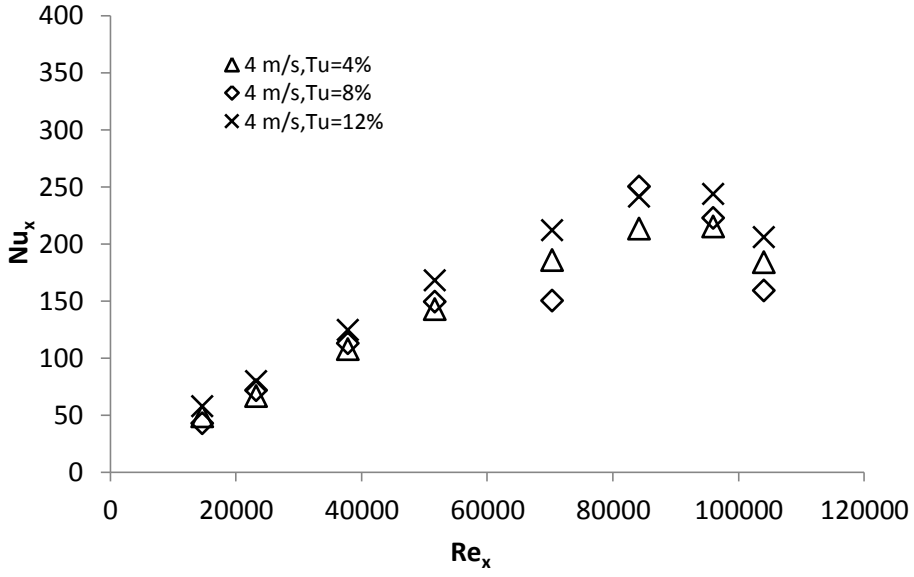

Figure 5.16: Nusselt number vs. Reynolds number at free stream velocity of 4 m/s and integral length scale of 0.015m; (a) tilt of 0°, (b) tilt of 20°.

5.2.2 Integral Length Scale of 0.021 m

By changing the perforated plate, the integral length scale of 0.021 m was established. All tests explained in Section 5.2.1 were repeated for the integral length scale of 0.021 m again at two different free stream velocities of 4 m/s and 8 m/s and two tilt angles of 0° and 20°.

Figures 5.17 and 5.18 illustrate the temperature distribution over the flat plate at free stream velocities of 8 m/s and 4 m/s respectively. It is seen that the flat plate temperature increases along the plate, however, there is temperature drop close to the trailing edge which is larger in the case of tilt=20°. The local convection heat transfer coefficient at free stream velocities of 8 m/s and 4 m/s is depicted respectively in Figures. 5.19 and 5.20. It is observed that the convection heat transfer coefficient decreases toward the trailing edge. However, it goes down with a sharper slope close to the end of the flat plate. Comparison of the convection heat transfer coefficient corresponding to different turbulence intensities indicates that higher turbulence intensity leads to a higher cooling capacity with the exception of those data shown in Figure 5.20. It is seen that the general trend of the diagrams corresponding to the integral length scale of 0.021 m is similar to what was observed for the integral length scale of 0.0150 m. A similar behavior was also identified for the integral length scale of 0.030 m. Hence to avoid repetition, only results related to integral length scales of 0.015 m and 0.021 m were presented here.

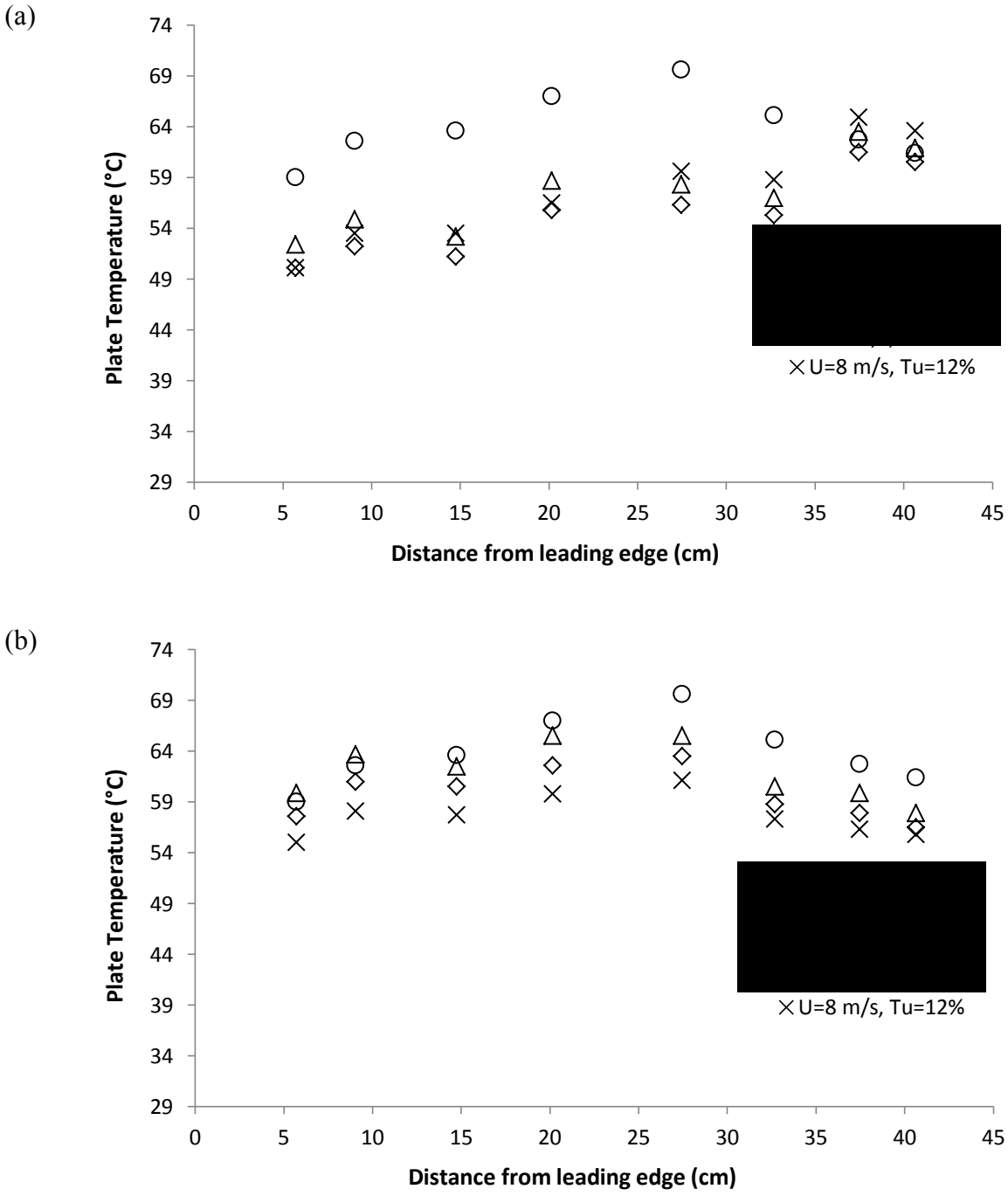

Figure 5.17: Flat plate temperature vs. distance from leading edge at free stream velocity of 8 m/s and integral length scale of 0.021 m; (a) tilt of 0°, (b) tilt of 20°.

(a)

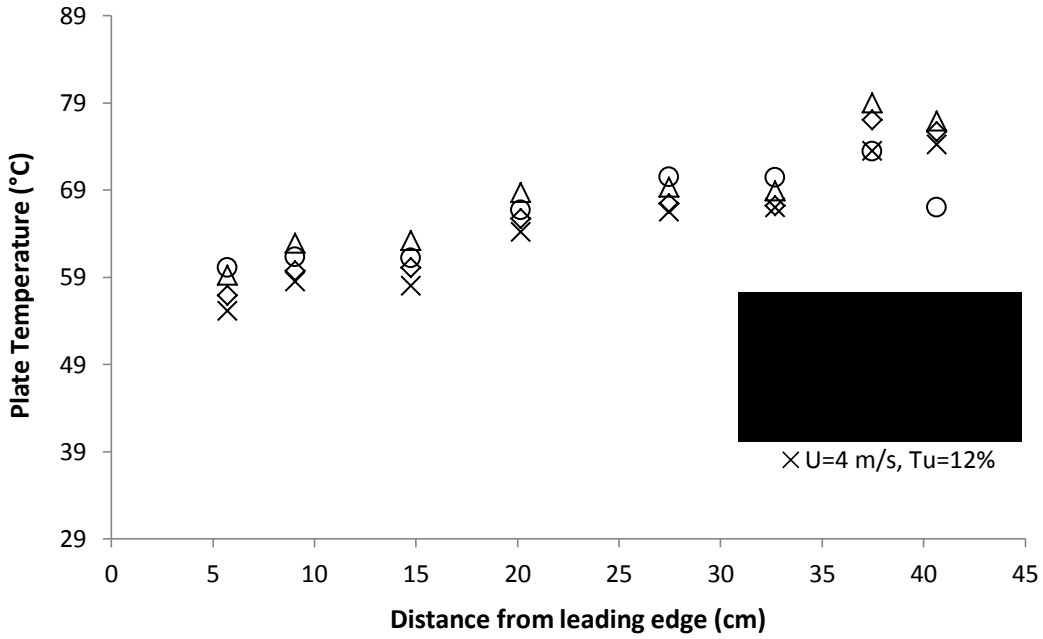

(b)

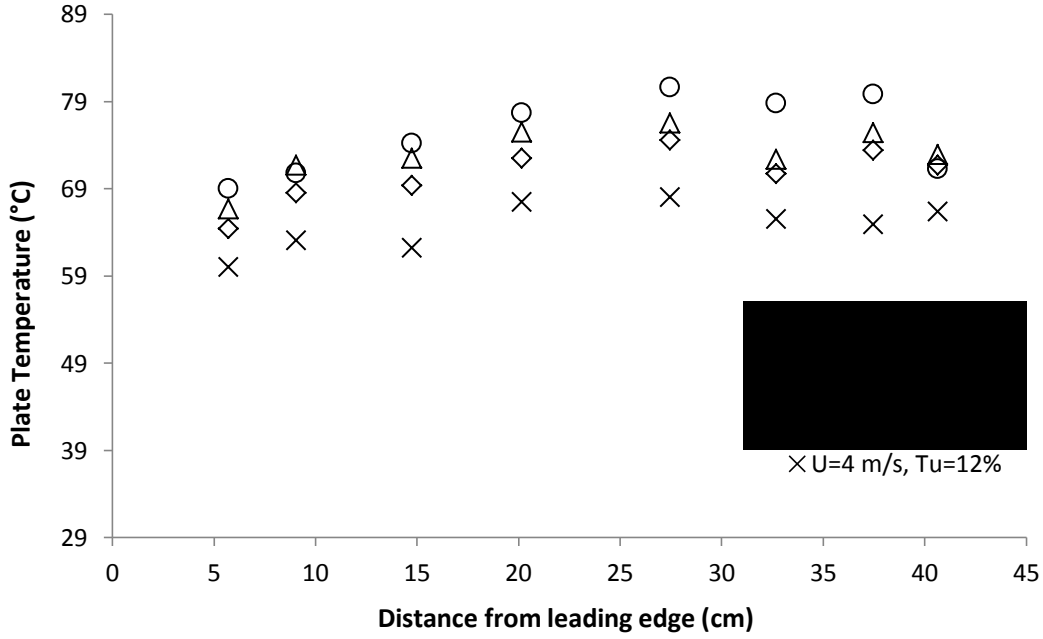

Figure 5.18: Flat plate temperature vs. distance from leading edge at free stream velocity of 4 m/s and integral length scale of 0.021 m; (a) tilt of 0°, (b) tilt of 20°.

(a)

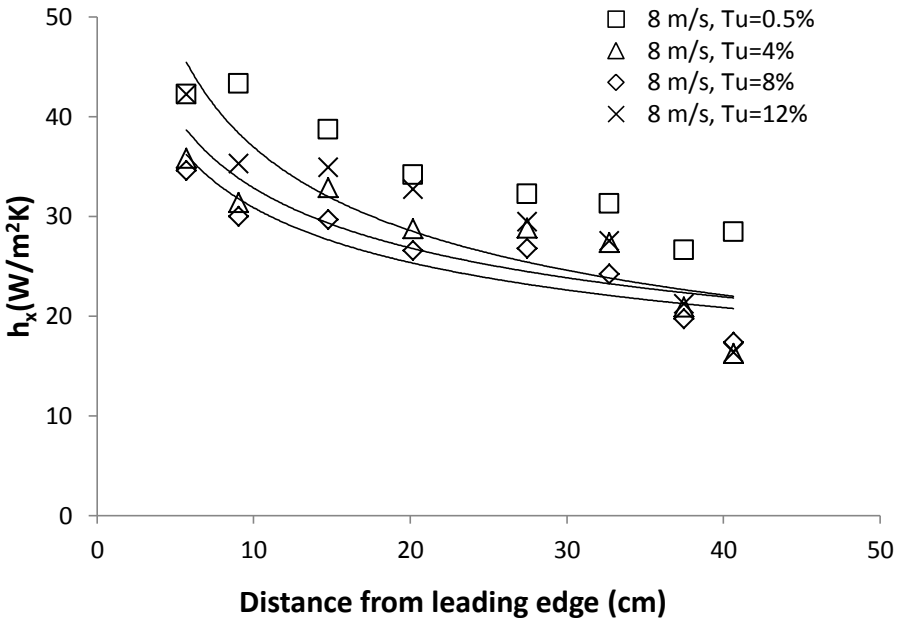

(b)

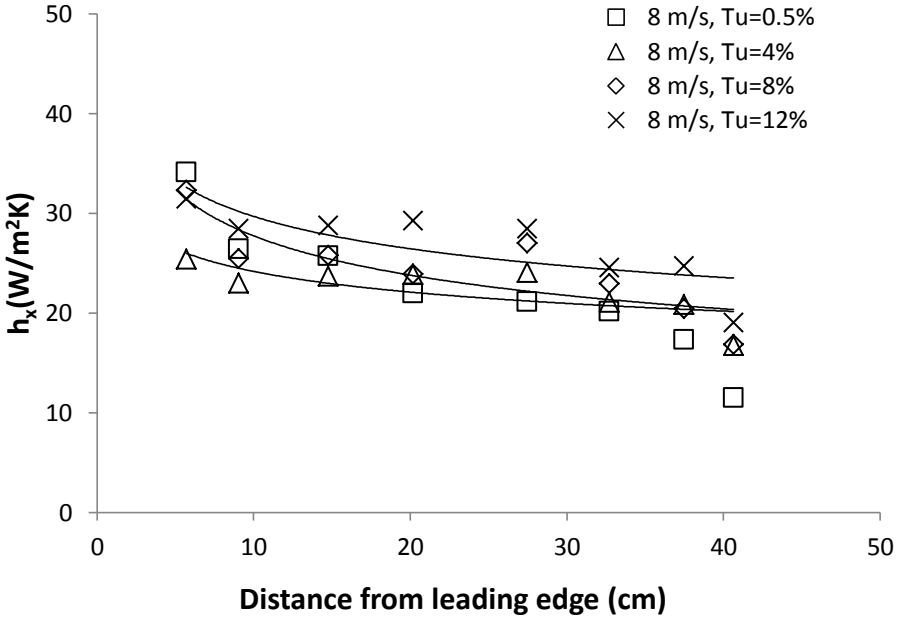

Figure 5.19: Local heat transfer coefficient vs. distance at free stream velocity of 8 m/s and integral length scale of 0.021 m; (a) tilt of 0°, (b) tilt of 20°.

(a)

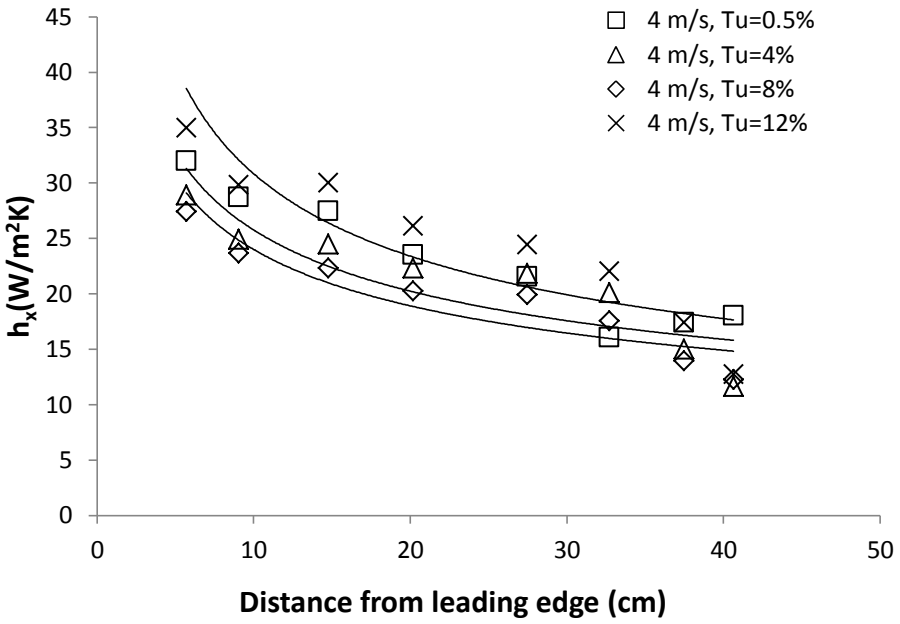

(b)

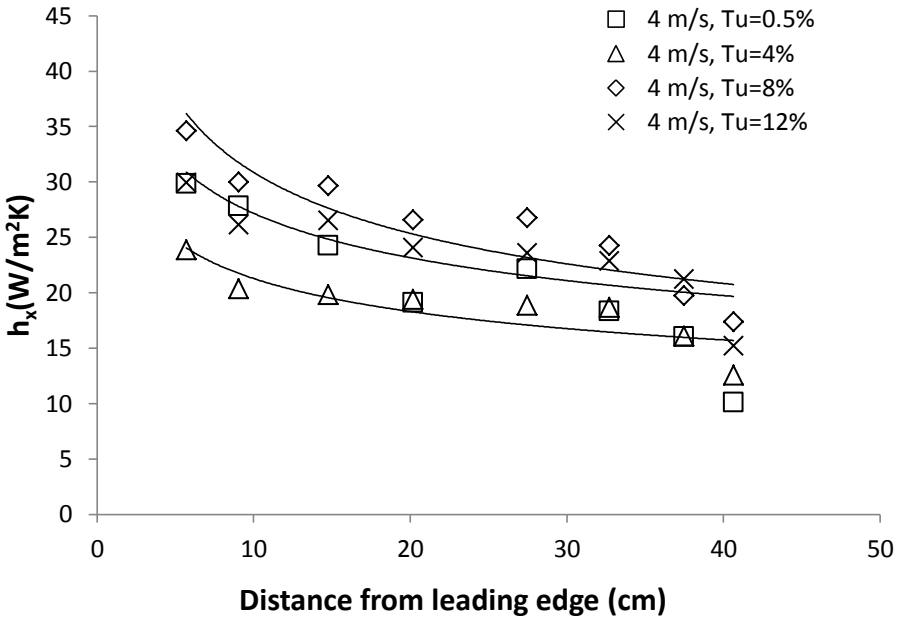

Figure 5.20: Local heat transfer coefficient vs. distance at free stream velocity of 4 m/s and integral length scale of 0.021 m; (a) tilt of 0°, (b) tilt of 20°.

The Nusselt number versus Reynolds number plots appear in Figures. 5.21 to 5.28 for integral length scales of 0.015 m, 0.021 m and 0.030 m to better elucidate the effects of integral length scale on convection heat transfer over the flat plate. Figures 5.23, 5.24 and 5.25 respectively, correspond to turbulence intensities of 4%, 8% and 12% at a free stream velocity of 8 m/s. Figures 5.26, 5.27 and 5.28 are related to the turbulence intensities of 4%, 8% and 12% at free stream velocity of 4 m/s.

(a)

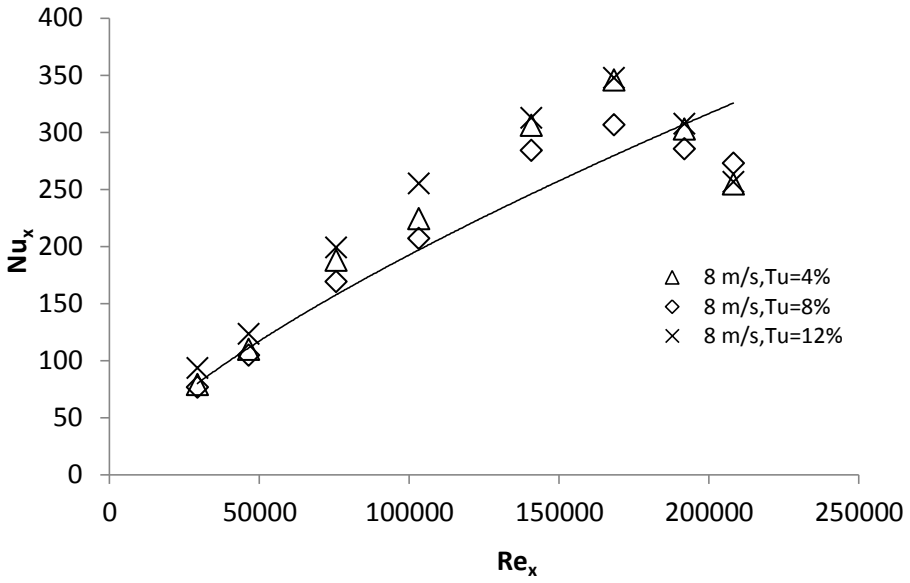

(b)

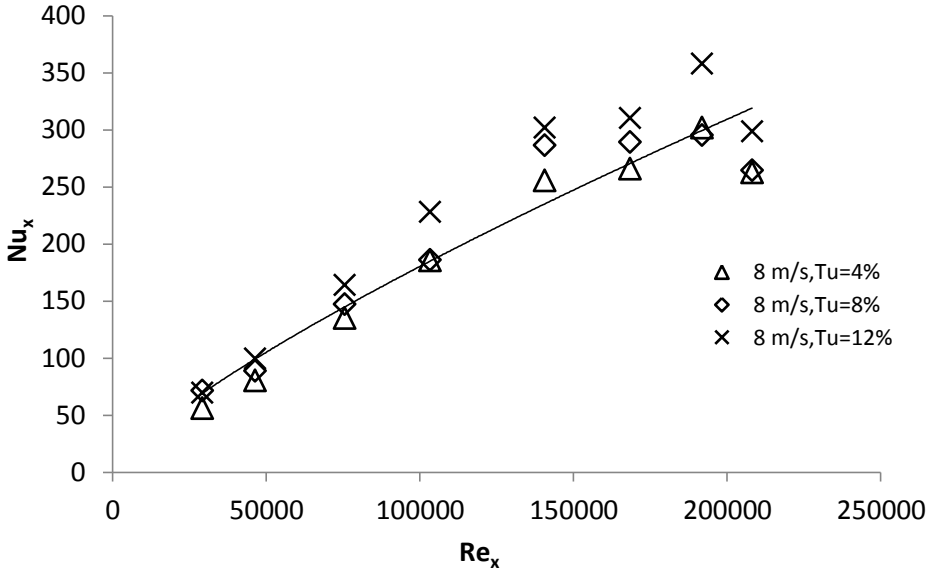

Figure 5.21: Nusselt number vs. Reynolds number at free stream velocity of 8 m/s and integral length scale of 0.021 m; (a) tilt of 0°, (b) tilt of 20°.

(a)

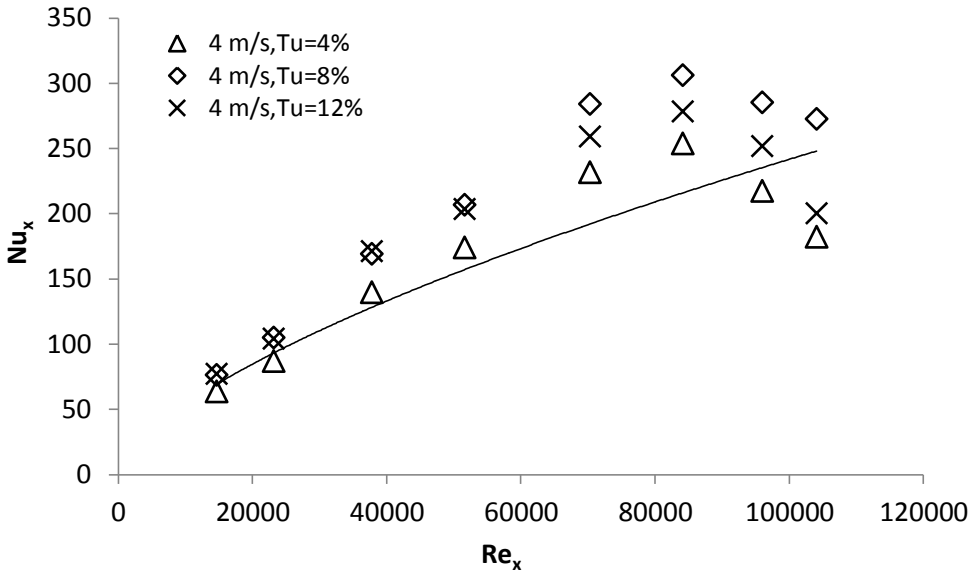

(b)

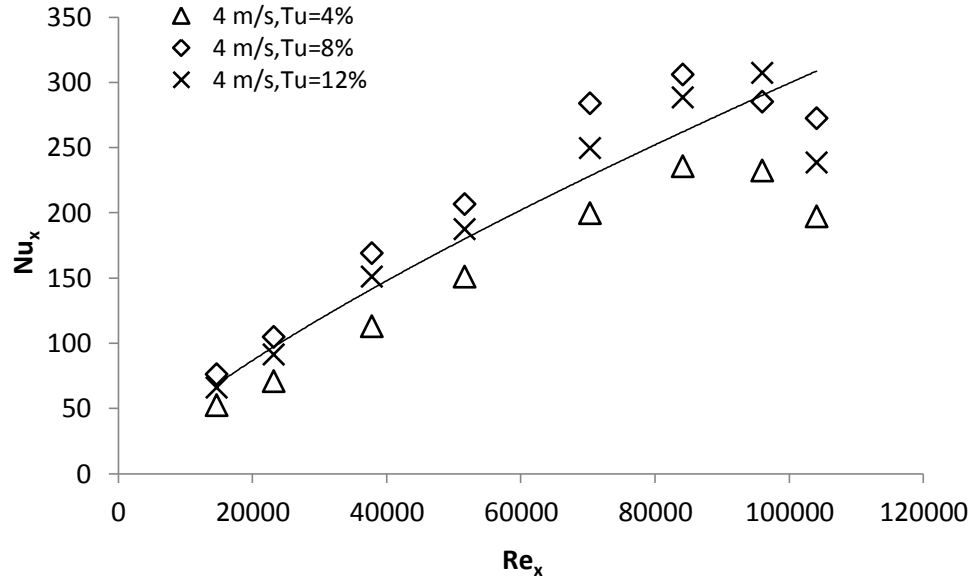

Figure 5.22: Nusselt number vs. Reynolds number at free stream velocity of 4 m/s and integral length scale of 0.021 m; (a) tilt of 0°, (b) tilt of 20°.

(a)

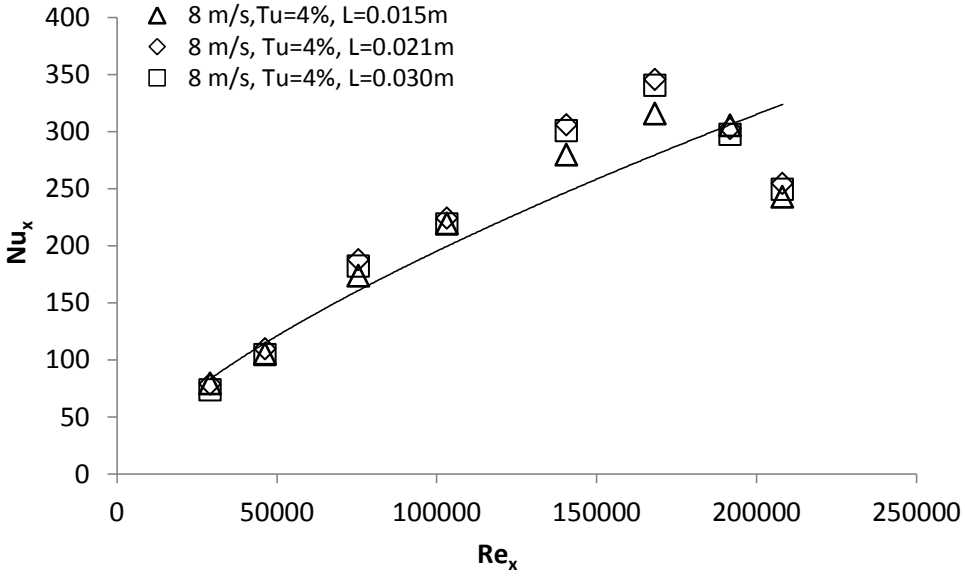

(b)

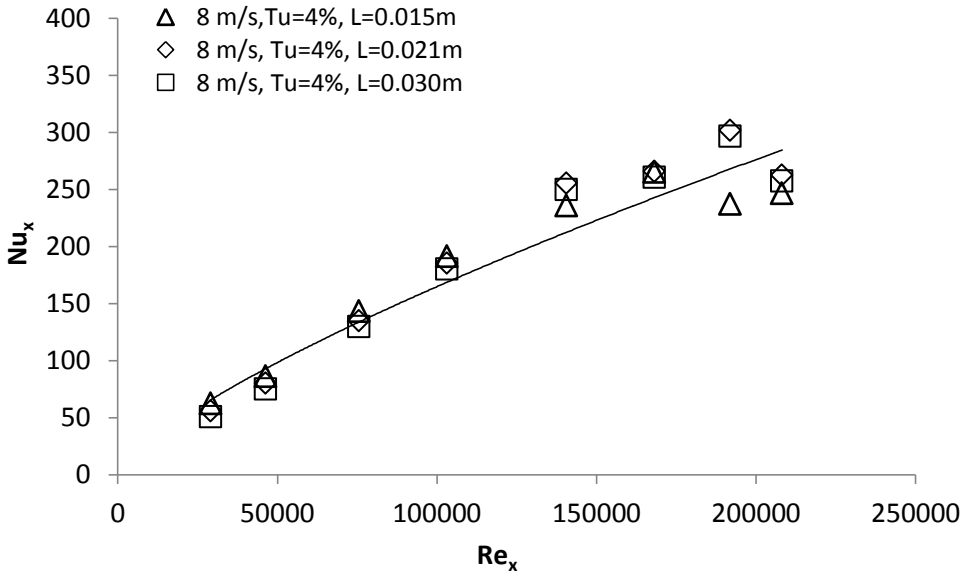

Figure 5.23: Nusselt number vs. Reynolds number at free stream velocity of 8 m/s and turbulence intensity of 4%; (a) tilt of 0°, (b) tilt of 20°.

(a)

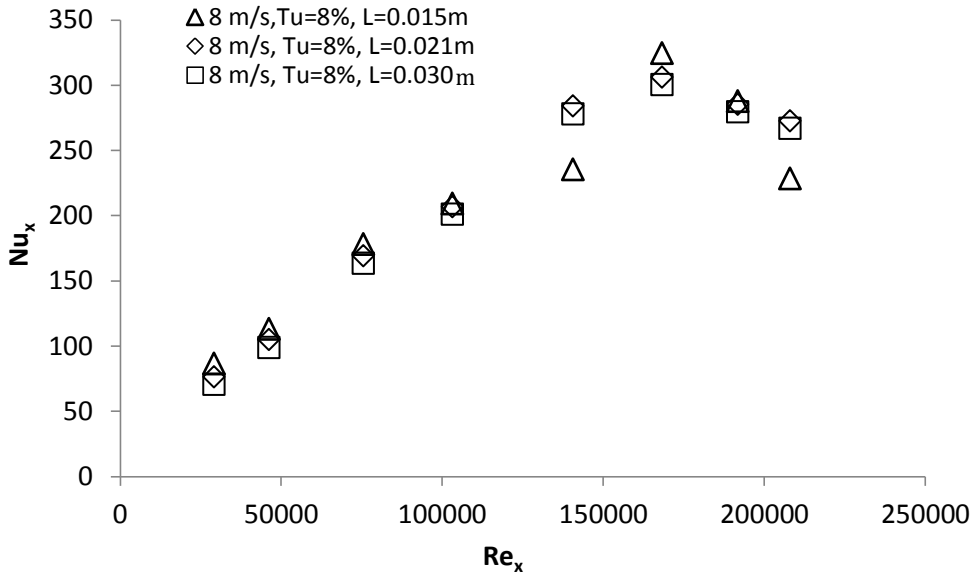

(b)

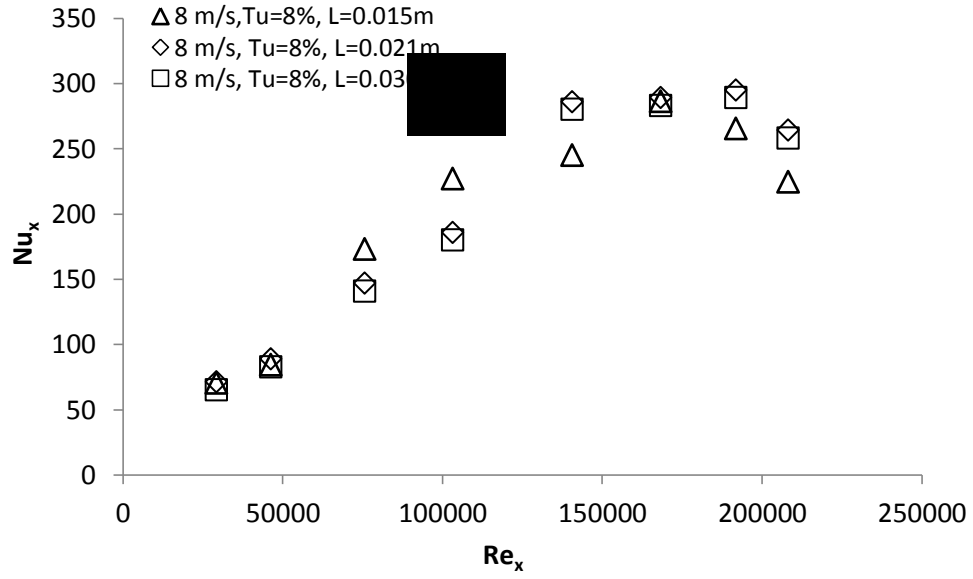

Figure 5.24: Nusselt number vs. Reynolds number at free stream velocity of 8 m/s and turbulence intensity of 8%; (a) tilt of 0°, (b) tilt of 20°.

(a)

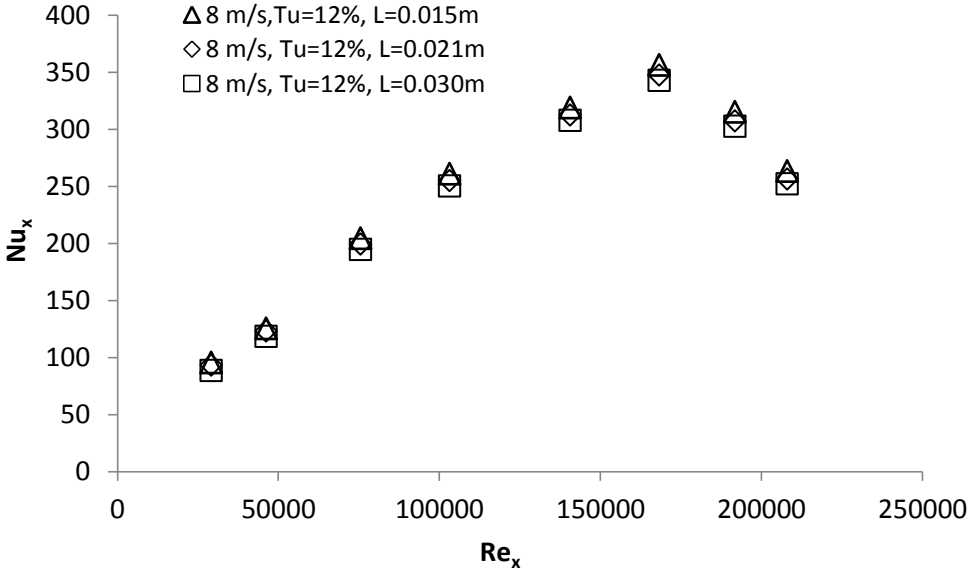

(b)

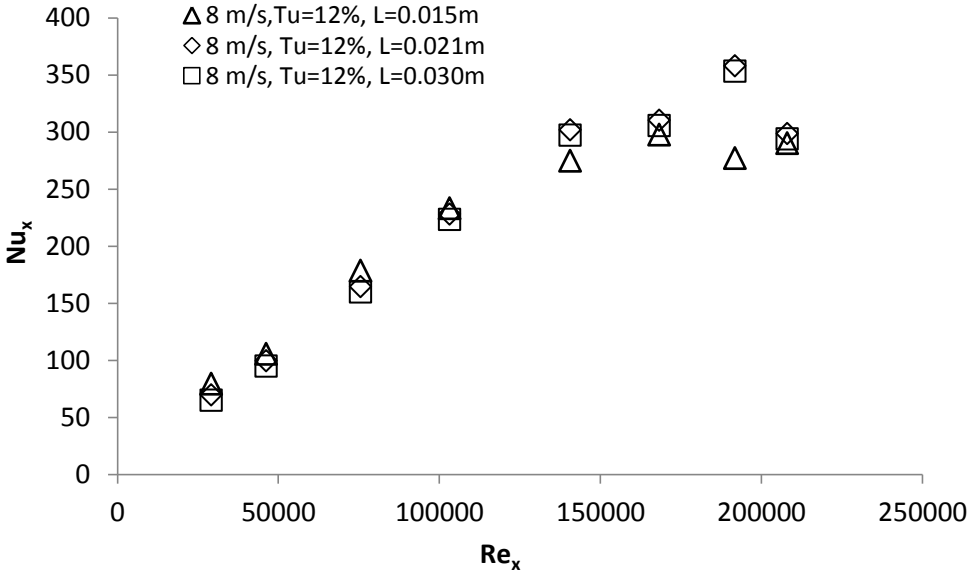

Figure 5.25: Nusselt number vs. Reynolds number at free stream velocity of 8 m/s and turbulence intensity of 12%; (a) tilt of 0°, (b) tilt of 20°.

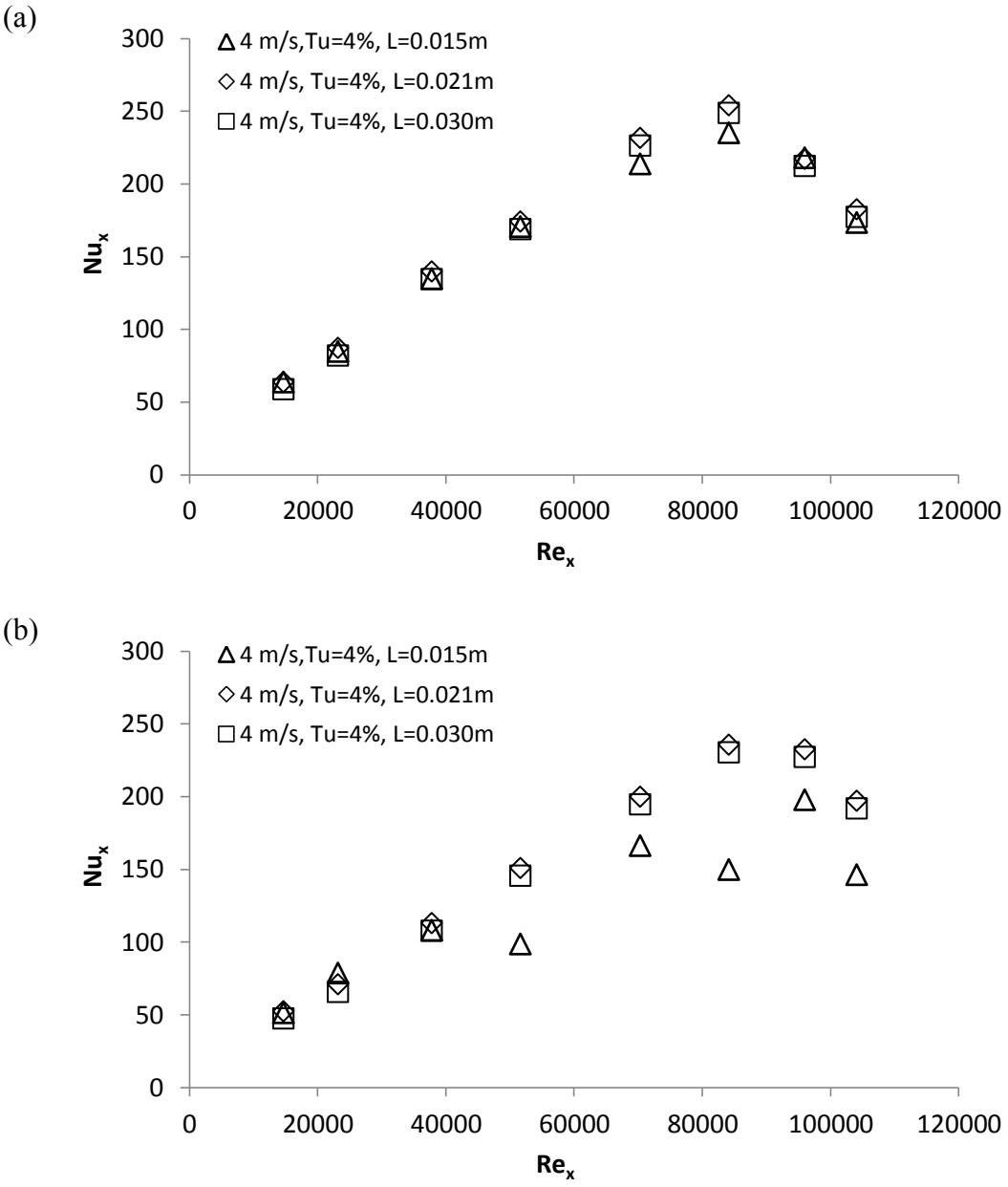

Figure 5.26: Nusselt number vs. Reynolds number at free stream velocity of 4 m/s and turbulence intensity of 4%; (a) tilt of 0°, (b) tilt of 20°.

(a)

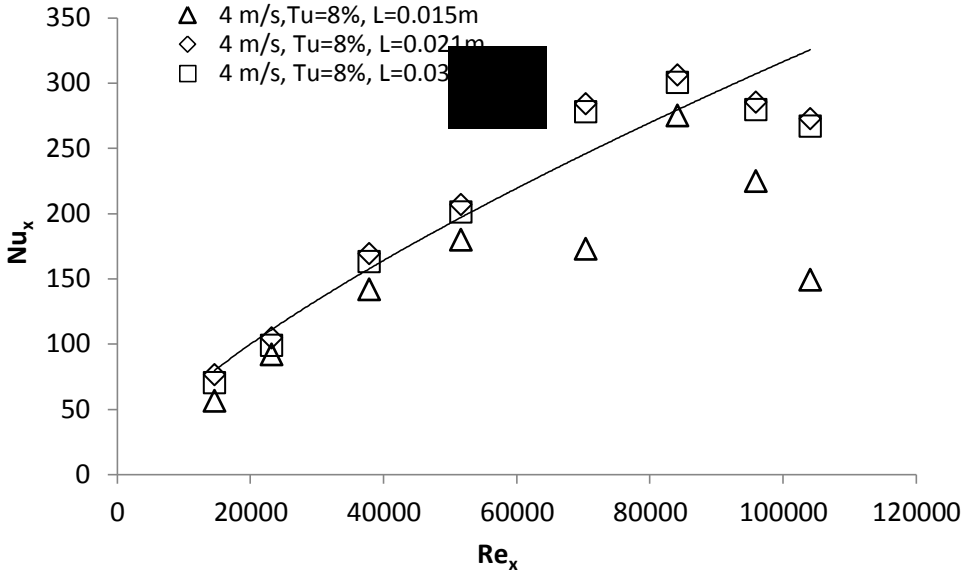

(b)

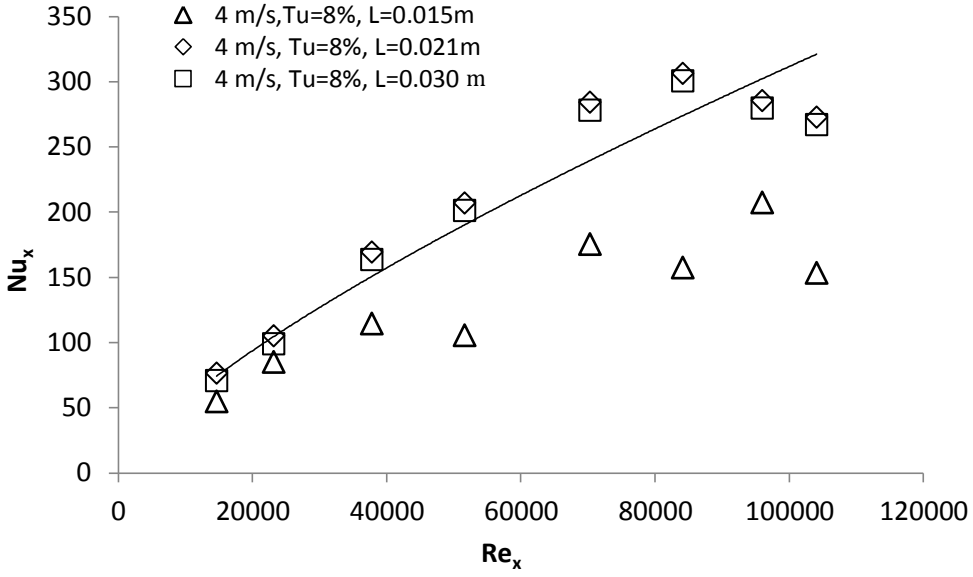

Figure 5.27: Nusselt number vs. Reynolds number at free stream velocity of 4 m/s and turbulence intensity of 8%; (a) tilt of 0°, (b) tilt of 20°.

(a)

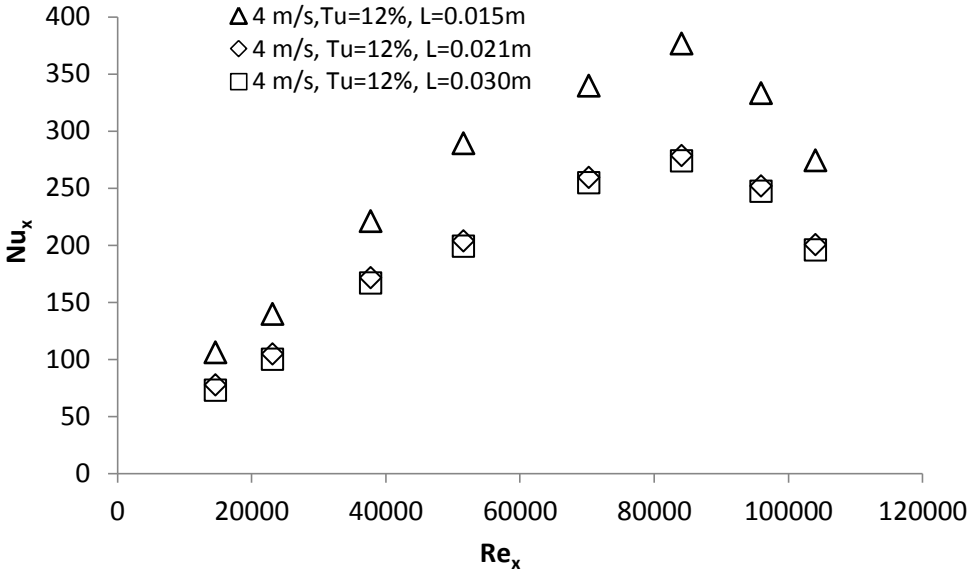

(b)

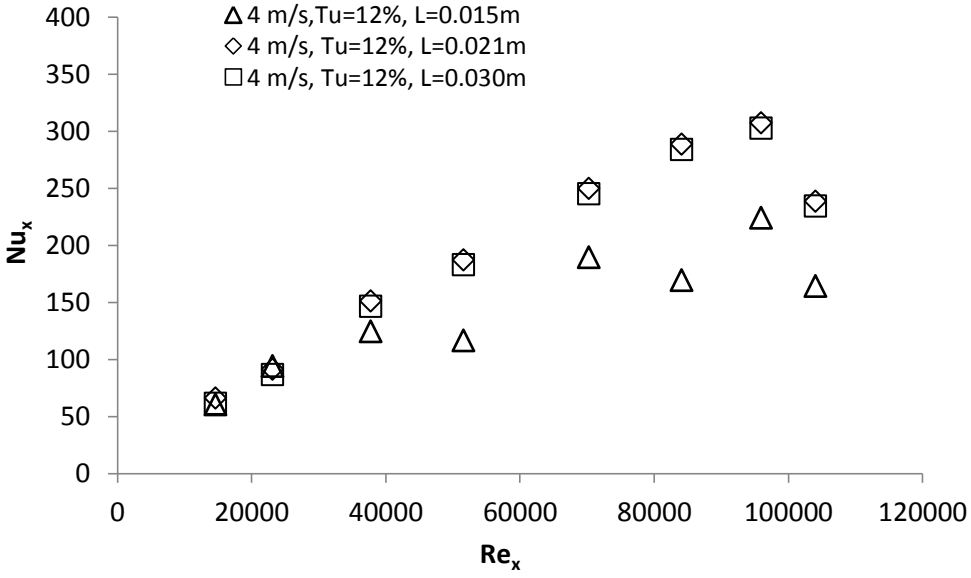

Figure 5.28: Nusselt number vs. Reynolds number at free stream velocity of 4 m/s and turbulence intensity of 12%; (a) tilt of 0°, (b) tilt of 20°.

Figure 5.29 compares the Nu number obtained in the current experiments with the literature data for tilt angle of 0°. The gray band represents the literature data reported in Table 2.2.

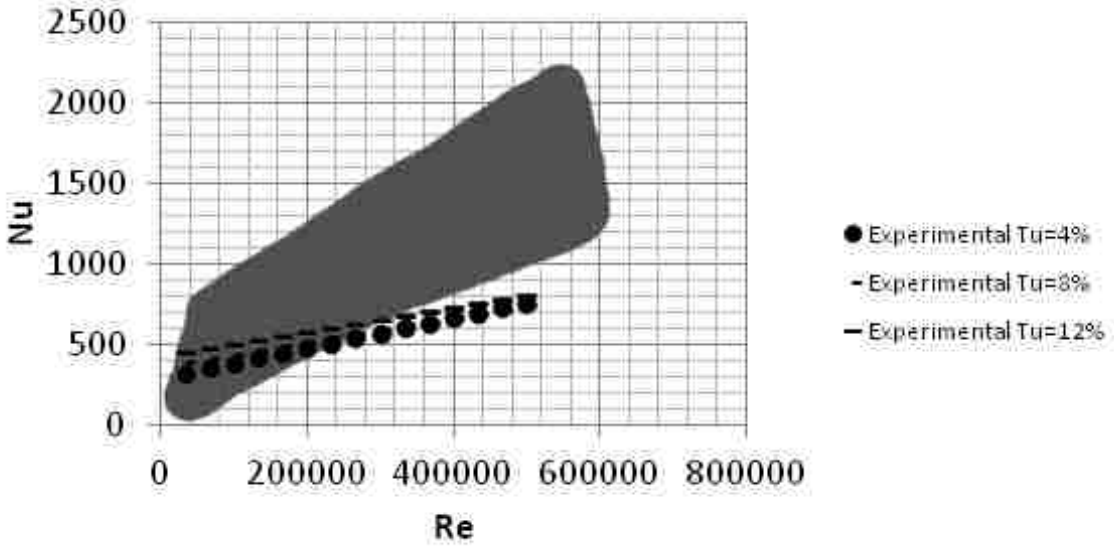

Figure 5.29: Comparison of the current study Nu number with the literature review band for the case of tilt=0°.

The effect of integral length scale on Nusselt number ratio ($Nu/Nu_{x,0G}$) is illustrated in Figure 5.30. $Nu_{x,0G}$ is the local Nusselt number in the absence of the grid, i.e. no turbulence generator. The results of the current study are compared with those of Hori & Junzo [20] which were discussed in chapter 2.

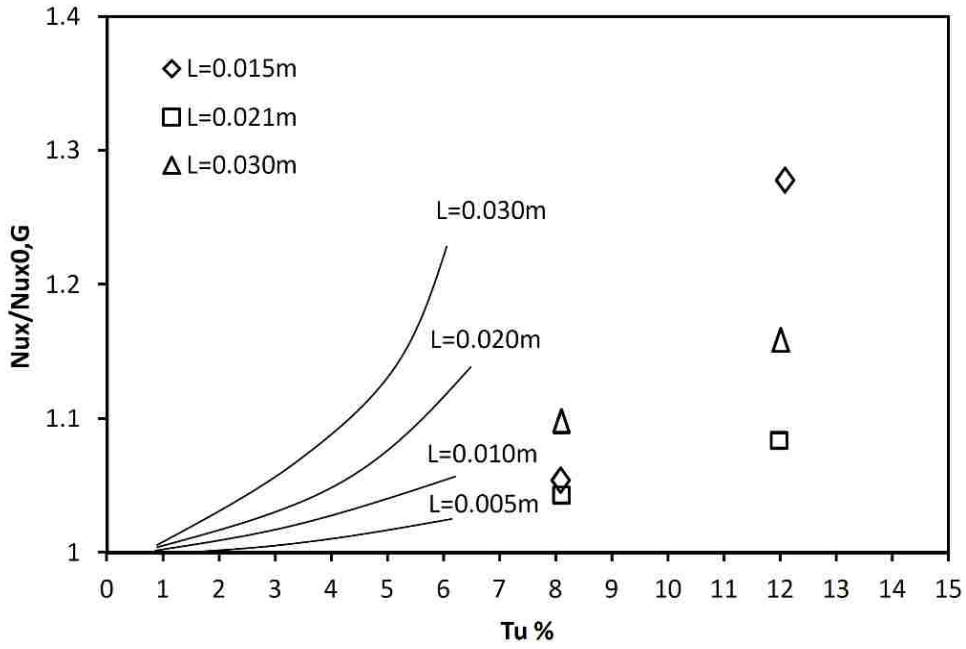

Figure 5.30: Effect of integral length on Nu-Tu relationship [20], $Re_x < 1.7 \times 10^6$.

The variation of Nusselt number ratio with turbulent Reynolds number Re_t and turbulence intensity Tu is also illustrated in 5.31. As was explained in Chapter 2 Hori & Junzo [20] defined the turbulence Reynolds number as $Re_t = \sqrt{\overline{u'^2}}L/\upsilon$ in which u' and L were velocity fluctuations and characteristic length respectively. The Nusselt number obtained in the current study is illustrated versus $Tu^{0.3}Re_t^{1.5} \times 10^{-4}$ in Figure 5.30. The results are also compared with those of Hori and Junzo [20], Blair [21] and Sugawara et al. [22].

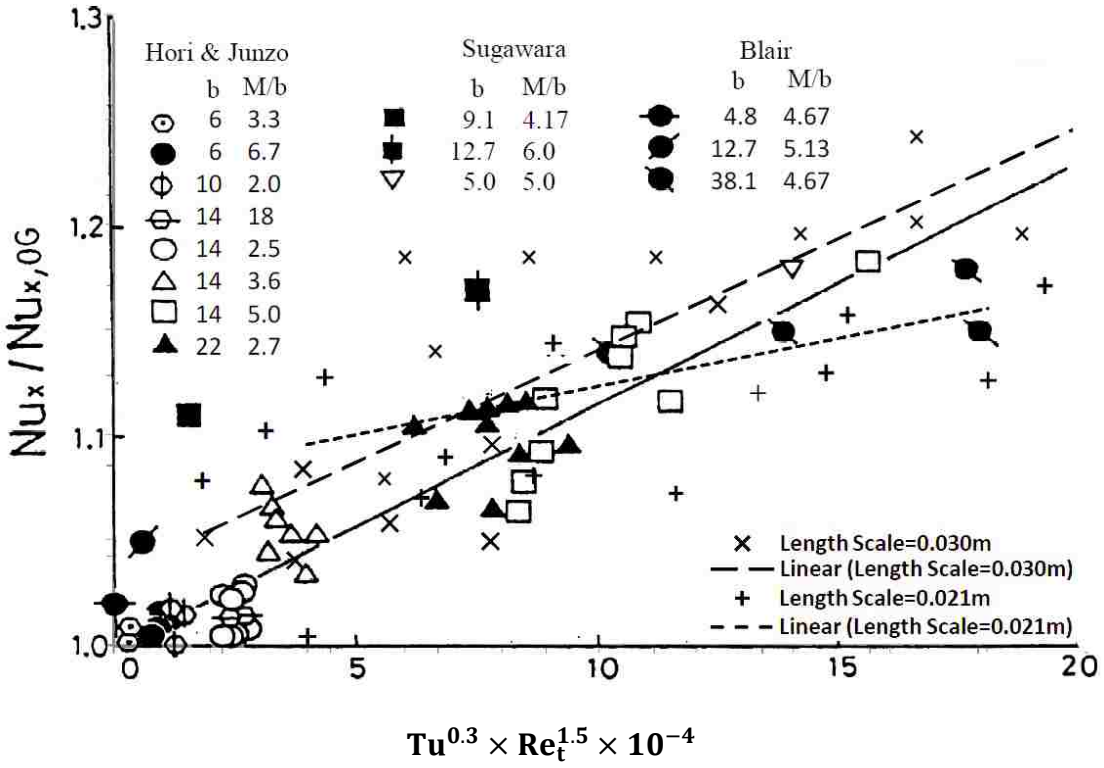

Figure 5.31: Nusselt number ratio versus turbulence intensity and turbulent Reynolds number [20].

The solid line indicates values calculated by the empirical equation $\frac{\mathrm{Nu_x}}{\mathrm{Nu_{x,0G}}} = 1.15 \times 10^{-6} \times \mathrm{Tu}^{0.3}\mathrm{Re_t}^{1.5} + 1$ which corresponds to results of Hori and Junzo [20], Blair [21] and Sugawara et al. [22]. In this figure the crosses (×) show the results of the current study for integral length scale of 0.030 m and the pluses (+) illustrates the results correspond to integral length scale of 0.021 m. It is observed that results of the current study are in good accordance with those of Hori and Junzo [20], Blair [21] and Sugawara et al. [22]

CHAPTER 6

CONCLUSIONS AND RECOMMENDATIONS

Conclusions

An experimental study was performed in a wind tunnel to investigate the convection heat transfer characteristics of a flat plate in laminar and turbulent flow. The air was forced to flow over a flat plate at four different velocities ranging between 4 m/s to 10 m/s that resulted in Reynolds numbers up to 346,670. Turbulent Intensities of 4%, 8% and 12% at the leading edge of the plate were kept constant while the Integral Length Scale (Λ) was varied from 0.030 m to 0.0150 m. For the two cases, laminar and turbulent, the flat plate was positioned at 0° and 20° tilt angles. The laminar case was tested at two different supplying powers; 52W and 224W. It was observed that in the case of 224W, the temperature distribution was more uniform, therefore, the turbulent case was performed only for 224W. The experimental results were compared with the field data given by Essex Energy Corp. The wind tunnel conditions were not exactly in accordance with the outdoor conditions; therefore, the experimental results had a significant difference to the field data. In fact, outdoor conditions have a higher level of turbulence intensity than indoor, so the convection heat transfer rate reported for the field data is larger than what was obtained in the current experiments. The main conclusions of the current study are highlighted as follows;

- An increase in the Reynolds number leads an increase in the heat transfer rate.
- The heat transfer rate is higher in the turbulent flow in comparison with the laminar one.
- The convection heat transfer coefficient increases with turbulence intensity.
- Integral length scale has no significant effect on convection heat transfer coefficient within the range of values tested in these experiments.

Recommendations

It is recommended that these experiments be repeated:

- with a wider plate to remove edge effects from the results.
- using a longer plate to let the boundary layer develop more.
- using more thermocouples to capture a more carefully the temperature field.
- using a larger heater to cover the entire surface of the flat plate. Currently, there was an approximately 5.08 cm (2 inch) unheated distance which created a negative gradient in the temperature close to the trailing edge.
- using several heaters to have a more efficient control of the temperature distribution.

APPENDICES

Appendix A Heat Loss due to Radiation and Conduction

For Radiation

As stated earlier the flat plate rejects heat to the surroundings by radiation, and this can be estimated as;

$Q_{rad} = \varepsilon\sigma A_s(T_s^4 - T_\infty^4)$

where,

ε = the emissivity for polished aluminum, 0.05

σ = Stefan Boltzmann constant, 5.67×10^{-8} W m^{-2} K^{-4}

A_s = Surface Area of the Aluminum Surface, 0.175 m^2

T_s = Surface Temperature of the Aluminum, 40°C

T_∞ = Ambient Temprature, 25°C

Q_{rad}= Heat Loss due to radiation, Watts

Solution

Therefore; $Q_{rad} = (0.05)(5.67 \times 10^{-8}\ W\ m^{-2}\ K^{-4})(0.175\ m^2)[(313°K)^4 - (298°K)^4]$

$= (4.99 \times 10^{-10}\ W\ K^{-4})(1.71 \times 10^9 K^4)$

$= 0.854$ W

For Conduction

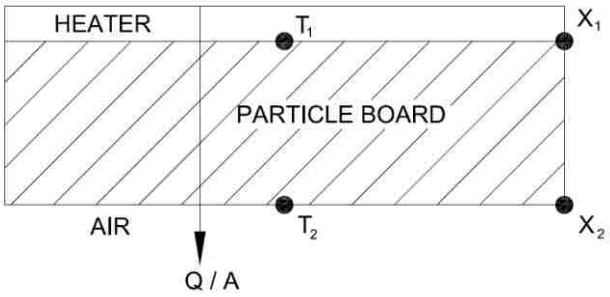

Figure A.1: Heat transfer by conduction of the flat plate.

Biot Number

The Biot number is a dimensionless value which indicates the ratio of convection at the surface of the body to conduction within the body. A small Biot number represents small temperature gradients within the body, and as such can be assumed to have a uniform temperature. This case is only applicable when the Biot number is less than 0.1 (Bi < 0.1)

The Biot number can be expressed as;

$Bi = hL_c / k_{al}$

where,

h = heat transfer coefficient (W/m^2K), for current study $4 \leq h \leq 60$

L_c= characteristic length, which is commonly defined as the volume of the body divided by the surface area of the body, which in the current study the body refers to the aluminum plate (V_s/A_s).

k_{al} = Thermal conductivity of the body (aluminum), taken as 250 W/mK

The length of the aluminum is 0.522m the width 0.337m and a thickness of 0.0015875m.

The area and volume can easily be calculated, $A_s = L \times W = 0.522m \times 0.337m = 0.176m^2$

And $V_s = L \times W \times H = 0.176m^2 \times 0.0015875m = 0.00028m^3$

Calculating (V_s/A_s) = 0.00159m

We have all parameters and can now calculate the Biot number based on the restraints of h.

For $h = 4\ W/m^2K$

$Bi = hL_c/ k_{al} = (4\ W/m^2K)(0.00159m) / 250\ W/mK$

$= 2.5 \times 10^{-5}$

And for $h = 60\ W/m^2K$

$Bi = hL_c/ k_{al} = (60\ W/m^2K)(0.00159m) / 250\ W/mK$

$= 3.8 \times 10^{-4}$

Appendix B Uncertainty Analysis

In general, the type of parameters that need to be considered in any uncertainty analysis can be safely divided into: independent and dependent parameters. Independent parameters are the parameters which are directly measured values from specific instruments like temperature and length. While the dependent parameters are calculated based on the values of the independent parameters such as Reynolds number and heat transfer coefficient.

B.1. Uncertainty of Independent Parameters

The errors of independent parameters are usually provided by the manufacturers. The errors are classified to be bias, *B*, and precision, *P*. The bias error includes the linearity, hysteresis, and accuracy while the precision error account for the repeatability. The combined error generated from the independent parameters is calculated from the following equation:

$$w = \sqrt{B^2 + P^2}$$

B.1.1. Uncertainty in surface temperature

The surface temperature is one of independent parameters which has been measured via Type T thermocouples. These thermocouples have ±1.0 ºC accuracy and 0.024 ºC resolution, so their bias uncertainty is $\sqrt{(1)^2 + \left(\frac{0.024}{2}\right)^2} = 1.00007\ °C$. The thermocouples measurements have been monitored via a Fluke meter Model#52 whose resolution and accuracy are 0.1 °C and ±0.3ºC respectively which gives total bias

uncertainty of $\sqrt{(0.3)^2 + \left(\frac{0.1}{2}\right)^2} = 1.0012\ ^\circ C$. Therefore, the total bias uncertainty in the surface temperature is $\sqrt{(1.00007)^2 + (1.0012)^2} = 1.415\ ^\circ C$.

On the other hand, the precision uncertainty has been deduced for a student t distribution with 95% confidence interval via:

$$W_P = t_{v,95} S_{\bar{X}}$$

where $t_{v,95}$ is the confidence interval with 95% level, $v=N-1$ is degree of freedom and $S_{\bar{X}}$ is standard deviation of mean values of the N measurements. In the present work four sets of independent experiments have been done for each flow case which yields to a value of $t_{v,95}=3.182$ for $v=3$ for a two tails distribution. As an example, in the flow case of U=8 m/s & Tu=8% the surface temperature at the first streamwise location has been measured as: 50.2, 51.2, 51.6, and 50.8 °C which results in a precision uncertainty of $W_P = 1.9003\ ^\circ C$. Taking into account the $W_B = 1.415\ ^\circ C$ bias uncertainty, gives a total uncertainty of $\sqrt{(1.9003)^2 + (1.415)^2} = 2.37\ ^\circ C$ in the surface temperature for that particular case. The uncertainty for other cases have also been calculated and displayed with errorbars on the relevant graphs.

B.2. Uncertainty of Dependent Parameters

The Kline-McClintock equation can be used to determine the uncertainty in a dependent parameter. If it is assumed that a dependent parameter R has a given function of the independent parameters of $x_1, x_2, x_3, \ldots, x_n$, Thus;

$$R = f(x_1, x_2, x_3, \ldots, x_n)$$

Then W_R, the uncertainty in the parameter R can be calculated as

$$W_R = \sqrt{\left(\frac{\partial R}{\partial x_1} w_{x_1}\right)^2 + \left(\frac{\partial R}{\partial x_2} w_{x_2}\right)^2 + \cdots + \left(\frac{\partial R}{\partial x_n} w_{x_n}\right)^2}$$

Two main parameters which have been reported throughout this study are Nusselt and Reynolds numbers. The following shows the procedure for estimating their uncertainty values.

B.2.1. Uncertainty in Nusselt number

The local Nusselt number can be found from the following relationship:

$$\mathrm{Nu_x} = \frac{\mathrm{h_x x}}{\mathrm{k_{air}}}$$

The total uncertainty associated with the Nusselt number is calculated as,

$$w_{Nu_x} = \sqrt{\left[\frac{\partial Nu_x}{\partial hx} w_{h_x}\right]^2 + \left[\frac{\partial Nu_x}{\partial L} w_L\right]^2 + \left[\frac{\partial Nu_x}{\partial k_{air}} w_{k_{air}}\right]^2}$$

The uncertainty associated with k_{air} is,

$$W_K = 0.00025\ W/mK$$

W_L is uncertainty in the length which was measured with a digital caliper (Mitutoyo 500-171). The caliper has a resolution of 0.01 mm and an accuracy of ±0.025 mm which gives the absolute uncertainty in length of the flat plate of:

$$W_L = 0.0255\ mm$$

The heat transfer coefficient was calculated as,

$$h_x = \left[\frac{Q_{tot}}{A_s(T_s - T_\infty)}\right]$$

Therefore the uncertainty associated with h_x is,

$$w_{h_x} = \sqrt{\left(\frac{\partial h}{\partial Q_{tot}} \times W_{Q_{tot}}\right)^2 + \left(\frac{\partial h}{\partial A_s} \times W_{A_s}\right)^2 + \left(\frac{\partial h}{\partial T_s} \times W_{T_s}\right)^2 + \left(\frac{\partial h}{\partial T_\infty} \times W_{T_\infty}\right)^2}$$

where, W_Q is the uncertainty in heat transfer which was supplied using a flexible heater Model# EFH-SH-12X18-10-115 whose uncertainty is:

$$W_{Qtot} = 9.5W$$

W_A is the uncertainty in the plate surface area whose dimensions are L=520 mm & b=340 mm. It has been calculated as:

$$w_{A_s} = \sqrt{\left(\frac{\partial A_s}{\partial L} \times W_L\right)^2 + \left(\frac{\partial A_s}{\partial b} \times W_b\right)^2} = 15.84\ mm$$

The temperature of the incoming flow has been measured via a Kestral 4500 whose resolution and accuracy are *1 °C* and *1 °C* respectively, so

$$W_{T\infty} = 1.11\ °C$$

The uncertainty in the surface temperature has been calculated earlier as:

$$W_{Ts} = 1.415\ °C$$

Calculating all terms for a flow case of U=8 m/s & Tu=8% at the first streamwise location, the uncertainty in heat transfer coefficient is:

$$w_{h_B} = 1.837\ \frac{W}{m^{2\circ}C}$$

Repeated experiments give the values of 39, 38, 37, 38 $\frac{W}{m^{2\circ}C}$ for that location which results in the precision uncertainty of:

$$w_{h_P} = 2.598\ \frac{W}{m^{2\circ}C}$$

Hence, the total uncertainty in heat transfer coefficient is:

$$w_{h_{x1}} = \sqrt{(1.837)^2 + (2.598)^2} = 3.189\ \frac{W}{m^{2\circ}C}$$

Following the same procedure, it gives the total uncertainty in Nusselt number for that specific case as:

$$w_{Nu_{x1}} = 13.068$$

B.2.2. Uncertainty in Reynolds number

The Reynolds number is calculated using the following equation:

$$Re = \frac{\rho U L}{\mu}$$

while the absolute uncertainty in the Reynolds number is found via:

$$W_{Re} = \sqrt{\left(\frac{\partial Re}{\partial L} \times W_L\right)^2 + \left(\frac{\partial Re}{\partial \rho} \times W_\rho\right)^2 + \left(\frac{\partial Re}{\partial U} \times W_U\right)^2}$$

assuming the uncertainty in the kinematic viscosity is negligible.

W_L is uncertainty in the length which was measured with a digital caliper (Mitutoyo 500-171) and has been calculated earlier as 0.0255 mm.

W_ρ is uncertainty in the air density. Air density has been calculated from the ideal gas equation:

$$\rho = P/RT$$

After neglecting the uncertainty of the gas constant, R, the uncertainty in the air density can be estimated via:

$$W_\rho = \sqrt{\left(\frac{\partial \rho}{\partial P} \times W_P\right)^2 + \left(\frac{\partial \rho}{\partial T} \times W_T\right)^2}$$

where the pressure has been measured using Kestral 4500 whose resolution and accuracy are 0.01 inHg and 0.05 inHg respectively, so

$$W_P = 0.0502 \text{ inHg}$$

The temperature of the wind flow has been measured via a Kestral 4500 whose resolution and accuracy are *1 °C* and *1 °C* respectively, so

$$W_{T\infty}=1.11\ °C$$

W_U is uncertainty in the free stream velocity in the wind tunnel. The free stream velocity is calculated by:

$$U = \sqrt{\frac{2\,\Delta p}{\rho_{air}}}$$

Then the uncertainty in free stream velocity can be estimated via:

$$w_U = \sqrt{\left(\frac{\partial U}{\partial \Delta p} U_{\Delta p}\right)^2 + \left(\frac{\partial U}{\partial \rho} U_{\rho}\right)^2}$$

Calculating all terms for a flow case of U=8 m/s & Tu=8%, the total uncertainty in local Reynolds number of the first streamwise location is:

$$w_{Re_{x1}} = 1754$$

It should be noted that, the uncertainty different flow cases have also been calculated and shown on the corresponding graphs with errorbars.

Appendix C MATLAB Code

This code is to designed plot out the turbulence intensity and integral length scales versus location. This program is written with temperature correction.

```
clc;
clear all;
 %--------------------------------------------------------------------------
%Conditioner Setting(need to be modified)
%--------------------------------------------------------------------------
gain=1;                                                    %Gain of the conditioner
offset=0;                                                  %Offset of the conditioner
sample=2000000;                                            %Sample Size
Fs=80000;                                                  %Sample Frequency Hz

 C=[-0.762692
0.761302
-0.231276
0.059089
-0.001341];
 %--------------------------------------------------------------------------
%Load Raw Data, which should already be corrected with the temperature
%--------------------------------------------------------------------------
zone = 1;
for index2=1:1;
   if index2<10
   Horizontal = ['0' int2str(index2)];
  else
  Horizontal = int2str(index2);
  end
     for index3=1:10;
     if index3<10;
     Vertical = ['0' int2str(index3)];
     else
     Vertical = int2str(index3);
     end

     name=[int2str(zone) Horizontal Vertical];
     type='.txt';
     file=[name type];
     E=load(file);                                         %Call"DataLoad" function
     Ea = E(1:sample)/4096*10/gain+offset;
     Ta(index3) = E(sample+1)/4096*10*30;
     Ecorr=TempCorr(Ea,Ta(index3));
     Ucorr=C(1)+C(2)*Ecorr+C(3)*Ecorr.^2+C(4)*Ecorr.^3+C(5)*Ecorr.^4;
     mu(index3)=mean(Ucorr);
     u=Ucorr-mu(index3);
     s(index3)=std(u);
```

```
    Tu(index3)=s(index3)/mu(index3);
    [rho_tau,tau]=autoCorrCoef(u(1:sample),Fs);
    k=1;
    while rho_tau(k)>0;                                  %if rho_tau is too small stop;
    k=k+1;
    end
    [Pxx(index3,:),f] = pwelch(u,2^14,[],2^17,80000);
     Tscale1=sum(rho_tau(1:i))*(1/Fs);                                    %equivalent  to
TScale=sum(rho_tau/Fs);
    Tscale(index3)=trapz(tau(1:k),rho_tau(1:k));
    L(index3)=Tscale(index3)*mu(index3);
    [L(index3),T(index3)]=ltscale(Ucorr,mu(index3),Fs,sample);
    end
end
 y=[4:-0.1:-4];
 plot(mu,[4:-0.1:-4])
```

- Following code is written to calculate the auto correlation function.

```
function [rho_tau,tau]=autoCorrCoef(u,Fs)

%Fs: Sampling Frequecy
%u : fluctuation term
%rho_tau=Rx_tau/Rx_0 where rho is auto-corr coefficient
%tau is in s
N=length(u);
Rx_0=mean(u.^2);
if N>2500000
disp('Sample Number should not exceed 2500000');
return

else
   d=N:-1:1;                 %or use d=1:n; fliplr(d);
   x=xcorr(u);
   x=x(N:length(x));          %trancate the symmetrical part
   Rx_tau=x./d';
   Rx_0=mean(u.^2);        %rho_tau=Rx_tau/Rx_0 where rho is a coefficient
   rho_tau=Rx_tau/Rx_0;
end
 tau=(0:N-1)/Fs;
```

- Following code is to calculate time scales

```
function [L,T,rho_tau,tau]=ltscale(U,mu,Fs,N)
%L: Integral length scale
%T: Integral time scale, U: Velocity, mu: sample mean, Fs: Sampling frequency, N: Sample
size
u=U-mu;           %fluctuation term
```

```
Rx_0=mean(u.^2);     %rho_tau=Rx_tau/Rx_0 where rho is a coefficient
if N>=2000000
n=N;
tau=(0:N-1)/Fs;
      for k=0:n-1;
      flag=0;      %A temporary value for continuous accumulated summation
      for i=1:n-k;
      flag=flag+u(i)*u(i+k);  %Accumulated summation
      end
      Rx_tau(k+1)=flag/(n-k);
      rho_tau(k+1)=(Rx_tau(k+1))/Rx_0;
      if rho_tau(k+1)<0;
      n1=k+1;
      break;
      end
      if tau(k+1)>0.030
      n1=k+1;
      break;
      end
      end

    for n2=1:n1;
    if rho_tau(n2)<0;
    break;
    end
    end
    T=sum(rho_tau(1:n1))*(1/Fs);    %equivalent to TScale=sum(rho_tau/Fs);
    L=T*mu;
    rho_tau;
   tau=(0:length(rho_tau)-1)/Fs;

else
d=N:-1:1;   %or use d=1:n; fliplr(d);
x=xcorr(u);
x=x(N:length(x));%trancate the symmetrical part
Rx_tau=x./d';
Rx_0=mean(u.^2); %rho_tau=Rx_tau/Rx_0 where rho is a coefficient
rho_tau=Rx_tau/Rx_0;

i=1;
while rho_tau(i)>0;   %if rho_tau is too small stop;
i=i+1;
end

n1=i-1;
tau=(0:10*n1-1)/Fs;
T=sum(rho_tau(1:n1))*(1/Fs);    %equivalent to TScale=sum(rho_tau/Fs);
L=TScale*mu;
end
```

- This part does the temperature correction

```
function Ecorr = TempCorr(Ea,Ta)
a = 0.8; %Overheat ration, 0.8 for air(default);
T0 = 24; %Ambient (reference) Temperature before calibration
alfa20 = 0.36/100;%Sensor temperature coefficient of resistance at T = 20C
alfa0 = alfa20/(1+alfa20*(T0-20)); %Sensor temperature coefficient of resistance at T =
T0
Tw = a/alfa0+T0; %Sensor hot temperature
Ecorr = Ea*((Tw-T0)/(Tw-Ta))^0.5;
```

Appendix D Snow effect on efficiency

There are some significant parameters which affect the efficiency of the PV modules installed in snowy weathers including

1. Snowfall/snow depth
2. Structure orientation (fixed or tracking with tilt, azimuth, and rotation angles as applicable and open-rack or building integrated mounting)
3. Visual record of snow buildup
4. Air and module temperatures
5. Plane of array irradiation
6. Wind speed and direction
7. Snow moisture content
8. Relative humidity

If these panels are covered by snow, they will produce little or no power, so they have been mounted at very steep tilt angles to shed snow quickly and to maximize the winter output. To estimate the best tilt angle at which the efficiency is the most the following formula is recommended:

- If the latitude is below 25°, use the latitude times 0.87.
- If your latitude is over 25°, use the latitude, times 0.76, plus 3.1 degrees.

Although it is simplest to mount your solar panels at a fixed steep tilt, however, sun is higher in the summer and lower in the winter, so it is possible to gain more energy during the whole year by changing the tilt of the panels with the season. The following table

presents the best dates to change the latitude angles for both northern and southern hemisphere:

	Northern hemisphere	Southern hemisphere
Adjust to summer angle on	March 30	September 29
Adjust to winter angle on	September 12	March 14

And for the best tilt angles use the following formula:

- If your latitude is between 25° and 50°, then the best tilt angle for summer is the latitude, times 0.93, minus 21 degrees. The best tilt angle for winter is the latitude, times 0.875, plus 19.2 degrees.

Having the tilt angle, the losses can be calculated through the following equation

Annual % loss = 0.1 x [Snow, in.] x $\cos^2$(tilt)

The first coefficient, 0.1, was not regression-fitted. It carries the implied units of % per inch. It was selected based on the observation that a near-20% annual loss corresponded to a near-200 inch annual snowfall, or 0.1%/yr/inch of snow. This correlation suggests a typical error of 2% for predicting annual energy loss, with the overall correlation looking pretty good up to about 45 degree tilt angles, and fairly poor for commercially invisible steeply tilted arrays. This is not good enough to call the job done, but, subject to additional data collection at other locations, potentially represents a considerable improvement over the current lack of any simple empirical estimating tools.

REFERENCES

[1] S. Kalagirou, 2009. Solar Energy Engineering, Elsevier.

[2] S. Fonash, 2010. Solar Cell Device Physics, Elsevier.

[3] T. Markvart, L. Castaner, 2003 Practical Handbook of Photovoltaics, Elsevier.

[4] S. Armstrong, W.G. Hurley, 2010. A thermal model for photovoltaic panels under varying atmospheric conditions, Applied Thermal Engineering v30, 1488-1495.

[5] M.K. Bhatt, S.N. Gaderia, S.A. Channiwala, 2011. Experimental Investigations on top loss coefficients of Solar Flat Plate Collector at Different Tilt Angle, World Academy of Science, v79, 432-436.

[6] M.K. Bhatt, S.A. Channiwala, 2010. Review of various losses occurring in single glazed flat plate collector – An experimental study, World Congress on Engineering, 1561-1566.

[7] J.A. Palyvos, E. Skoplaki, 2009. On the temperature dependence of photovoltaic module electrical performance: a review of efficiency/power correlations, Solar Energy, v83, 614-624.

[8] J. Stafford, E. Walsh, V. Egan, R. Grimes, 2010. Flat plate heat transfer with impinging axial fan flows, International Journal of Heat and Mass Transfer, v53, 5629-5638.

[9] K-F.V Wong, 2003. Intermediate Heat Transfer. Marcel Dekker Inc.

[10] Y. Çengel, M.A. Boles 2008, A. Heat and Mass Transfer: A practical Approach. Sixth Edition. New York: McGraw Hill.

[11] P. Oosthuizen, 1999. An Introductive to Convective Heat Transfer Analysis. McGraw – Hill.

[12] H. Schlichting, 1979. Boundary-layer theory New York: McGraw-Hill.

[13] F.P Incropera, D.P DeWitt, 1996. Fundamentals of Heat and Mass Transfer, third ed. John Wiley & Sons, New York.

[14] W.H. McAdams, 1954. Heat Tranmission, Third Edition. McGraw-Hill, New York

[15] J.H. Watmuff, W.W.S. Charters, D. Proctor, 1977. Solar and Wind Induced External Coefficients Solar Collectors 2nd Quarter, Revue Internationaled'Helio-technique, p.56.

[16] E.M. Sparrow, J.W Ramsey, 1979. Laminar Effect of finite width on heat transfer and fluid flow about an inclined rectangular plate, ASME Journal of Heat transfer v101, 199-204.

[17] P.J. Lunde, 1980. Solar Thermal Engineering, John Wiley and Sons.

[18] E. Sartori, 2006. Convection coefficient equations for forced air flow over flat surfaces, Solar Energy, v.80, 1063-1071.

[19] D.S-K. Ting, 2011. Some Basics of Engineering Flow Turbulence, Naomi Ting's Books.

[20] M. Hori, Y. Junzo, 1997. Effects of free stream turbulence on turbulent boundary layer on a flat plate with zero pressure gradient, Journal of Heat Transfer, v26, 97-106.

[21] M.F. Blair, 1983. ASME, Journal of Heat Transfer, v.105, 33-47.

[22] S. Sugawara, T. Sato, H. Komatsu, H.Osaka,1951. The effect of free stream turbulence on heat transfer from a flat plate. JSME, v.17, 122.

[23] D. Hubble, P. Pavlos, 2009. An investigation of the physical mechanism of heat transfer augmentation in boundary layer flows subject to free stream turbulence, ASME Summer Heat Transfer Conference, v1, 597-604.

[24] R.J. Kind, D.H. Gladstone, A.D. Moizer, 1983. Convective heat losses from flat plate solar collectors in turbulent winds. ASME Journal of Solar Energy Engineering, v105, 80–85.

[25] M.C. Smith, A.M. Kuethe, 1966. Effects of turbulence on laminar skin friction and heat transfer, Physics of Fluids, v9, 2337-2344.

[26] L.P.M. Colombo, C.La Briola, A. Niro, 2008. Infrared thermographic measurements of heat transfer enhancement over ribbed surfaces, European Thermal Sciences Conference.

[27] E. Sanz, C. Nicot, R. Point, F. Plaza, 2007. Study of transition from laminar to turbulent boundary layer on a tilted flat plate using heat transfer measurements, Journal of Thermal Science, v.16, 186-191.

[28] H.Y Li, W.M. Yan, 2003. Identification of wall heat flux for turbulent forced convection by inverse analysis, International Journal of Heat and Mass Transfer, v.46, 1041-1048.

[29] P. Karava, C.M. Jubayer, E. Savory, 2011. Numerical modelling of forced convective heat transfer from the inclined windward roof of an isolated low-rise building

with application to photovoltaic/thermal systems, Applied Thermal Engineering, v31, 1950-1963.

[30] O. Turgut, N. Onur, 2010. An experimental and three dimensional numerical study on the wind related heat transfer from a rectangular flat plate model collector flush mounted on the roof of a model house, Heat Mass Transfer, v46, 1345-1354.

[31] F. Peneau, H.C. Boisson, A. Kondjoyan, N. Djilali, 2004, Structure of a flat plate boundary layer subjected to free stream turbulence. International Journal of Computational Fluid Dynamics, v18, 175–188.

[32] M.C.A. Garcia, J.L. Balenzategui, 2004. Estimation of photovoltaic module yearly temperature and performance based on nominal operation cell temperature calculations, Renewable Energy, v29, 1997-2010.

[33] Gh. Juncu, 2005. Unsteady forced convection heat/mass transfer from a flat plate. Heat Mass Transfer, v41, 1095-1102.

[34] G. L. Lioznov, V. G. Lushchik, M. S. Makarova, and A. E. Yakubenko, 2012. Freestream turbulence effect on flow and heat transfer in the flat plate boundary layer, Fluid Dynamics, v47, 590-592.

[35] X. Wu, 2010. Transitional and turbulent boundary layer with heat transfer, Physics of Fluids, v22

[36] A.A. Kendoush, 2009. Theoretical analysis of heat and mass transfer to fluids flowing across a flate plate, International Journal of Thermal Sciences, v48, 188-194.

[37] A. Campo, 2001. Numerical study of turbulent flow with heat removal from a flat plate using the finite volume-based method of lines, International Journal of Numerical Methods for Heat and Fluid Flow, v11, 511-523.

[38] R.J. Ribando, K.A. O'Leary, W. Gerald, 1998. Teaching module for laminar and turbulent forced convection on a flat plate, Computer Applications in Engineering Education, v6, 115-125.

[39] F.L. Test, R.C. Lessmann, A. Johary, 1980. Heat transfer during wind flow over rectangular bodies in the natural environment, Journal of Heat Transfer, v103, 262-267.

[40] N.S. Sturrock, R.J. Cole, 1977. The convective heat exchange at the external surface of buildings, Building and Environment, v12, 207-214.

[41] S. Sharples, P.S. Charlesworth, 1998. Full scale measurements of wind induced convective heat transfer from a roof mounted flat plate solar collector, Solar Energy, v62,n2, 69-77.

[42] R. Lui, D. Ting, G. Rankin, 2004. On the generation of turbulence with a perforated plate, Experimental Thermal and Fluid Science, v28, 307-316.

[43] C. Ramirez, D.B. Murray, J.A. Fitzpatrick, 2002. Convective heat transfer of an inclined rectangular plate. Experimental Heat Transfer, v15, 1-18.

[44] D.L Evans, L.W. Florschuetz. 1977, Cost studies on terrestrial photovoltaic power systems with sunlight concentration. Solar Energy v19, 255–262.

[45] ASHRAE Fundamentals Handbook. 2009 Climatic Design Information. Chapter 14.

[46] G.E. Ahmad, H.M.S. Hussein, 2001. Comparative study of PV modules with and without a tilted plane reflector, Energy Conversion and Management, v42, 1327-1333.

[47] Lj.T. Kostić, T.M. Pavlović, Z.T. Pavlović. 2010, Optimal design of orientation of PV/T collector with reflectors, Applied Energy, v87, 3023-3029.

[48] Ji Jie, He Wei, H.N. Lam, 2002. The annual analysis of the power output and heat gain of a PV-wall with different integration mode in Hong Kong, Solar Energy Materials and Solar Cells,v71, 435-448.

[49] M. Kacira, M. Simsek, Y. Babur, S. Demirkol, 2004. Determining optimum tilt angles and orientations of photovoltaic panels in Sanliurfa, Turkey,Renewable Energy, v29, 1265-1275.

[50] J. Deb Mondol, Y.G. Yohanis, B. Norton, 2007. The impact of array inclination and orientation on the performance of a grid-connected photovoltaic system, Renewable Energy, v32,118-140.

[51] L. Lu, K.M. Law, 2013. Overall energy performance of semi-transparent single-glazed photovoltaic (PV) window for a typical office in Hong Kong, Renewable Energy, v49,250-254.

[52] S. Nakagawa, T. Tokoro, T. Nakano, K. Hayama, H. Ohyama and T. Yamaguchi, 2003. An effect of snow for electric energy generation by 40KW PV system, 3rd World conference on photovoltaic energy conversion May 11-18, Osaka, Japan

[53] L. Powers, J. Newmiller T. Townsend, 2010. Measuring and modeling the effect of snow on photovoltaic system performance, IEEE, 973-978.

VITA AUCTORIS

Name: Frantzis Iakovidis

Place of Birth: Windsor, Ontario, Canada

Year of Birth: 1980

In 2003, Frantzis completed a Bachelor's Degree in Applied Mechanical Engineering from Cleveland State University in Ohio, United States of America. Upon graduation, he worked as a consulting engineer in Ohio. He then moved back to Canada in 2006 due to the death of his father Anestis. He is currently pursuing a higher educational degree. He is currently a candidate for a Master Degree in Applied Science in Mechanical Engineering at the University of Windsor, Windsor, Ontario, Canada.